Supplementary Information

Cluster *versus* coordination: the chemistry of cyclopentadienyl titanium and vanadium complexes with B- and C-functionalized carborane-thiols, $[C_2B_{10}H_{12-n}(SH)_n]$ (n = 2 or 3)

Subhash Bairagi,[‡a] Deepak Kumar Patel,[‡a,b,c] Debipada Chatterjee,[a] Monika Kučeráková,[d] Jan Macháček,[c] Tomas Base,*[c] Thalappil Pradeep,*[a,b] and Sundargopal Ghosh*[a]

[a]Department of Chemistry, Indian Institute of Technology Madras, Chennai 600036, India, E-mail: sghosh@iitm.ac.in

[b]DST Unit of Nanoscience (DST UNS) and Thematic Unit of Excellence (TUE), Department of Chemistry, Indian Institute of Technology, Madras, Chennai 600036, India, Email: pradeep@iitm.ac.in

[c]Institute of Inorganic Chemistry, The Czech Academy of Science, 25068 Rez, Czech Republic, Email: tbase@iic.cas.cz

[d]Institute of Physics, The Czech Academy of Science, 182 21 Prague 8, Czech Republic.

[‡]These authors contributed equally to this work.

Table of contents

I Experimental Details

General Procedures and Instrumentation

All the manipulations were conducted under an Ar/N_2 atmosphere using standard Schlenk line techniques or in a glove box. Toluene, hexane, and THF solvents were distilled from purple solutions of benzophenone ketyl. Dichloromethane and $CDCl_3$ were distilled from calcium hydride before use. Metal precursors $[Cp^*TiCl_3]$[1], $[Cp^*VCl_2]_3$[2] and di/tri-thiol-*o*-carborane ligands $[1,2\text{-}(SH)_2\text{-}1,2\text{-}C_2B_{10}H_{10}]$[3], $[9,12\text{-}(SH)_2\text{-}1,2\text{-}C_2B_{10}H_{10}]$[4], and $[8,9,12\text{-}(SH)_3\text{-}1,2\text{-}C_2B_{10}H_9]$[5] were synthesized according to the literature methods while $LiBH_4$ (2.0 M in THF) and $[Cp_2TiCl_2]$ were used as received (Sigma Aldrich). Thin layer chromatography (TLC) was carried out on 250-μm diameter aluminum-supported silica gel TLC plates (MERCK TLC Plates) to separate the reaction mixtures. NMR spectra were recorded on a Bruker Avance III 500 MHz spectrometer. The residual solvent protons ($CDCl_3$, δ = 7.26 ppm) and carbon ($CDCl_3$, δ = 77.1 ppm) were employed as a reference for the ^1H and $^{13}C\{^1H\}$ NMR spectra, respectively. The ^{11}B decoupled ^1H spectrum was obtained with inverse gated decoupling (zgig) and power gated decoupling (zgpr) pulse sequences, respectively. $^{11}B\{^1H\}$ NMR spectra were processed with a backward linear prediction algorithm to eliminate the broad ^{11}B background signal of the NMR tube.[6] All pulse sequences are available in a commercial Bruker spectrometer. Electrospray mass (ESI-MS) spectrometric data were obtained on a Qtof Micro YA263 HRMS and 6545 Qtof LC/MS instrument. Infrared (IR) spectra were recorded on a JASCO FT/IR-1400 spectrometer. UV-vis spectra were recorded in dichloromethane on a Thermo Scientific (Evolution 300) UV-vis spectrometer.

Synthesis of 1 and 2: In a flame-dried Schlenk tube, $[(Cp^*TiCl_3]$ (0.100 g, 0.35 mmol) was suspended in 10 mL dry toluene and it was charged with lithium borohydride solution of 2.0 M in THF (0.6 mL, 1.2 mmol) dropwise at -78 °C and kept under constant stirring for 1 h. The red reaction mixture converted to dark green after 1 h. To this in situ-generated unstable dark green intermediate, one equivalent of $[1,2\text{-}(SH)_2\text{-}1,2\text{-}C_2B_{10}H_{10}]$ (0.038 g, 0.18 mmol) was added and kept at 90 °C for 48 h under stirring conditions. After the addition of $[1,2\text{-}(SH)_2\text{-}1,2\text{-}C_2B_{10}H_{10}]$, the mixture becomes brown and, after 48 h, changes to dark brown. After the completion of the reaction, the solvent was removed under vacuum. The residue was extracted with *n*-hexane /dichloromethane mixture (70:30 v/v) through a frit using 3 cm of celite. The filtrate was concentrated, and the residue was subjected to chromatographic workup on 250-μm diameter aluminium-supported silica gel TLC plates (MERCK TLC Plates). Note that we have done the chromatographic workup using TLC plates inside beakers, which were filled with Ar before and after filling them with properly distilled eluting solvents. Elution with a *n*-hexane/dichloromethane (50:50 v/v) mixture yielded brown **1** (0.010 g, 12%) and brown **2** (0.015 g, 18%).

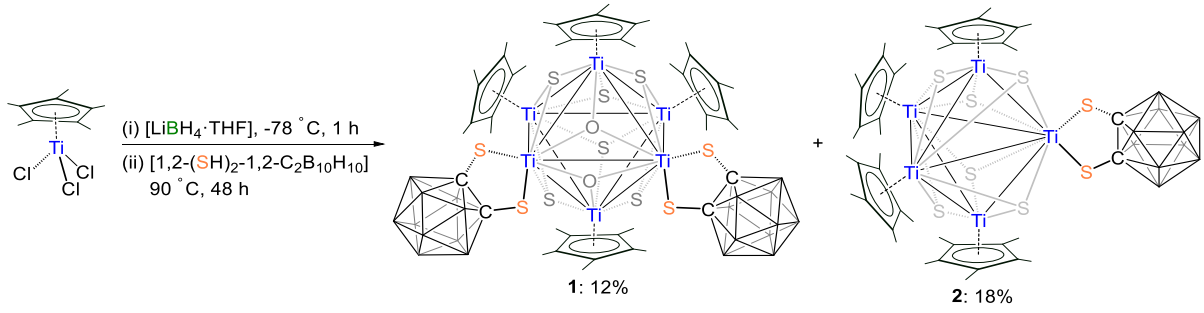

Scheme S1. Synthesis of **1** and **2**.

1: MS (ESI^+): *m/z* calculated for $[C_{44}H_{80}B_{20}S_{10}O_2Ti_6 + K]^+$: 1504.1911, found: 1504.2403; $^{11}B\{^1H\}$ NMR (160 MHz, $CDCl_3$, 22 °C): δ = -12.5 and -7.9 (vrey broad peak ranging from -11.0 to -1.0) ppm (br, 20B, *B*-H); ^{11}B NMR (160 MHz, $CDCl_3$, 22 °C): δ = -13.0 and -11.4 (d, $^1J_{B\text{-}H}$ = 209.0 Hz), -7.0 (vrey broad peak ranging from -10.0 to -1.0) ppm (br, 20B, *B*-H), ppm; ^1H NMR (500 MHz, $CDCl_3$, 22 °C): δ = 2.22 (s, 15H, 1Cp*), 2.25 (s, 15H, 1Cp*), 2.28 (s, 30H, 2Cp*) ppm; $^1H\{^{11}B\}$ NMR (500 MHz, $CDCl_3$, 22 °C): δ = 2.22 (s, 15H, 1Cp*), 2.25 (s, 15H, 1Cp*), 2.28 (s, 30H, 2Cp*), 2.52-2.98 (br, 20H, Carborane-B*H*) ppm; $^{13}C\{^1H\}$ NMR

(125 MHz, $CDCl_3$, 22 °C): δ = 14.7, 15.1, 15.3, and 15.5 ($4C_5\mathit{Me}_5$), 132.5, 132.9, and 133.6 ($4\mathit{C}_5Me_5$) ppm; IR (KBr, cm^{-1}): $\bar{\upsilon}$ = 2956, 2925, 2854, 2773, 2580 (B-H_t), 1740, 1643, 1459, 1262, 1088, 1024, 801, 699; UV-Vis (CH_2Cl_2): λ = 252, 375, 490 nm.

2: MS (ESI^+): *m/z* calculated for $[C_{42}H_{70}B_{10}S_8Ti_5 + CH_3OH + CH_3CN + Na]^+$: 1291.1833, found: 1291.1251; $^{11}B\{^1H\}$ NMR (160 MHz, $CDCl_3$, 22 °C): δ = -12.4, -9.8, -8.7, -8.4, -4.9, -3.7, -1.5, and -0.8 ppm (br, 10B, *B*-H); ^{11}B NMR (160 MHz, $CDCl_3$, 22 °C): δ = -12.8 and -11.4 (d, $^1J_{B\text{-}H}$ = 178 Hz), -10.4 (d, merged wih other peak), -9.0 and –7.9 (d, $^1J_{B\text{-}H}$ = 144 Hz), -5.3, -4.2 and -3.1 {(d, $^1J_{B\text{-}H}$ = 157 Hz) and (d, $^1J_{B\text{-}H}$ = 153 Hz)}, -2.1, -0.9 and -0.2 {(d, $^1J_{B\text{-}H}$ = 121 Hz) and (d, $^1J_{B\text{-}H}$ = 109 Hz)} ppm; ^1H NMR (500 MHz, $CDCl_3$, 22 °C): δ = 2.21 (s, 30H, 2Cp*), 2.23 (s, 30H, 2Cp*) ppm; $^1H\{^{11}B\}$ NMR (500 MHz, $CDCl_3$, 22 °C): δ = 2.21 (s, 30H, 2Cp*), 2.23 (s, 30H, 2Cp*), 2.47, 2.52 and 3.04 (br, 10H, Carborane-B*H*) ppm; $^{13}C\{^1H\}$ NMR (125 MHz, $CDCl_3$, 22 °C): δ = 14.3 ($2C_5\mathit{Me}_5$), 14.4 ($2C_5\mathit{Me}_5$), 68.1 (Carborane-*C*H), 132.2 ($2\mathit{C}_5Me_5$), 133.3 ($2\mathit{C}_5Me_5$) ppm; IR (KBr, cm^{-1}): $\bar{\upsilon}$ = 2961, 2925, 2854, 2800, 2589 (B-H_t), 1740, 1638, 1450, 1410, 1262, 1092, 1024, 867, 801, 692; UV-Vis (CH_2Cl_2): λ = 252, 365, 463 nm.

Synthesis of 3 and 4a: In a flame-dried Schlenk tube, $[(Cp^*TiCl_3]$ (0.100 g, 0.35 mmol) was suspended in 10 mL dry toluene and it was charged with lithium borohydride solution 2.0 M in THF (0.6 mL, 1.2 mmol) dropwise at -78 °C and kept under constant stirring for 1 h. The red reaction mixture converted to dark green after 1 h. To this in situ generated intermediate, one equivalent of $[9,12\text{-}(SH)_2\text{-}1,2\text{-}C_2B_{10}H_{10}]$ (0.073 g, 0.35 mmol) was added and kept at 90 °C for 24 h under stirring condition. After the addition of $[9,12\text{-}(SH)_2\text{-}1,2\text{-}C_2B_{10}H_{10}]$, the mixture becomes brown and, after 24 h, changes to yellow. After the completion of the reaction, the solvent was removed under vacuum. The residue was extracted with hexane/dichloromethane mixture (50:50 v/v) through a frit using 3 cm of celite. The filtrate was concentrated, and the residue was subjected to chromatographic workup on 250-µm diameter aluminium-supported silica gel TLC plates (MERCK TLC Plates). Elution with a hexane/dichloromethane (30:70 v/v) mixture yielded yellow **3** (0.089 g, 64%).

Under similar reaction conditions, treatment of the above-mentioned in situ generated intermediate with one equivalent of $[8,9,12\text{-}(SH)_3\text{-}1,2\text{-}C_2B_{10}H_9]$ (0.084 g, 0.35 mmol) yielded yellow solid **4a** (0.104 g, 72%).

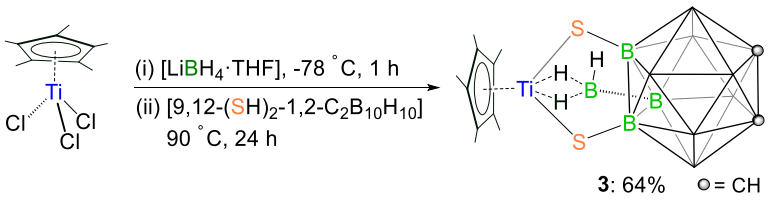

Scheme S2. Synthesis of **3**.

3: MS (ESI^+): *m/z* calculated for $[C_{12}H_{27}B_{11}S_2Ti + H]^+$: 403.2216, found: 403.2129; $^{11}B\{^1H\}$ NMR (160 MHz, $CDCl_3$, 22 °C): δ = -15.8 (br, 2B, *B*-H), -11.2 (br, 2B, *B*-H), -10.1 (br, 2B, *B*-H), -6.8 (br, 2B, *B*-H), -3.1 (br, 1B, BH_3), 8.4 (br, 2B, *B*-S) ppm; ^{11}B NMR (160 MHz, $CDCl_3$, 22 °C): δ = -16.5 and -15.2 (d, $^1J_{B\text{-}H}$ = 168 Hz, 2B, *B*-H), -11.8, -10.7 and -9.5 {(d, $^1J_{B\text{-}H}$ = 136 Hz, 2B, *B*-H) and (d, $^1J_{B\text{-}H}$ = 153 Hz, 2B, *B*-H)}, -6.8 (br, 2B, *B*-H), -3.2 (br, 1B, BH_3), 8.4 (br, 2B, *B*-S) ppm; ^1H NMR (500 MHz, $CDCl_3$, 22 °C): δ = -0.86 (br, 2H, Ti-*H*-B), 2.24 (s, 15H, 1Cp*), 2.58, 2.92 and 3.21 (br, 8H, Carborane-B*H*), 3.54 (br, 2H, Carborane-C*H*) ppm; $^1H\{^{11}B\}$ NMR (500 MHz, $CDCl_3$, 22 °C): δ = -0.87 (br, 2H, Ti-*H*-B), 2.24 (s, 15H, 1Cp*), 1.92, 2.43, 2.73 and 2.84 (br, 8H, Carborane-B*H*), 3.54 (br, 2H, Carborane-C*H*) ppm; $^{13}C\{^1H\}$ NMR (125 MHz, $CDCl_3$, 22 °C): δ = 13.9 ($C_5\mathit{Me}_5$), 44.3 (Carborane-*C*H), 127.8 (C_5Me_5) ppm; IR (KBr, cm^{-1}): $\bar{\upsilon}$ = 3060, 2954, 2923, 2852, 2738, 2602 (B-H_t), 2480 (B-H_t of *exo*-BH_3), 2117, (B-H_b),1707, 1459, 1259, 1094, 1021, 799; UV-Vis (CH_2Cl_2): λ = 238, 288, 336 nm.

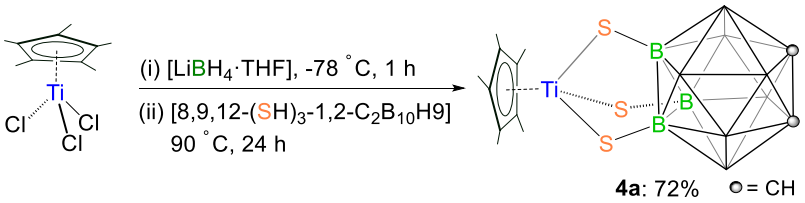

Scheme S3. Synthesis of **4a**.

4a: MS (ESI$^+$): *m/z* calculated for $[C_{12}H_{24}B_{10}S_3Ti + H]^+$: 421.1608, found: 421.1511; $^{11}B\{^1H\}$ NMR (160 MHz, $CDCl_3$, 22 °C): δ = -22.3 (br, 1B, *B*-H), -16.4 (br, 2B, *B*-H), -12.5 (br, 2B, *B*-H), -11.3 (br, 2B, *B*-H), 1.3 (br, 1B, *B*-S), 6.3 (br, 2B, *B*-S) ppm; ^{11}B NMR (160 MHz, $CDCl_3$, 22 °C): δ = -23.1 and -21.9 (d, $^1J_{B\text{-}H}$ = 160 Hz, 1B, *B*-H), -17.1 and -15.8 (d, $^1J_{B\text{-}H}$ = 167 Hz, 2B, *B*-H), -13.4, -12.0 and -10.8 {(d, $^1J_{B\text{-}H}$ = 170 Hz, 2B, *B*-H) and (d, $^1J_{B\text{-}H}$ = 161 Hz, 2B, *B*-H)}, 1.3 (br, 1B, *B*-S), 6.3 (br, 2B, *B*-S) ppm; ^1H NMR (500 MHz, $CDCl_3$, 22 °C): δ = 2.24 (s, 15H, 1Cp*), 2.50, 2.97 and 3.29 (br, 8H, Carborane-B*H*), 3.49 (br, 2H, Carborane-C*H*) ppm; $^1H\{^{11}B\}$ NMR (500 MHz, $CDCl_3$, 22 °C): δ = 2.24 (s, 15H, 1Cp*), 2.03, 2.79 and 2.99 (br, 8H, Carborane-B*H*), 3.49 (br, 2H, Carborane-C*H*) ppm; $^{13}C\{^1H\}$ NMR (125 MHz, $CDCl_3$, 22 °C): δ = 13.8 (C_5Me_5), 39.7 (Carborane-*C*H), 127.7 (C_5Me_5) ppm; IR (KBr, cm^{-1}): $\bar{\upsilon}$ = 3072, 3033, 2995, 2918, 2850, 2605 (B-H_t), 2569 (B-H_t), 1636, 1425, 1085, 1021, 867, 799, 738; UV-Vis (CH_2Cl_2): λ = 230, 257, 289, 371 nm.

Synthesis of 4b: In a flame-dried Schlenk tube, $[(Cp_2TiCl_2]$ (0.100 g, 0.34 mmol) was suspended in 10 mL dry toluene and it was charged with lithium borohydride solution of 2.0 M in THF (0.6 mL, 1.2 mmol) dropwise at -78 °C and kept under constant stirring for 1 h. The red reaction mixture converted to dark blue after 1 h. To this in situ-generated unstable dark blue intermediate, one equivalent of $[8,9,12\text{-}(SH)_3\text{-}1,2\text{-}C_2B_{10}H_9]$ (0.084 g, 0.35 mmol) was added and kept at 90 °C for 24 h under stirring conditions. After the addition of $[8,9,12\text{-}(SH)_3\text{-}1,2\text{-}C_2B_{10}H_9]$, the mixture becomes brown and, after 24 h, changes to yellow. After the completion of the reaction, the solvent was removed under vacuum. The residue was extracted with *n*-hexane /dichloromethane mixture (50:50 v/v) through a frit using 3 cm of celite. The filtrate was concentrated, and the residue was subjected to chromatographic workup on 250-μm diameter aluminium-supported silica gel TLC plates (MERCK TLC Plates). Elution with a *n*-hexane /dichloromethane (30:70 v/v) mixture yielded yellow **4b** (0.080 g, 57%).

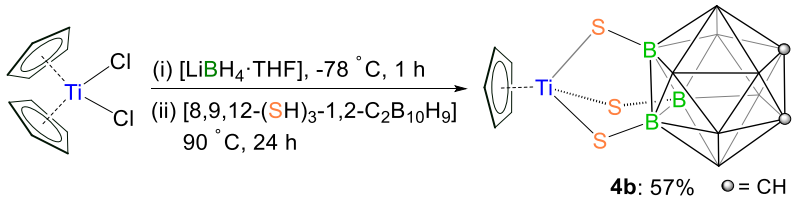

Scheme S4. Synthesis of **4b**.

4b: MS (ESI$^+$): *m/z* calculated for $[2(C_7H_{14}B_{10}S_3Ti) + H]^+$: 723.1394, found: 723.1343; $^{11}B\{^1H\}$ NMR (160 MHz, $CDCl_3$, 22 °C): δ = -22.2 (br, 1B, *B*-H), -16.6 (br, 2B, *B*-H), -11.8 (br, 2B, *B*-H), -10.7 (br, 2B, *B*-H), 2.1 (br, 1B, *B*-S), 7.1 (br, 2B, *B*-S) ppm; ^{11}B NMR (160 MHz, $CDCl_3$, 22 °C): δ = -23.0 and -21.6 (d, $^1J_{B\text{-}H}$ = 181 Hz, 1B, *B*-H), -17.4 and -16.1 (d, $^1J_{B\text{-}H}$ = 167 Hz, 2B, *B*-H), -12.4, -11.4 and -10.2 {(d, $^1J_{B\text{-}H}$ = 139 Hz, 2B, *B*-H) and (d, $^1J_{B\text{-}H}$ = 156 Hz, 2B, *B*-H)}, 2.1 (br, 1B, *B*-S), 7.1 (br, 2B, *B*-S) ppm; ^1H NMR (500 MHz, $CDCl_3$, 22 °C): δ = 2.55, 3.11 and 3.40 (br, 8H, Carborane-B*H*), 3.59 (br, 2H, Carborane-C*H*), 6.65 (s, 15H, 1Cp*) ppm; $^1H\{^{11}B\}$ NMR (500 MHz, $CDCl_3$, 22 °C): δ = 2.08, 2.92 and 3.13 (br, 8H, Carborane-B*H*), 3.59 (br, 2H, Carborane-C*H*), 6.65 (s, 15H, 1Cp*) ppm; $^{13}C\{^1H\}$ NMR (125 MHz, $CDCl_3$, 22 °C): δ = 39.8 (Carborane-*C*H), 114.0 (C_5H_5) ppm; IR (KBr, cm^{-1}): $\bar{\upsilon}$ = 3082, 3013, 2986, 2925, 2850, 2623 (B-H_t), 2598 (B-H_t), 1638, 1435, 1257, 1017, 872, 818, 741; UV-Vis (CH_2Cl_2): λ = 230, 256, 293, 330, 388 nm.

Synthesis of 5: In a flame-dried Schlenk tube, $[(Cp^*VCl_2)_3]$ (0.100 g, 0.13 mmol) was suspended in 10 mL dry toluene and it was charged with lithium borohydride solution 2.0 M in THF (0.5 mL, 1.0 mmol) dropwise at -78 °C through a syringe. Then, the reaction mixture was allowed to come to room temperature for over 1 h under stirring conditions, and no such drastic color change was observed in the brownish reaction mixture. After 1 h, three equivalents of $[8,9,12\text{-}(SH)_3\text{-}1,2\text{-}C_2B_{10}H_9]$ (0.093 g, 0.39 mmol) was added and kept at 90 °C for 24 h under stirring conditions. After 24 h, the mixture becomes brownish green. After the completion of the reaction, the solvent was removed under vacuum. The residue was extracted with hexane/dichloromethane mixture (70:30 v/v) through a frit using 3 cm of celite. The filtrate was concentrated, and the residue was subjected to chromatographic workup on 250-µm diameter aluminium-supported silica gel TLC plates (MERCK TLC Plates). Elution with a hexane/dichloromethane (50:50 v/v) mixture yielded green **5** (0.032 g, 26%).

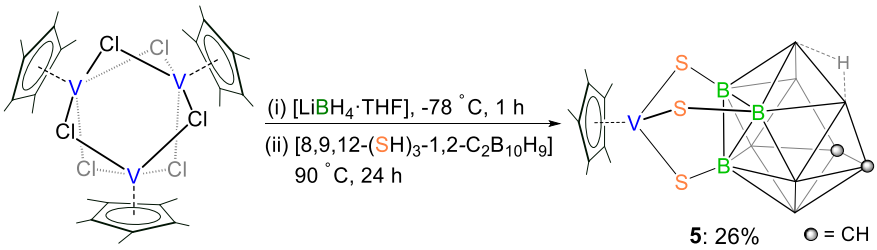

Scheme S5. Synthesis of **5**.

5: $^{11}B\{^1H\}$ NMR (160 MHz, $CDCl_3$, 22 °C): δ = -30.3 (br, 2B, *B*-H), -25.8 (br, 2B, *B*-H), -22.0 (br, 1B, *B*-S), -6.4 (br, 2B, *B*-H), -4.6 (br, 2B, *B*-S) ppm; ^{11}B NMR (160 MHz, $CDCl_3$, 22 °C): δ = -30.8 and -29.8 (d, $^1J_{B\text{-}H}$ = 160 Hz, 2B, *B*-H), -26.3 and -25.1 (d, $^1J_{B\text{-}H}$ = 161 Hz, 2B, *B*-H), -21.9 (br, 1B, *B*-S), -7.0 and -5.8 (d, $^1J_{B\text{-}H}$ = 150 Hz, 2B, *B*-H), -4.6 (br, 2B, *B*-S) ppm; ^1H NMR (500 MHz, $CDCl_3$, 22 °C): δ = -0.43 (br, 1H, B-*H*-B), 2.28 (s, 15H, 1Cp*), 2.01, 2.52, 2.79, 3.10 and 3.39 (br, 7H, Carborane-B*H*) ppm; $^1H\{^{11}B\}$ NMR (500 MHz, $CDCl_3$, 22 °C): δ = -0.39 (br, 1H, B-*H*-B), 2.28 (s, 15H, 1Cp*), 2.01, 2.25, 2.95 and 3.49 (br, 7H, Carborane-B*H*) ppm; $^{13}C\{^1H\}$ NMR (125 MHz, $CDCl_3$, 22 °C): δ = 14.2 (C_5Me_5), 25.8 (Carborane-*C*H), 127.6 (C_5Me_5) ppm; IR (KBr, cm^{-1}): $\bar{\upsilon}$ = 3054, 2981, 2921, 2852, 2683 (B-H_t), 2619 (B-H_t), 1725, 1430, 1364, 1264, 1094, 1019, 897, 741; UV-Vis (CH_2Cl_2): λ = 230, 283, 335, 424, 591, 652 nm.

I.1 UV-visible Studies

In order to investigate the optical properties of these coloured clusters **1**-**5**, we have carried out UV-vis study in CH_2Cl_2 solution. The UV-vis absorption spectra of all the complexes were measured in the range of 200-800 nm in CH_2Cl_2 solution at 298 K (Figures S54-S55). All of them display the most intense peaks at higher energy regions 230-293 nm due to the π–π* transition of Cp* ligands, characteristic bands for most Cp* based metal complexes.[7] The absorptions with λ>300 nm exhibit mainly two to three absorption bands. These comparatively low energy bands, around 330-652 nm, have been assigned to the charge transfer bands.[8,9] Unlike other complexes, in complex **5**, relatively low energy absorption bands have been observed at 591 and 652 nm.[10]

To reproduce the UV-vis spectrum and get some idea about the electronic transitions, Time-Dependent DFT formalism was used. The studies show that the possible number of electronic transitions is more in hexa- and pentametallic clusters **1** and **2** compared to the monometallic complexes **3**-**5** (Figures S71, S73, S75, S77, S79, S81, and Tables S6-S11). The molecular orbitals of **1**-**5**, exhibiting the most intense electronic transitions, are shown in Figures S72, S74, S76, S78, S80, and S82. In complex **1** and **2**, the low-intensity absorption bands near 365-490 nm may be assigned as an intramolecular LMCT transition that correspond to electron density flow from the sulfur or carborane ring to the metal centers. The absorptions in 330-388 nm region for complexes **3**, **4a**, and **4b** are mainly due to the electron density flow from the Cp*

ligand or sulfur atoms to the metal center. In the contrary, the absorption bands at 335 and 652 nm for **5** are due to LMCT transition that correspond to electron density flow from the carborane ring to the metal center. This is mainly due to the zwitterionic nature of complex **5**, where the anionic charge delocalized onto the pendant [C_2B_3] ring of the *nido*-carborane (C_2B_9).

I.2 Supplementary Data

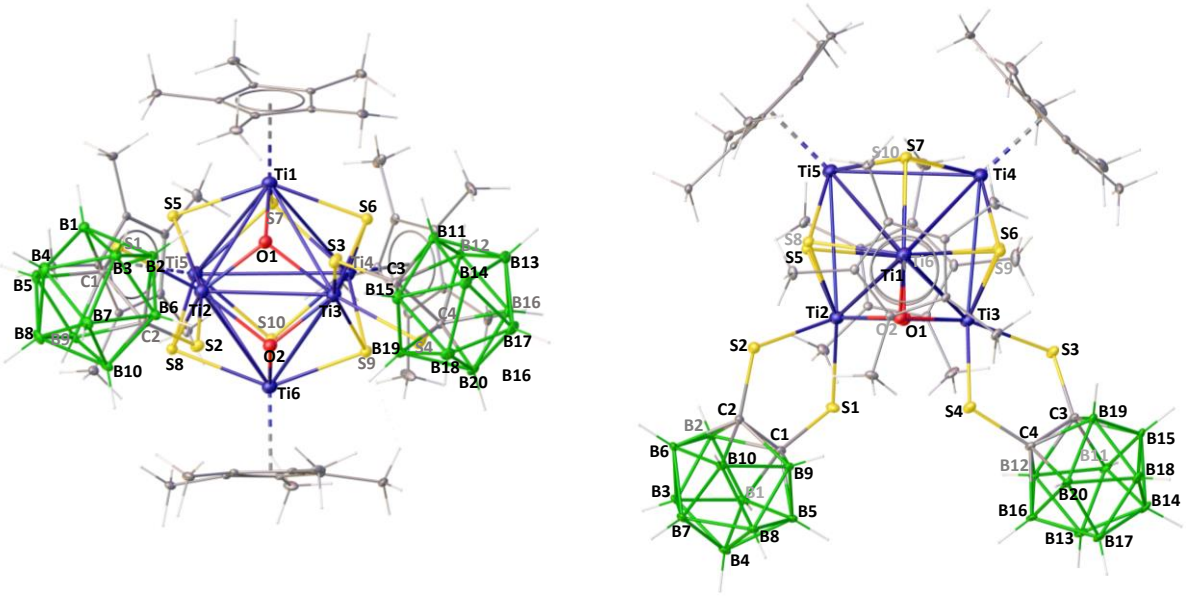

Figure S1. Molecular structure and labelling diagram of **1**. (left) side view; (right) top view. Selected bond lengths (Å) and bond angles (˚): Ti···Ti 3.130-3.598, Ti1-S5 2.4274(12), Ti1-O1 1.919(2), Ti2-S5 2.4835(12), Ti2-S1 1.3963(13), C1-S1 1.785(4), B1-C1 1.703(7), Ti3-Ti2-Ti5 93.913, Ti1-S5-Ti2 82.52(4).

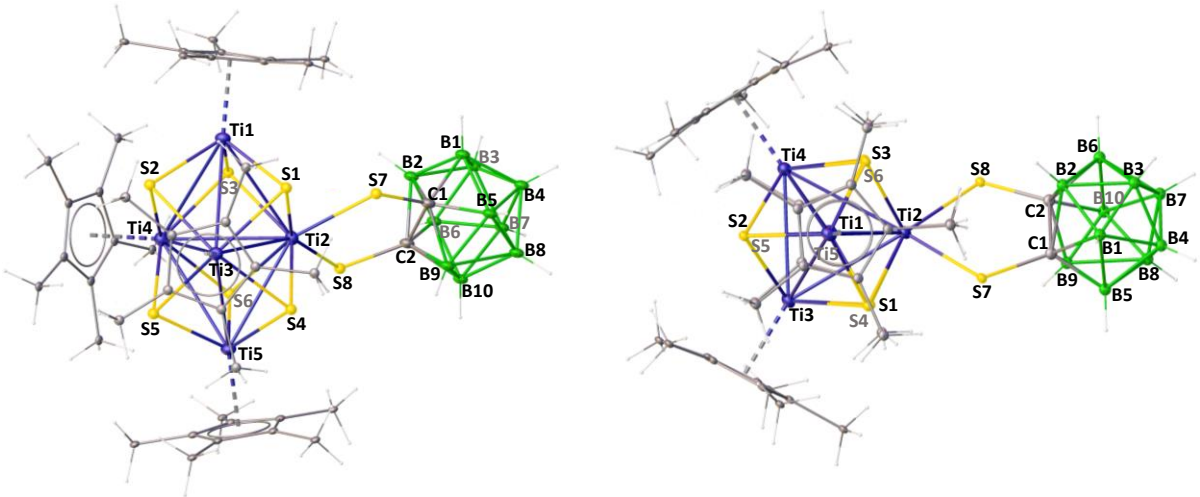

Figure S2. Molecular structure and labelling diagram of **2**. (left) side view; (right) top view. Selected bond lengths (Å) and bond angles (˚): Ti···Ti 3.201-3.305, Ti1-S1 2.2839(17), Ti2-S1 1.5004(16), Ti2-S7 1.446(4), Ti3-S1 2.5089(17), C2-S8 1.782(9), Ti3-Ti2-Ti4 58.270, S7-Ti2-S8 81.09(12), Ti1-S1-Ti2 82.24(5).

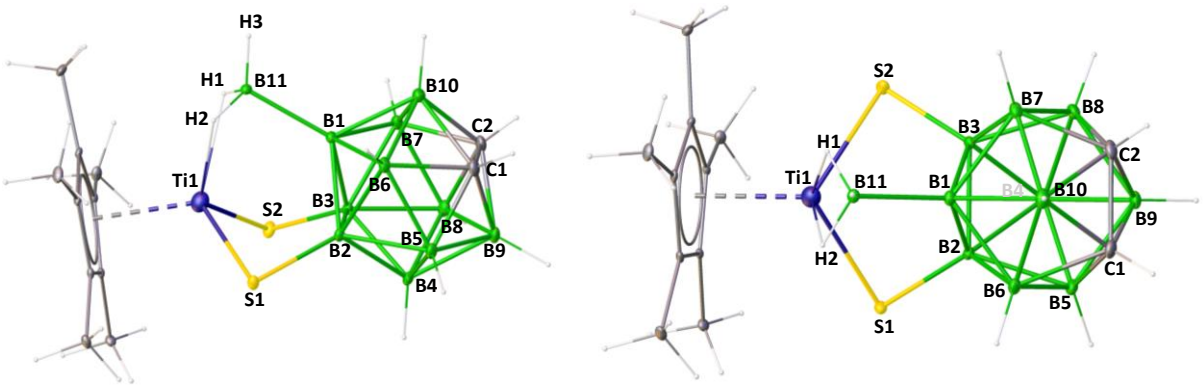

Figure S3. Molecular structure and labelling diagram of **3**. (left) side view; (right) top view. Selected bond lengths (Å) and bond angles (˚): Ti1-S1 2.3321(9), Ti1-S2 2.3214(9), Ti1···B11 2.259(4), Ti1-H1 2.00(3), Ti-H2 1.93(3), B11-H1 0.90(3), B11-H2 1.03(4), B1-B11 1.750(5), B2-S1 1.851(4) C1-C2 1.626(6), Ti1-S1-B2 81.17(11), B2-B1-B11 121.9(3).

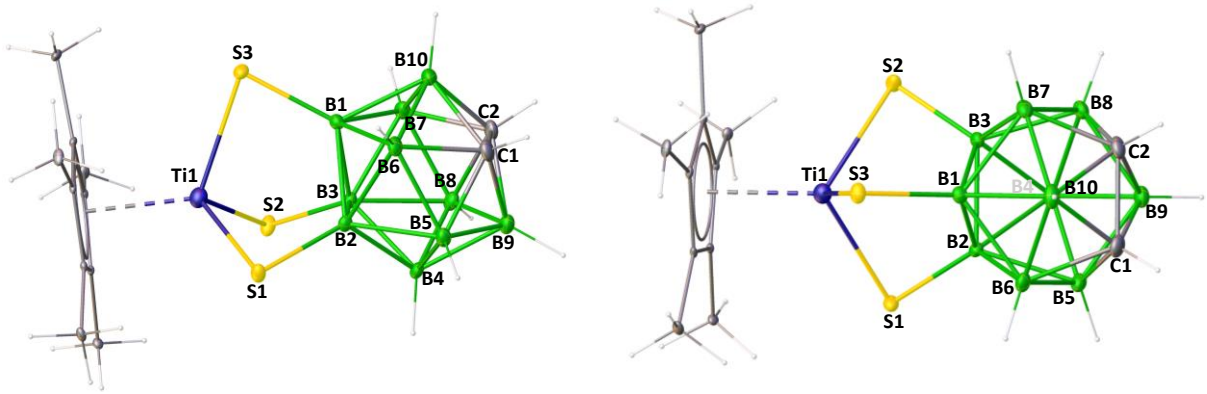

Figure S4. Molecular structure and labelling diagram of **4a**. (left) side view; (right) top view. Selected bond lengths (Å) and bond angles (˚): Ti1-S1 2.3095(12), Ti1-S3 2.3231(12), B1-S3 1.849(5), B1-B2 1.829(5), C1-C2 1.635(7), C1-B10 1.713(7), Ti1-S1-B2 80.72(14).

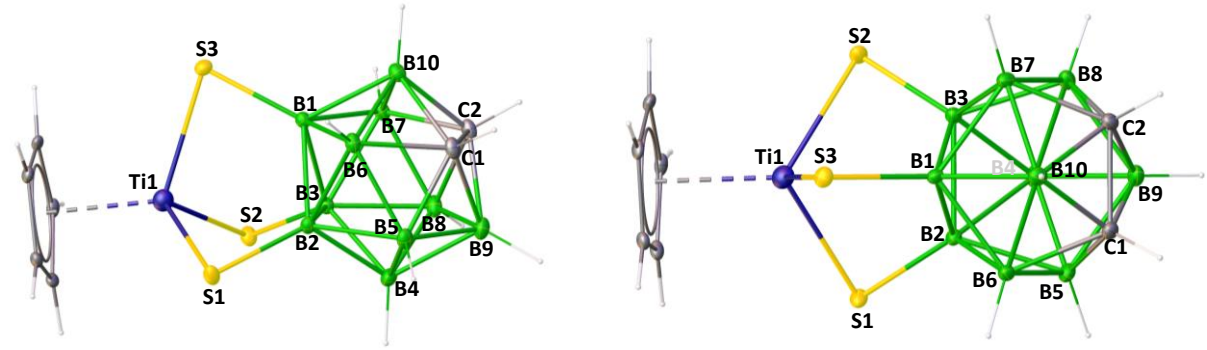

Figure S5. Molecular structure and labelling diagram of **4b**. (left) side view; (right) top view. Selected bond lengths (Å) and bond angles (˚): Ti1-S1 2.2992(7), Ti1-S3 2.3223(7), Ti1-S3 2.3182(7), B1-S3 1.843(3), B1-B2 1.835(3), C1-C2 1.629(3), C1-B10 1.711(4), Ti1-S1-B2 80.89(8).

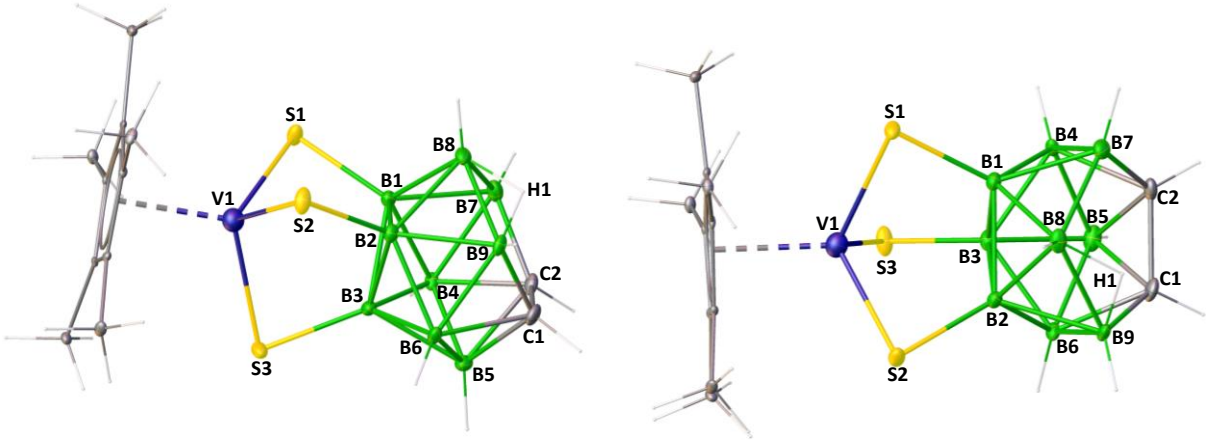

Figure S6. Molecular structure and labelling diagram of **5**. (left) side view; (right) top view. Selected bond lengths (Å) and bond angles (˚): V1-S1 2.2194(16), V1-S3 2.2099(15), B3-S3 1.859(6), B1-B8 1.780(9), C1-C2 1.555(8), C2-B7 1.596(8), B8-H_b 1.15(2), B9-H_b 1.16(2), V1-S1-B1 81.01(19), V1-S3-B3 79.42(17), B7-B8-B9 101.7(5), C1-C2-B7 114.3(5).

I.3 Spectroscopic Details

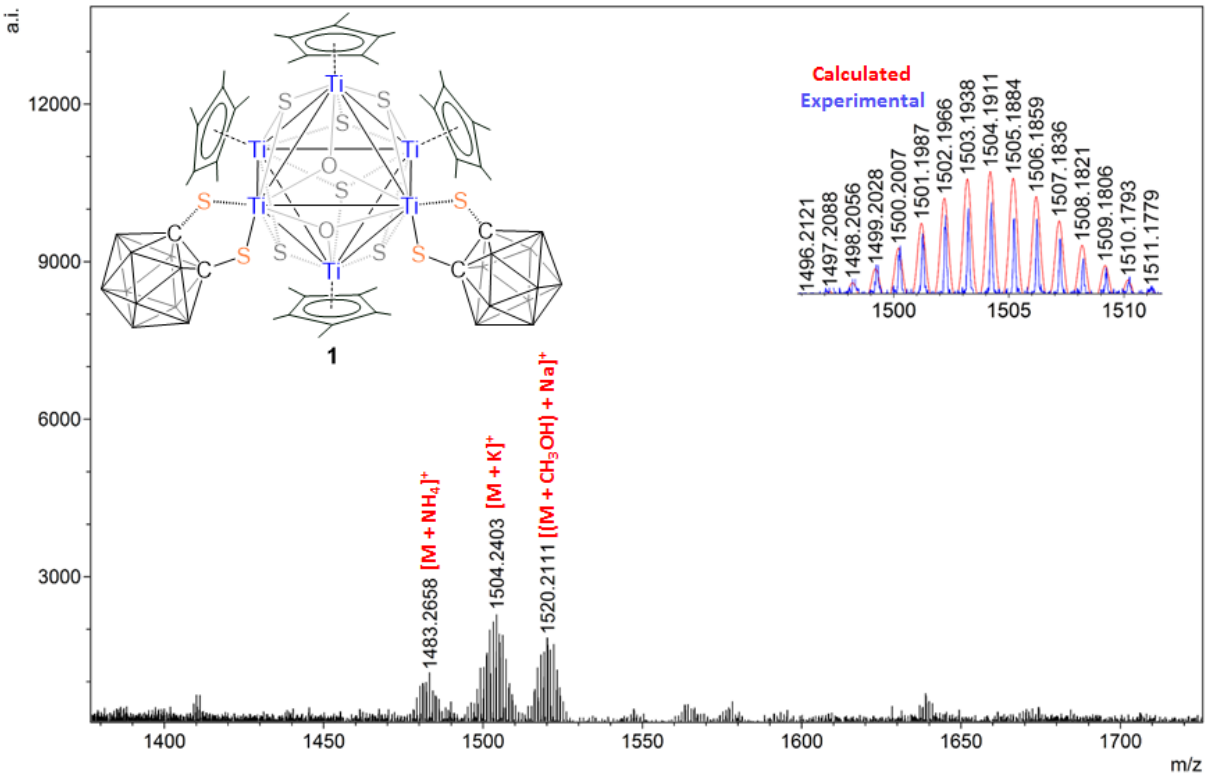

Figure S7. ESI-MS spectrum of **1**.

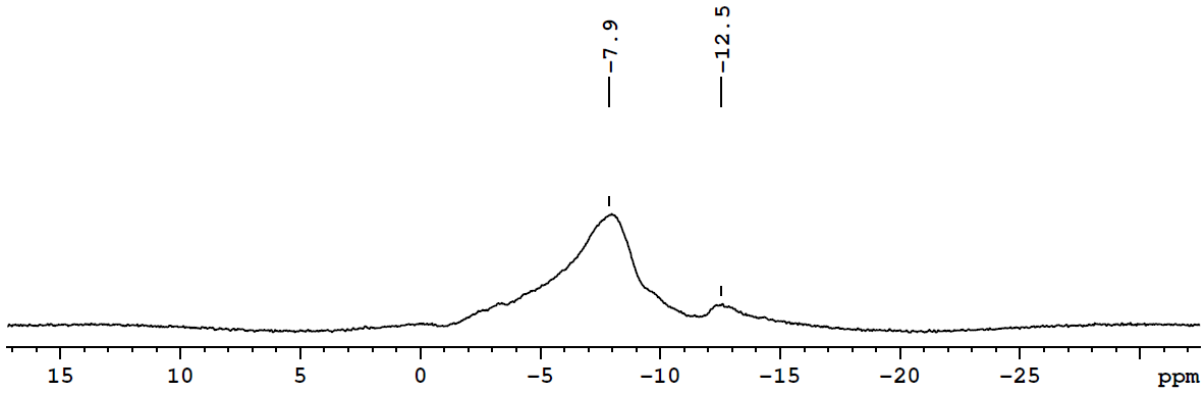

Figure S8. $^{11}B\{^{1}H\}$ NMR spectrum of **1** in $CDCl_3$. $^{11}B\{^{1}H\}$ NMR spectra were processed with a backward linear prediction algorithm to eliminate the broad ^{11}B background signal of the NMR tube.[6]

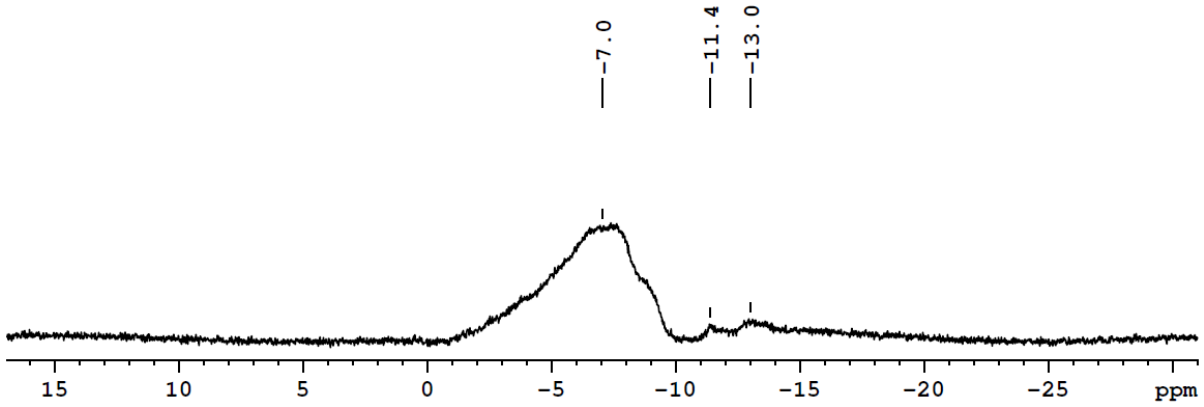

Figure S9. ^{11}B NMR spectrum of **1** in $CDCl_3$. $^{11}B\{^{1}H\}$ NMR spectra were processed with a backward linear prediction algorithm to eliminate the broad ^{11}B background signal of the NMR tube.[6]

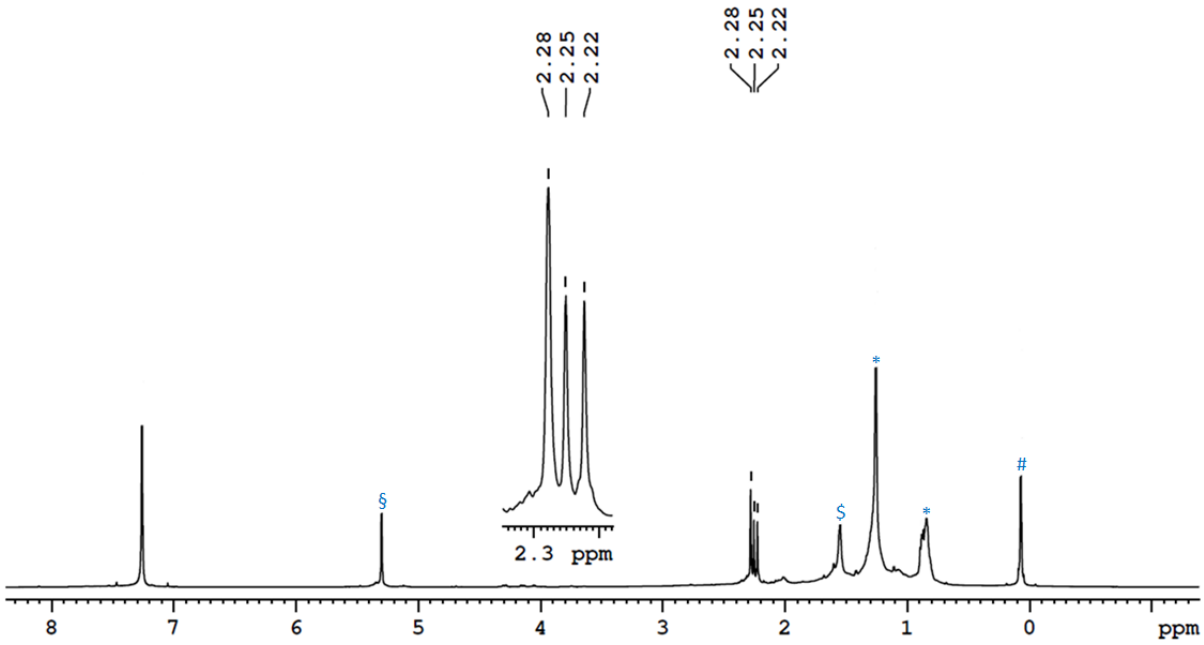

Figure S10. ^{1}H NMR spectrum of **1** in $CDCl_3$ (§Dichloromethane, $$H_2O$, *Grease, #Silicon grease).

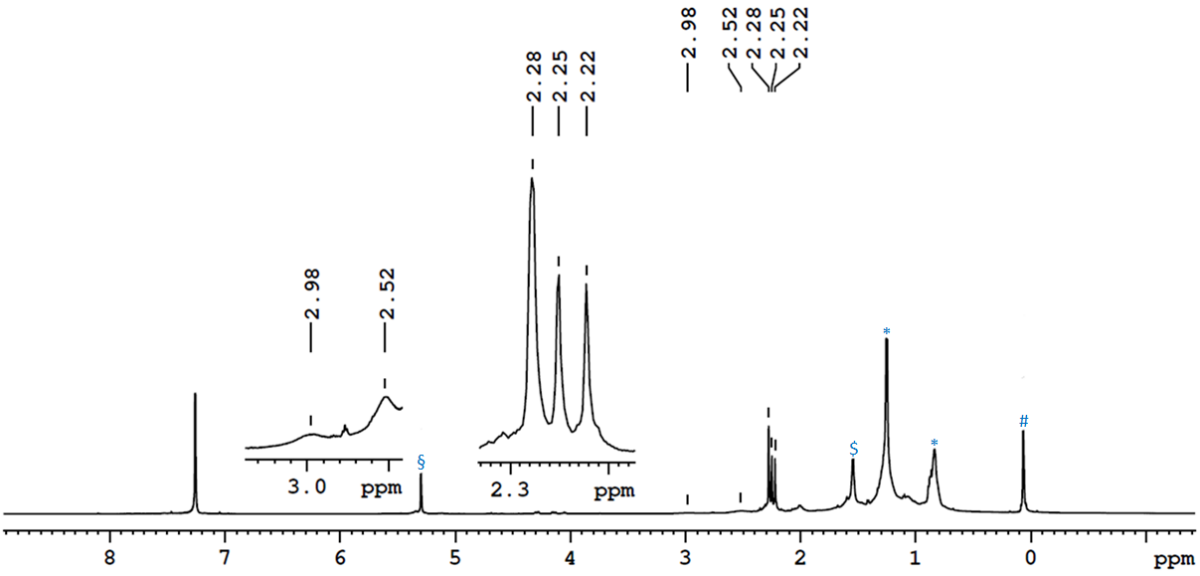

Figure S11. $^{1}H\{^{11}B\}$ NMR spectrum of **1** in $CDCl_3$ (§Dichloromethane, $$H_2O$, *Grease, #Silicon grease).

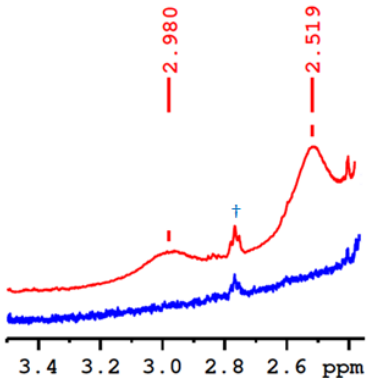

Figure S12. Stacked ^{1}H (bottom) and $^{1}H\{^{11}B\}$ NMR (top) spectra of **1** in $CDCl_3$ (†Inseparable impurity).

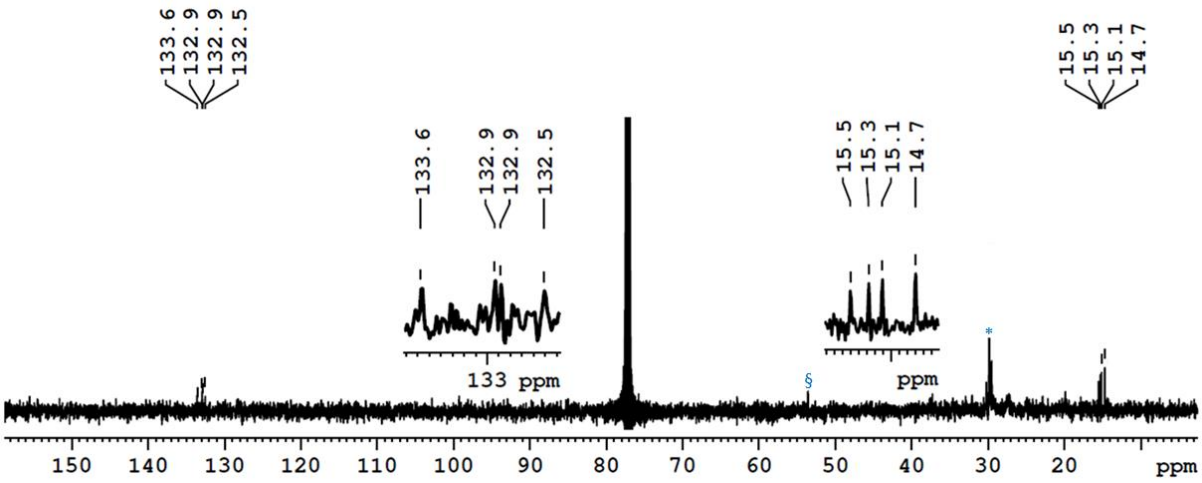

Figure S13. $^{13}C\{^{1}H\}$ NMR spectrum of **1** in $CDCl_3$ (§Dichloromethane, *Grease).

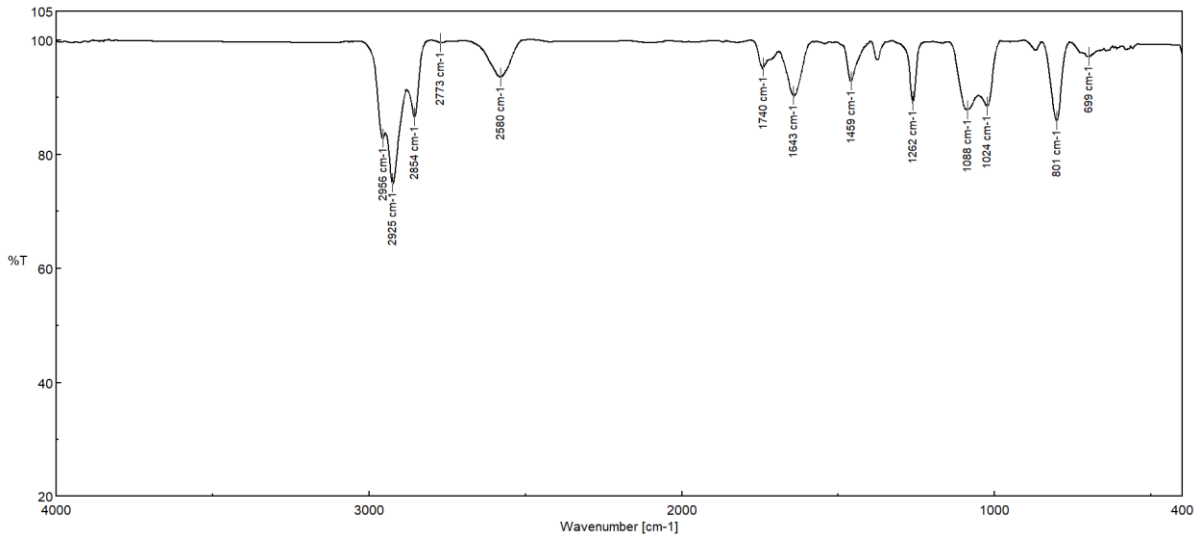

Figure S14. IR spectrum of **1**.

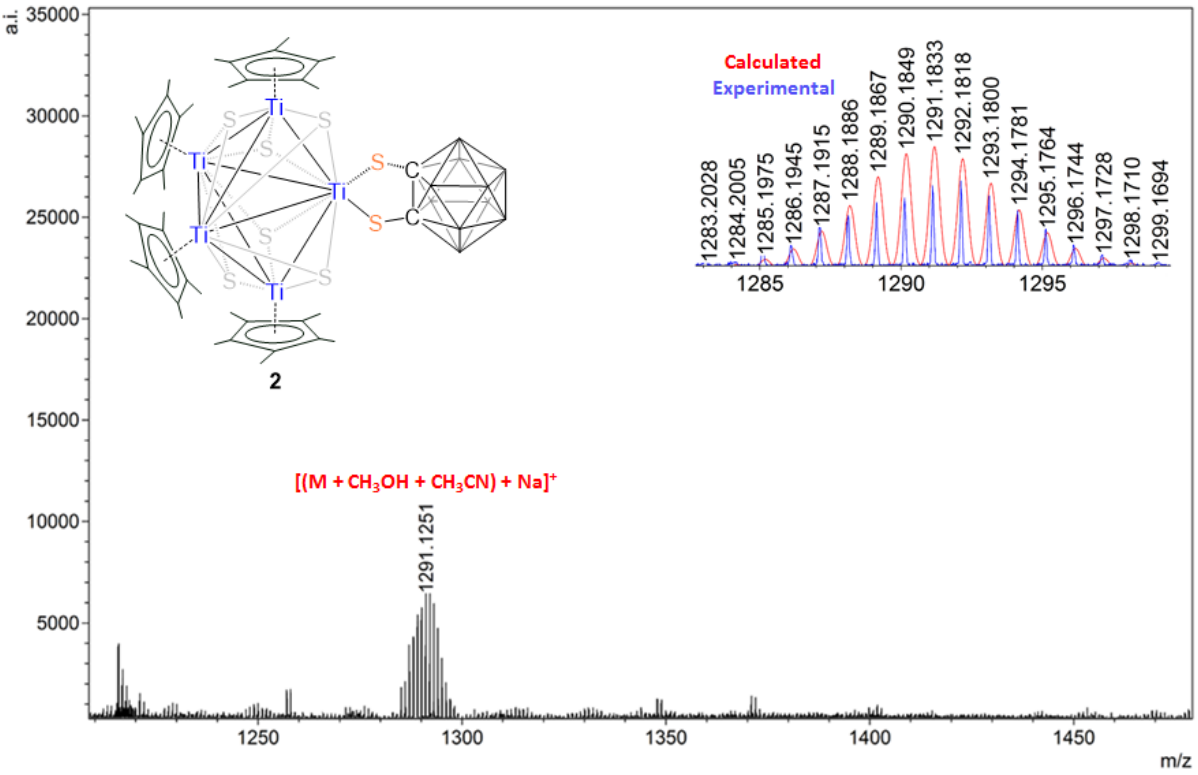

Figure S15. ESI-MS spectrum of **2**.

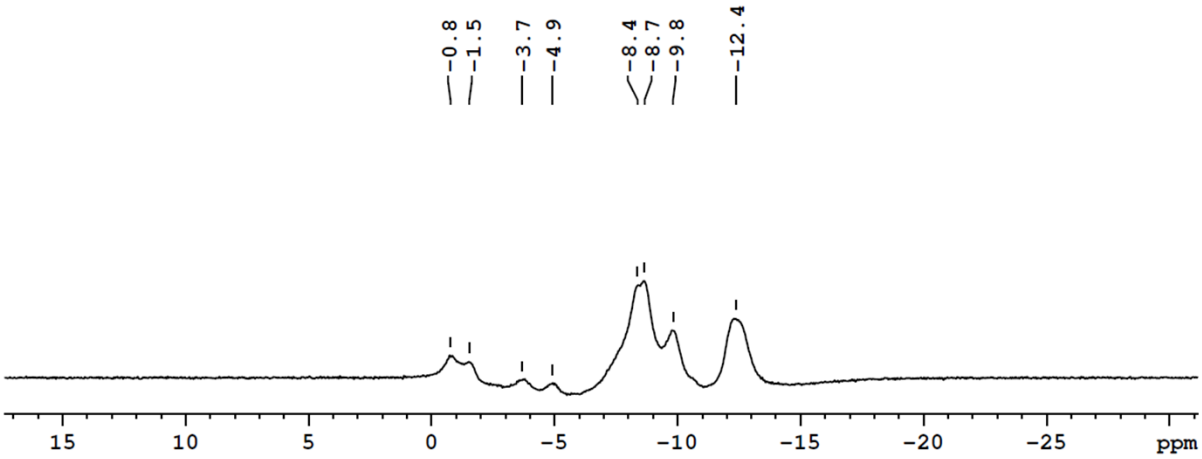

Figure S16. $^{11}B\{^{1}H\}$ NMR spectrum of **2** in $CDCl_3$. $^{11}B\{^{1}H\}$ NMR spectra were processed with a backward linear prediction algorithm to eliminate the broad ^{11}B background signal of the NMR tube.[6]

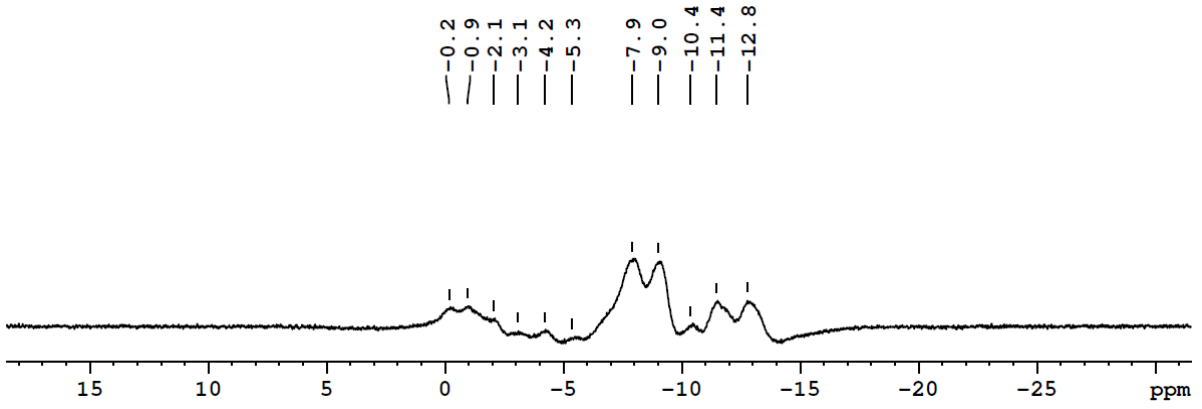

Figure S17. ^{11}B NMR spectrum of **2** in $CDCl_3$. $^{11}B\{^{1}H\}$ NMR spectra were processed with a backward linear prediction algorithm to eliminate the broad ^{11}B background signal of the NMR tube.[6]

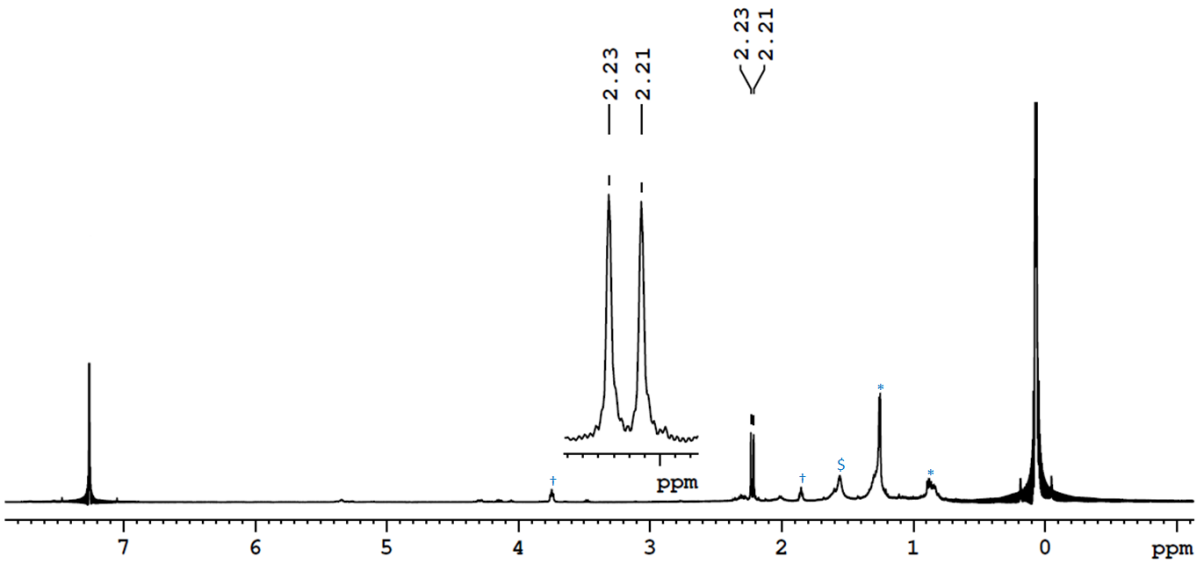

Figure S18. ^{1}H NMR spectrum of **2** in $CDCl_3$ (†Inseparable impurity, $\$H_2O$, *Grease, #Silicon grease).

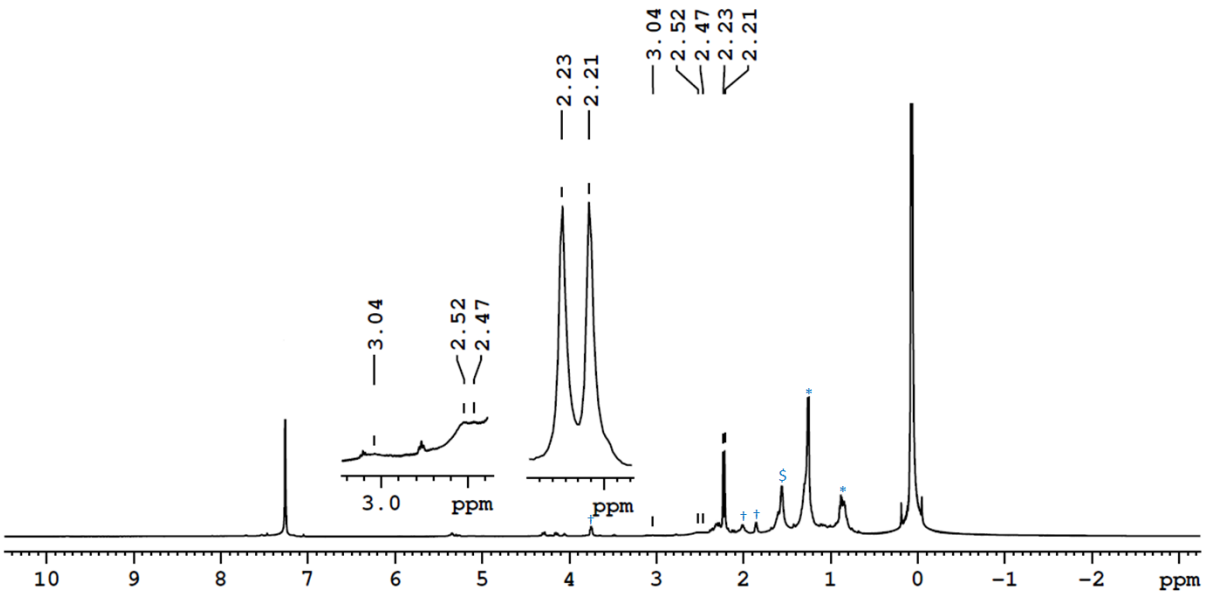

Figure S19. $^{1}H\{^{11}B\}$ NMR spectrum of **2** in $CDCl_3$ (†Inseparable impurity, $\$H_2O$, *Grease, #Silicon grease).

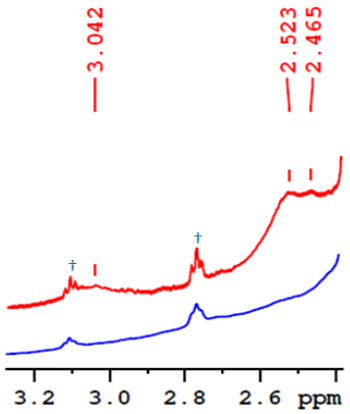

Figure S20. Stacked ^{1}H (bottom) and $^{1}H\{^{11}B\}$ NMR (top) spectra of **2** in $CDCl_3$ (†Inseparable impurity).

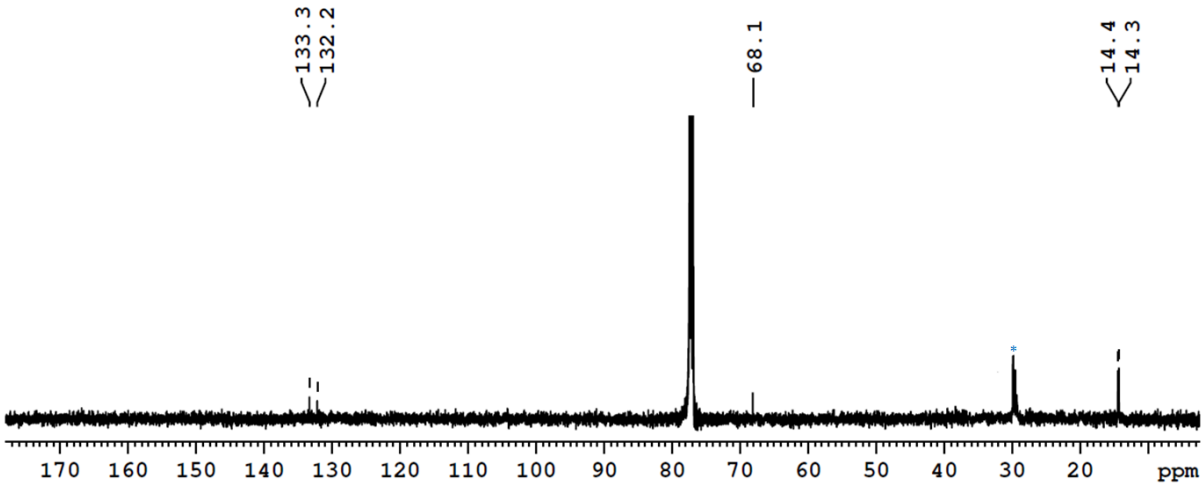

Figure S21. $^{13}C\{^{1}H\}$ NMR spectrum of **2** in $CDCl_3$ (*Grease).

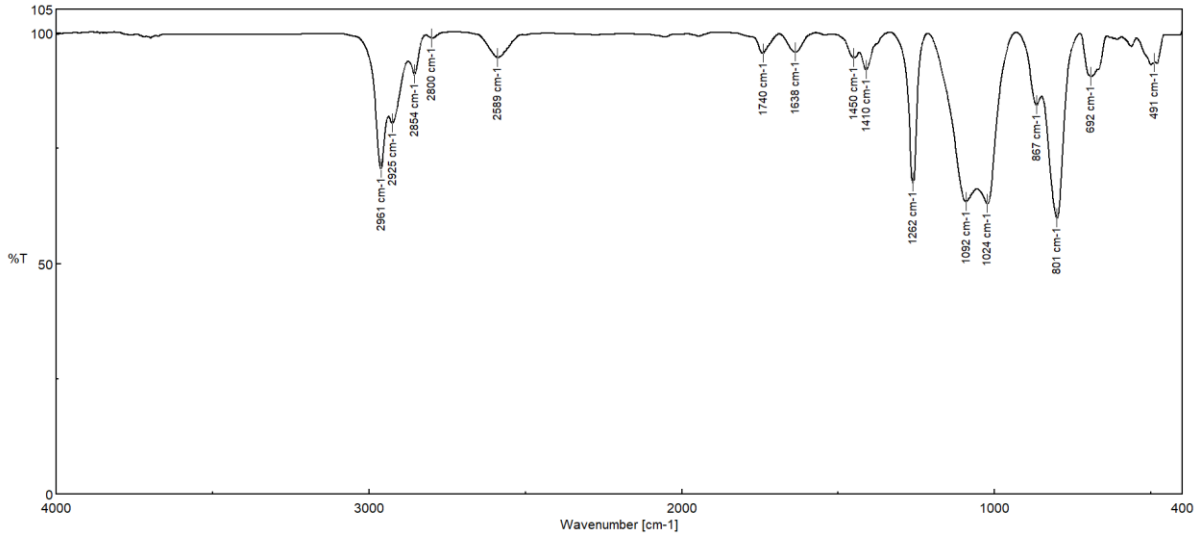

Figure S22. IR spectrum of **2**.

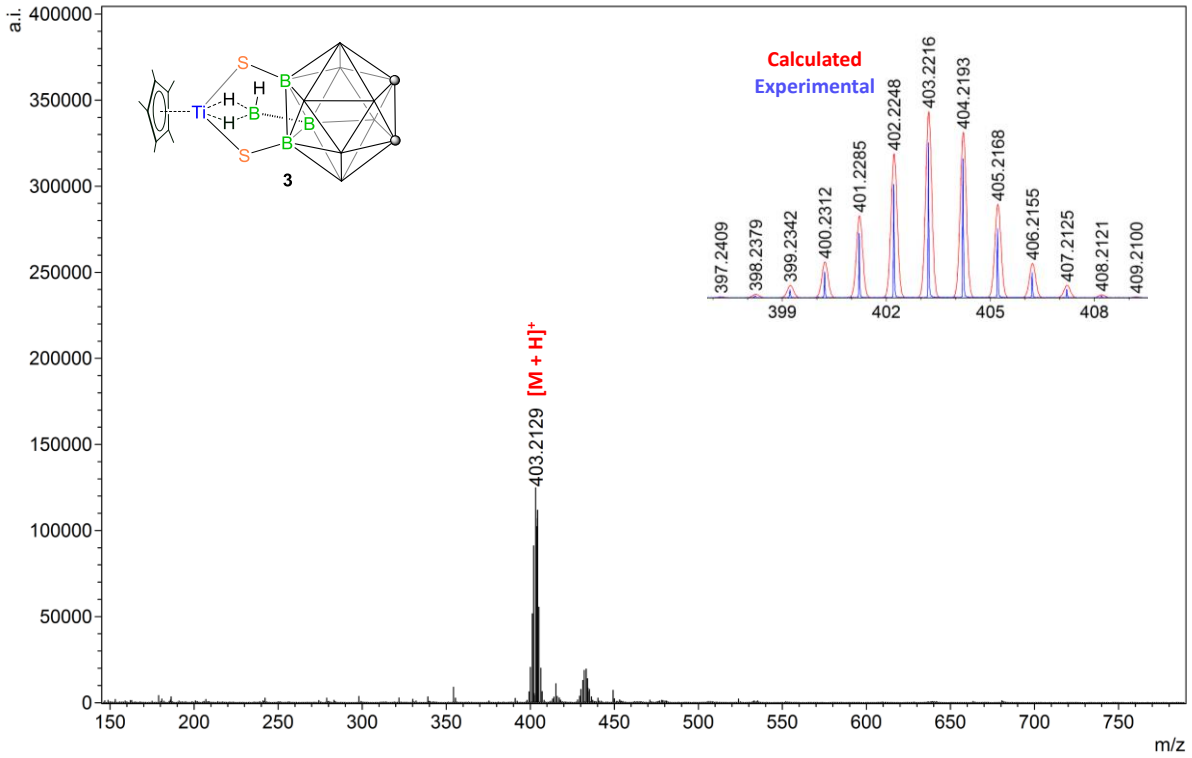

Figure S23. ESI-MS spectrum of **3**.

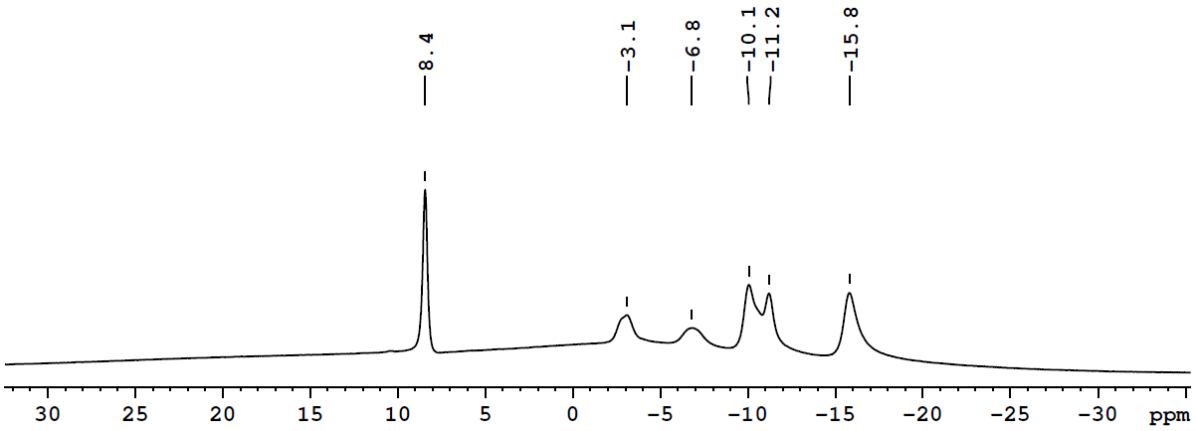

Figure S24. $^{11}B\{^{1}H\}$ NMR spectrum of **3** in $CDCl_3$.

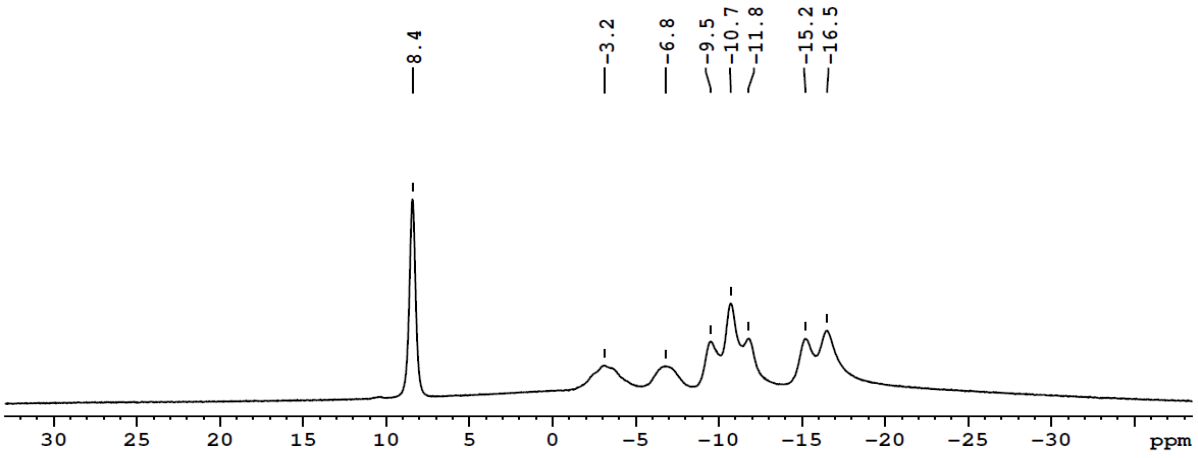

Figure S25. ^{11}B NMR spectrum of **3** in $CDCl_3$.

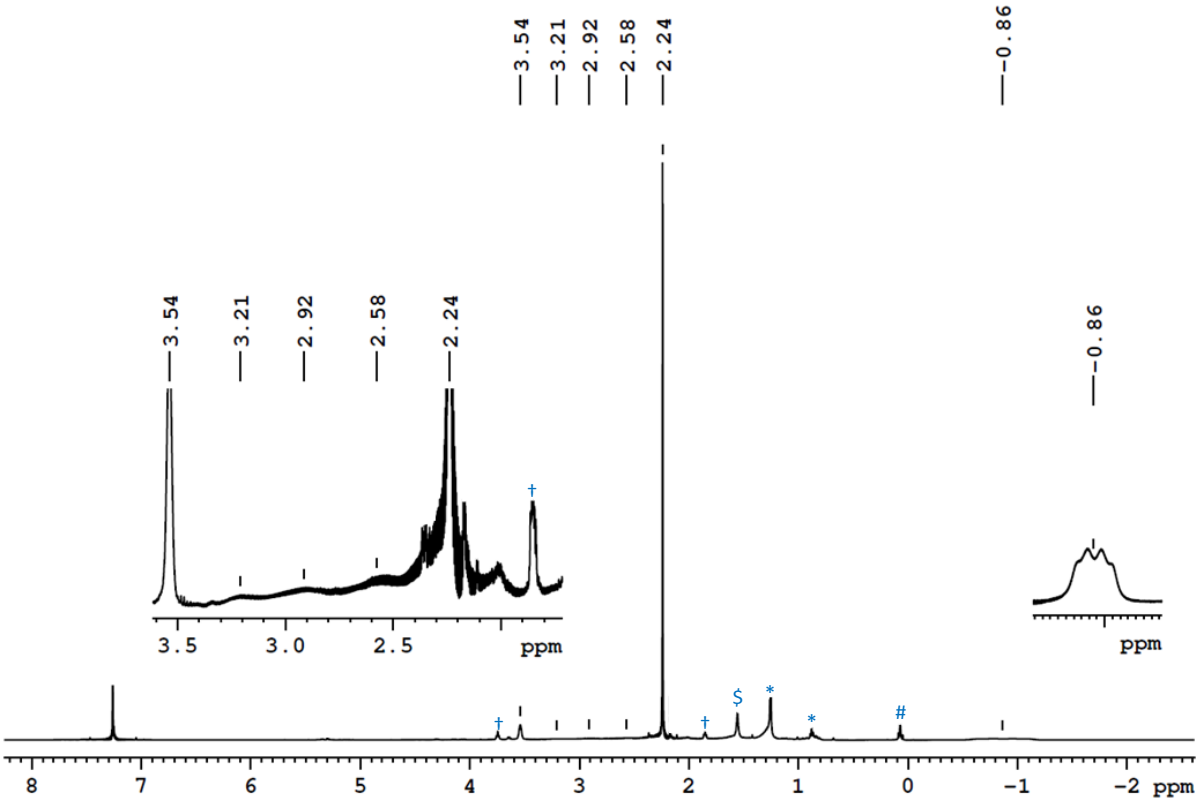

Figure S26. ^{1}H NMR spectrum of **3** in $CDCl_3$ (†Inseparable impurity, $$H_2O$, *Grease, #Silicon grease).

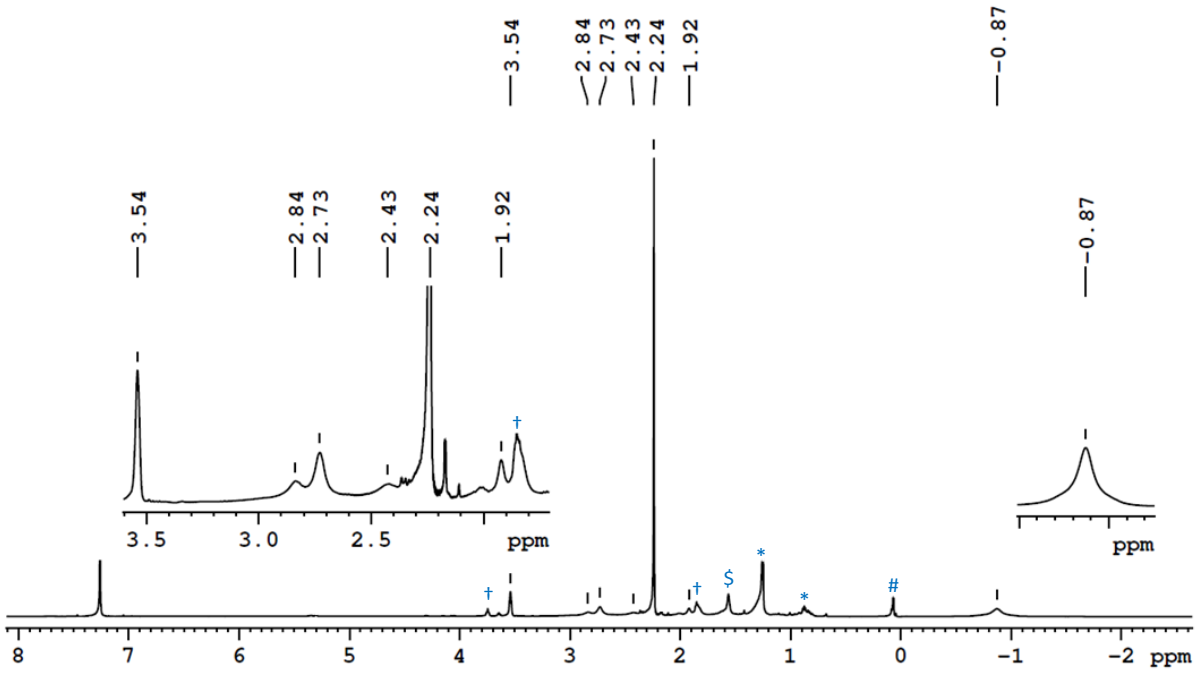

Figure S27. ^{1}H{^{11}B} NMR spectrum of **3** in $CDCl_3$ (†Inseparable impurity, $$H_2O$, *Grease, #Silicon grease).

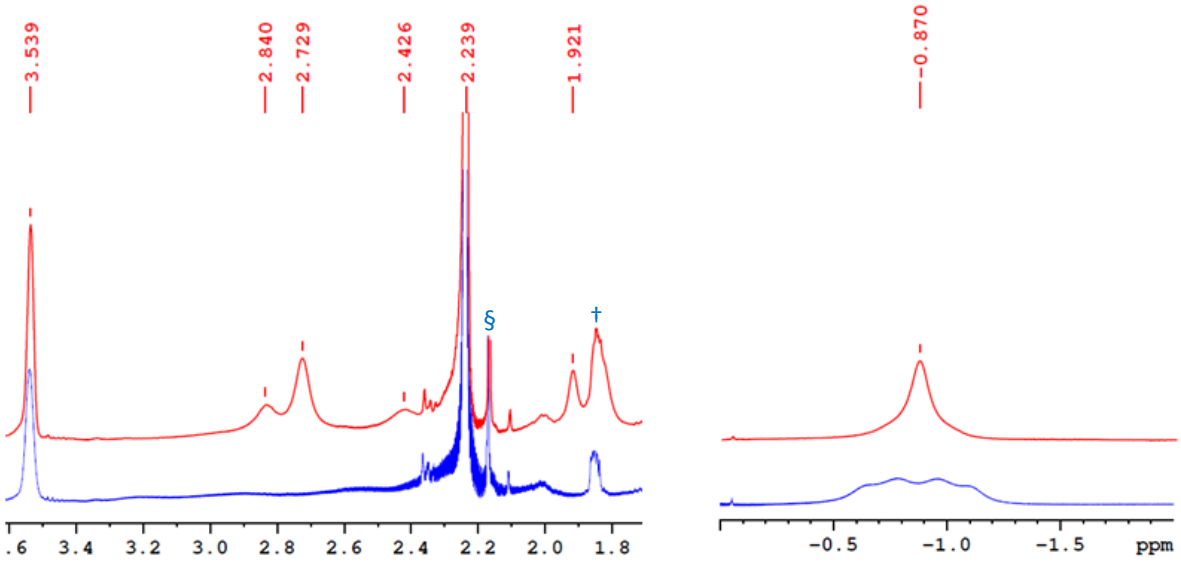

Figure S28. Stacked ^{1}H (bottom) and $^{1}H\{^{11}B\}$ NMR (top) spectra of **3** in $CDCl_3$ (§Acetone, †Inseparable impurity).

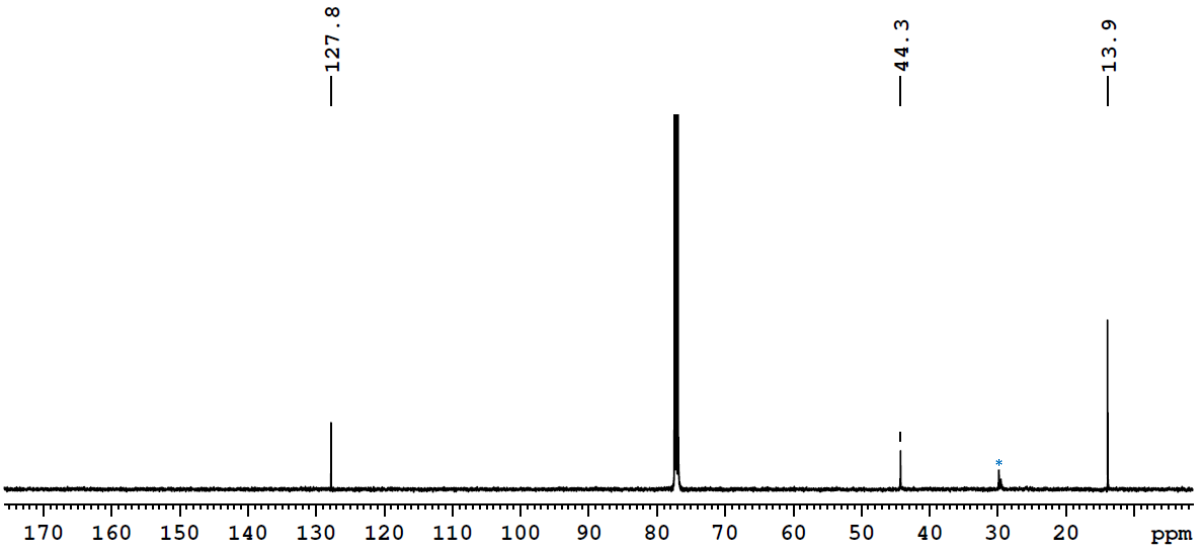

Figure S29. $^{13}C\{^{1}H\}$ NMR spectrum of **3** in $CDCl_3$ (*Grease).

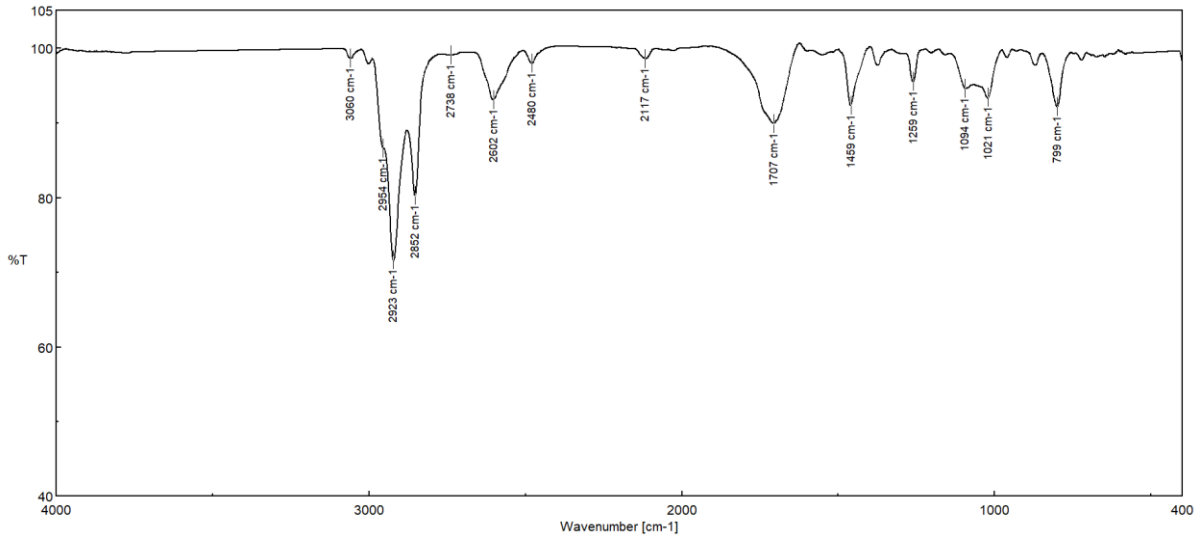

Figure S30. IR spectrum of **3**.

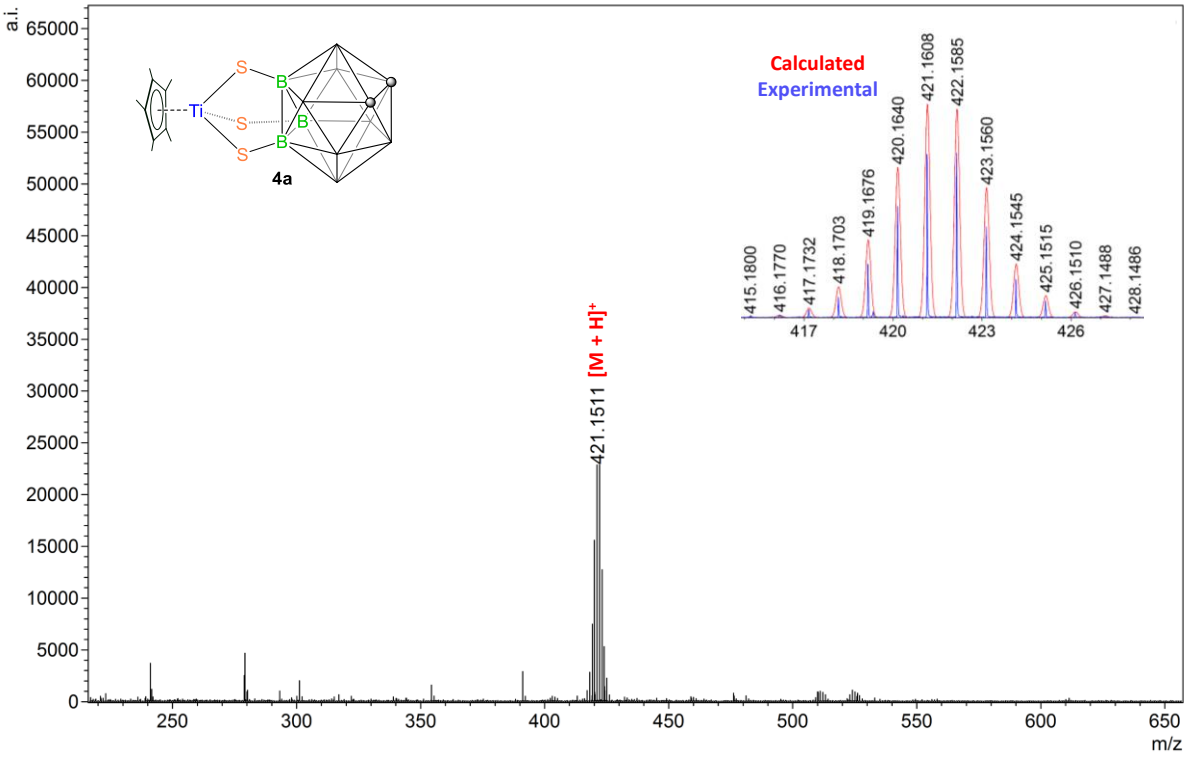

Figure S31. ESI-MS spectrum of **4a**.

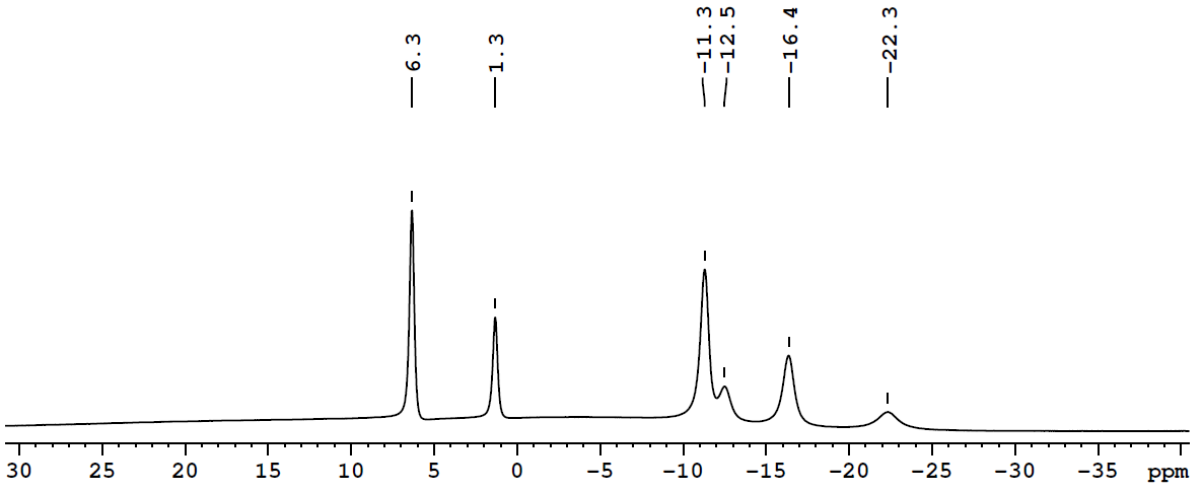

Figure S32. $^{11}B\{^{1}H\}$ NMR spectrum of **4a** in $CDCl_3$.

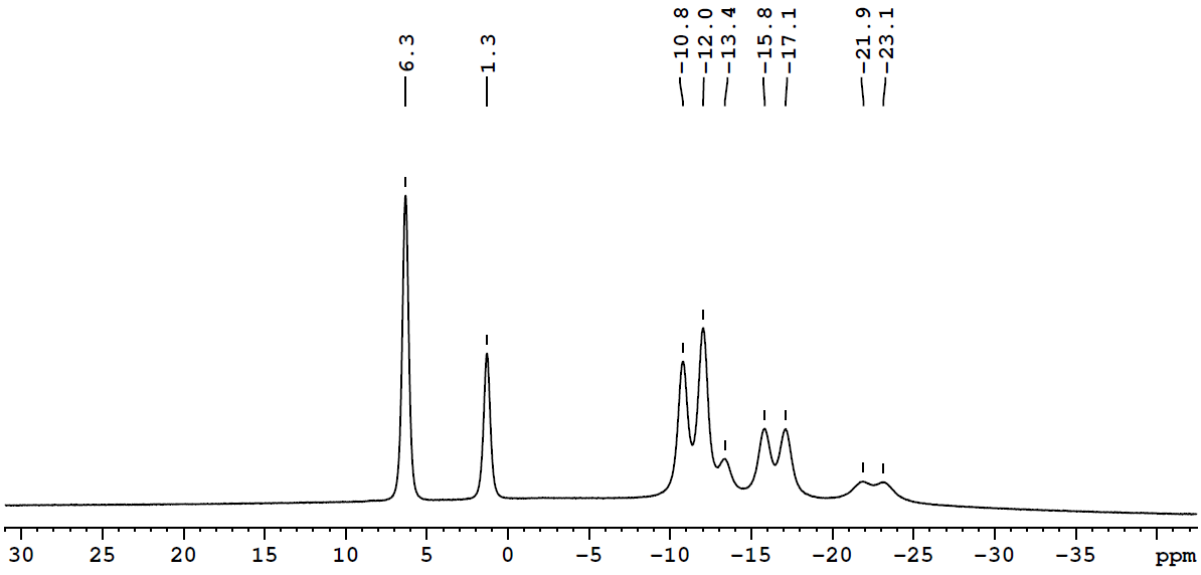

Figure S33. ^{11}B NMR spectrum of **4a** in $CDCl_3$.

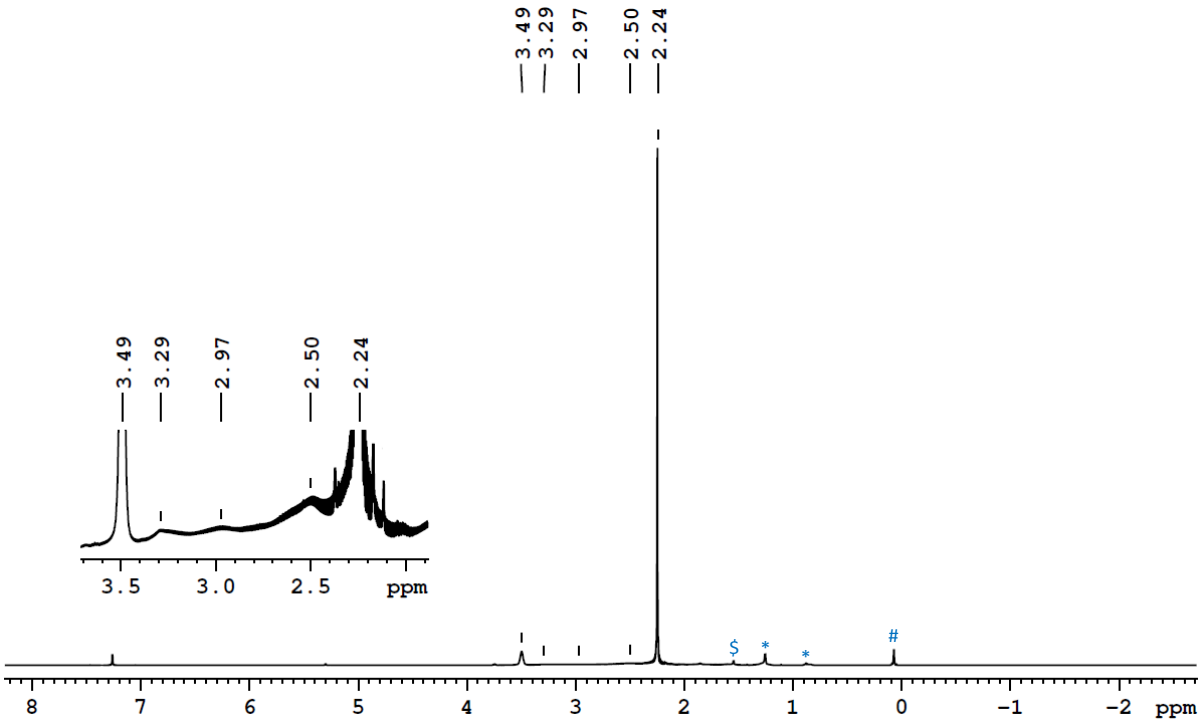

Figure S34. ^{1}H NMR spectrum of **4a** in $CDCl_3$ ($H_2O, *Grease, #Silicon grease).

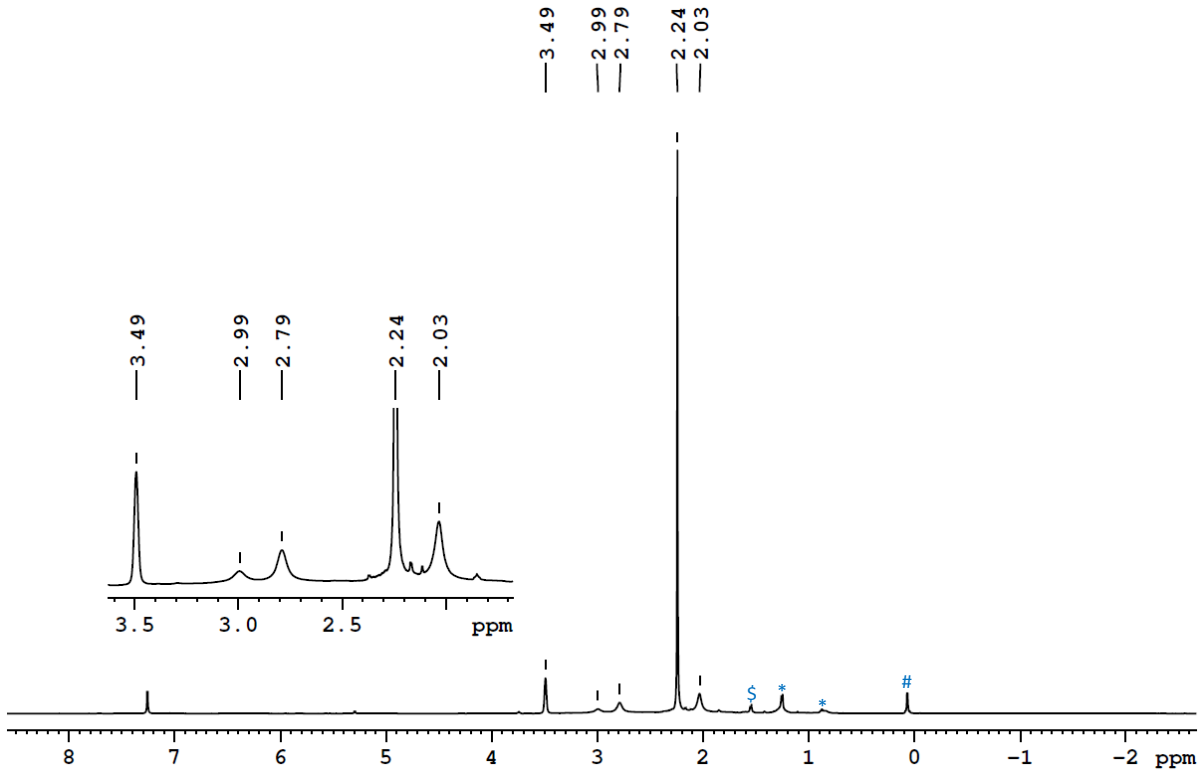

Figure S35. $^{1}H\{^{11}B\}$ NMR spectrum of **4a** in $CDCl_3$ ($H_2O, *Grease, #Silicon grease).

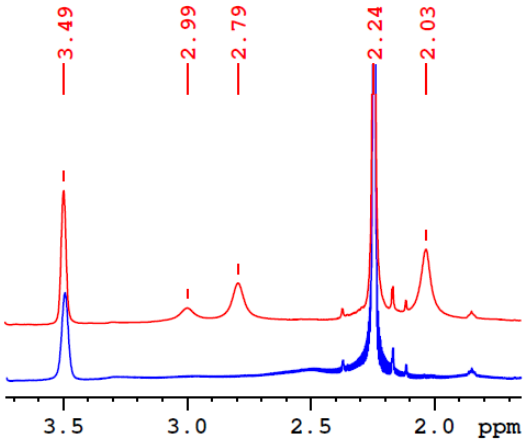

Figure S36. Stacked ^{1}H (bottom) and $^{1}H\{^{11}B\}$ NMR (top) spectra of **4a** in $CDCl_3$.

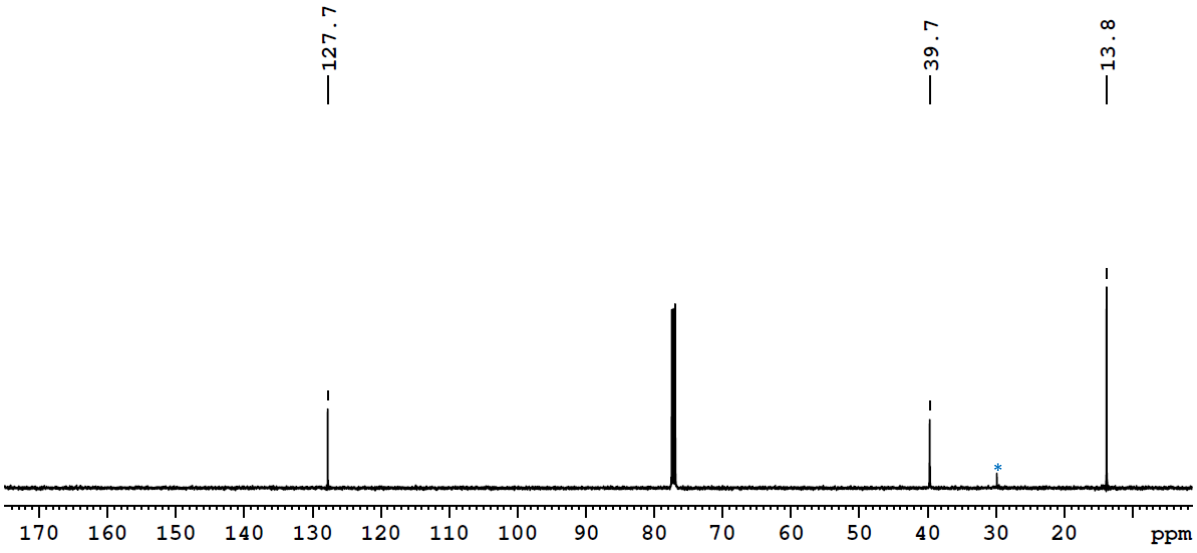

Figure S37. $^{13}C\{^{1}H\}$ NMR spectrum of **4a** in $CDCl_3$ (*Grease).

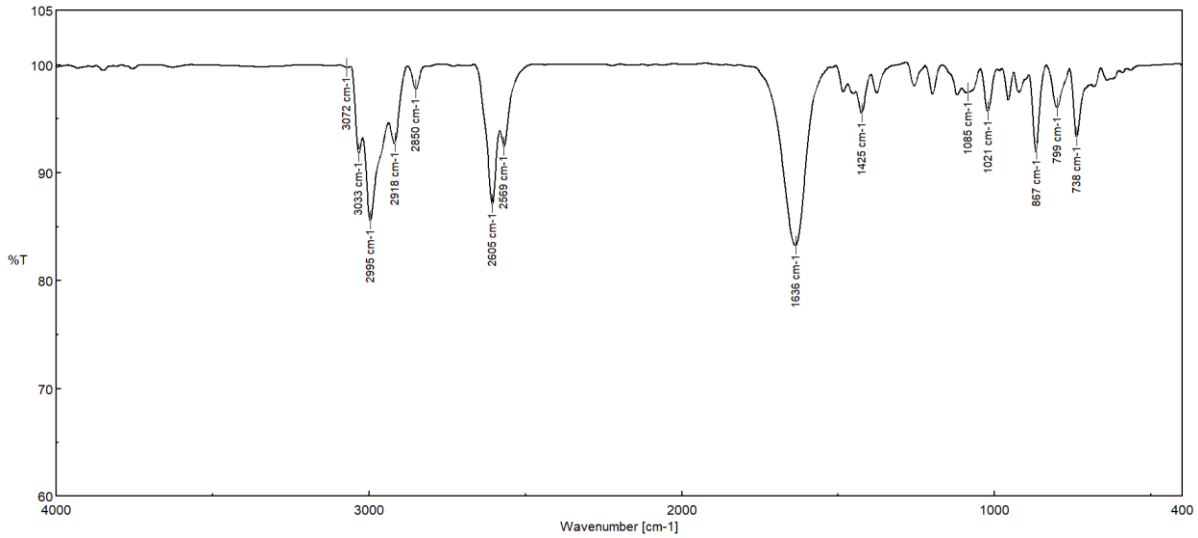

Figure S38. IR spectrum of **4a**.

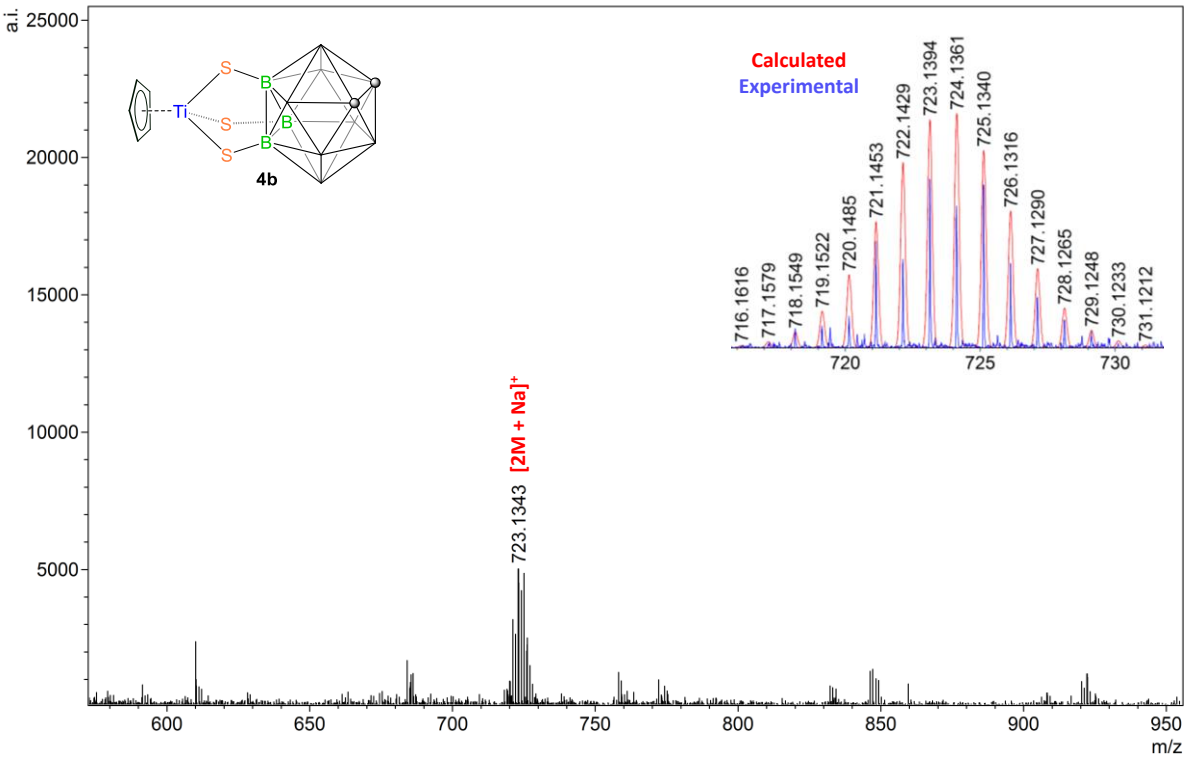

Figure S39. ESI-MS spectrum of **4b**.

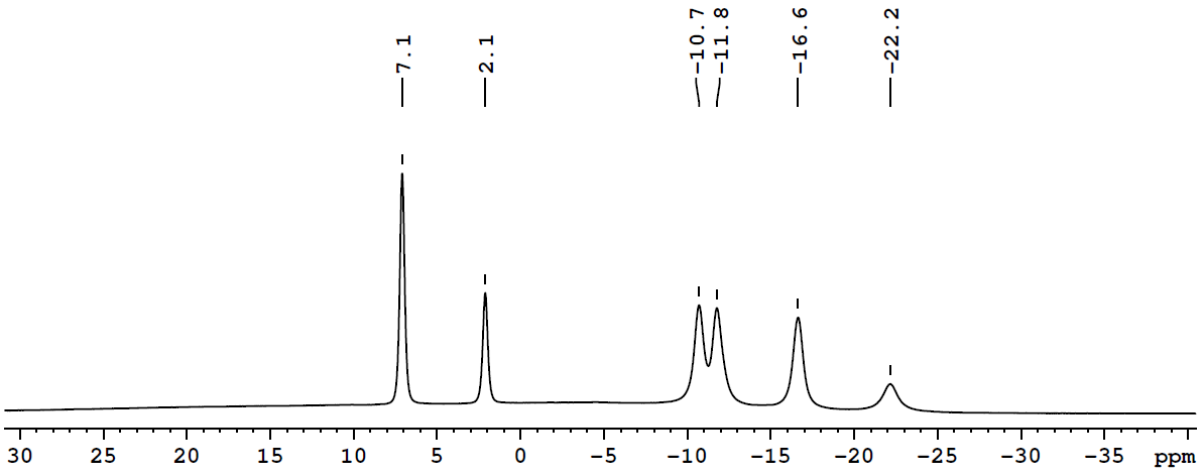

Figure S40. $^{11}B\{^{1}H\}$ NMR spectrum of **4b** in $CDCl_3$.

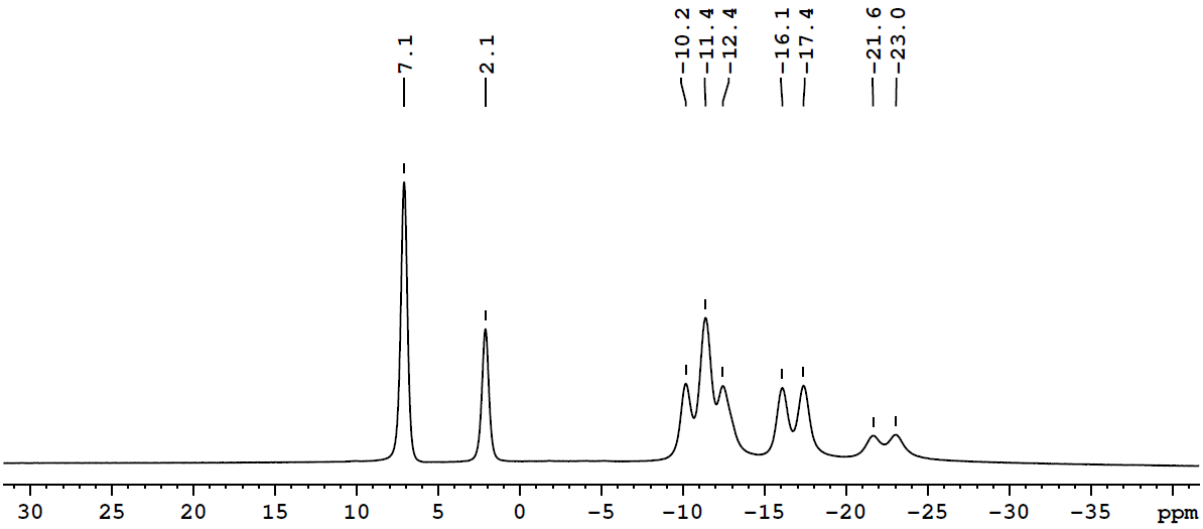

Figure S41. ^{11}B NMR spectrum of **4b** in $CDCl_3$.

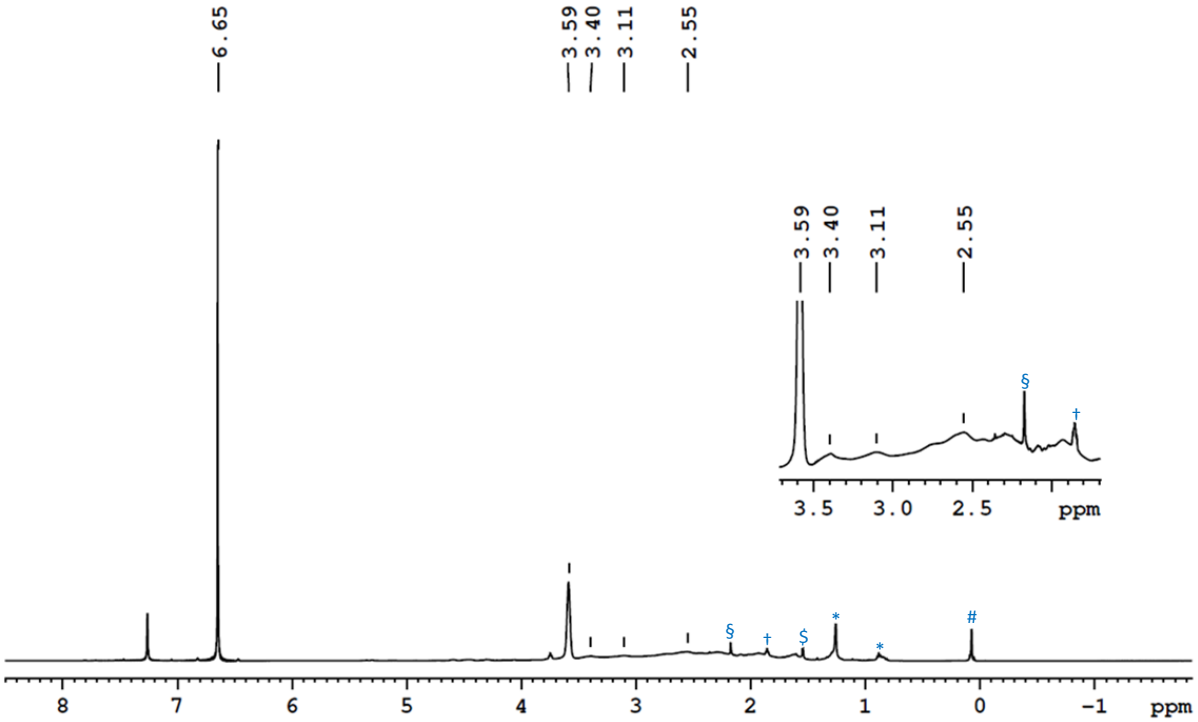

Figure S42. ^{1}H NMR spectrum of **4b** in $CDCl_3$ (§Acetone,†Inseparable impurity, $$H_2O$, *Grease, #Silicon grease).

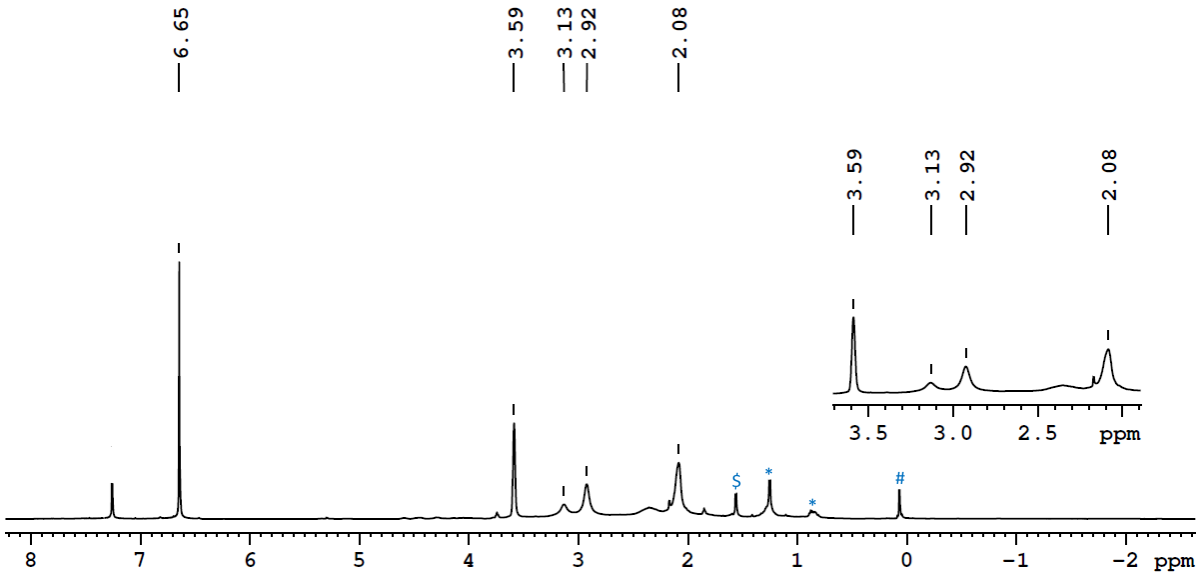

Figure S43. $^{1}H\{^{11}B\}$ NMR spectrum of **4b** in $CDCl_3$ ($$H_2O$, *Grease, #Silicon grease).

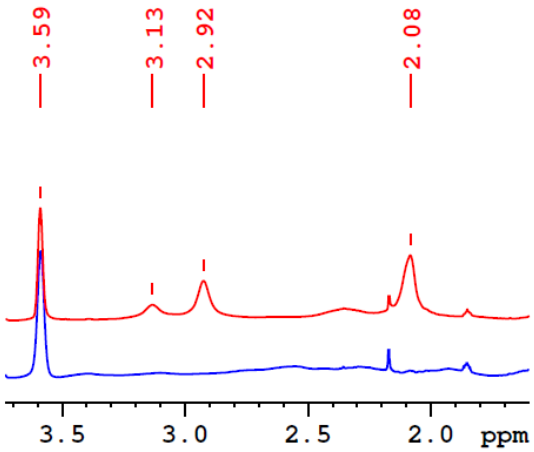

Figure S44. Stacked ^{1}H (bottom) and $^{1}H\{^{11}B\}$ NMR (top) spectra of **4b** in $CDCl_3$.

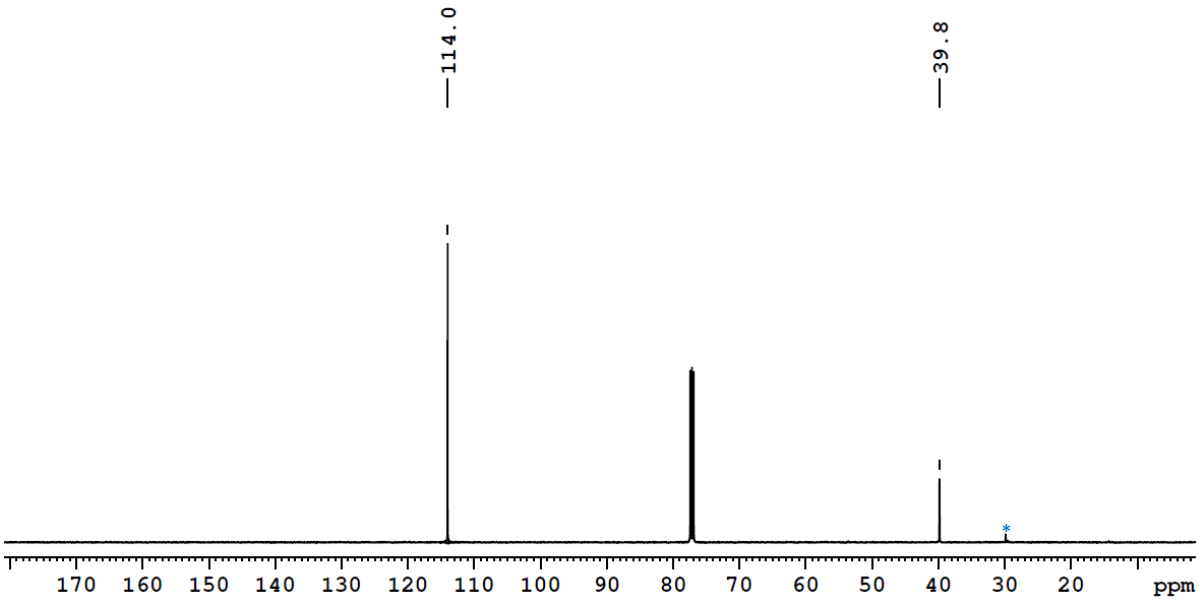

Figure S45. $^{13}C\{^{1}H\}$ NMR spectrum of **4b** in $CDCl_3$ (*Grease).

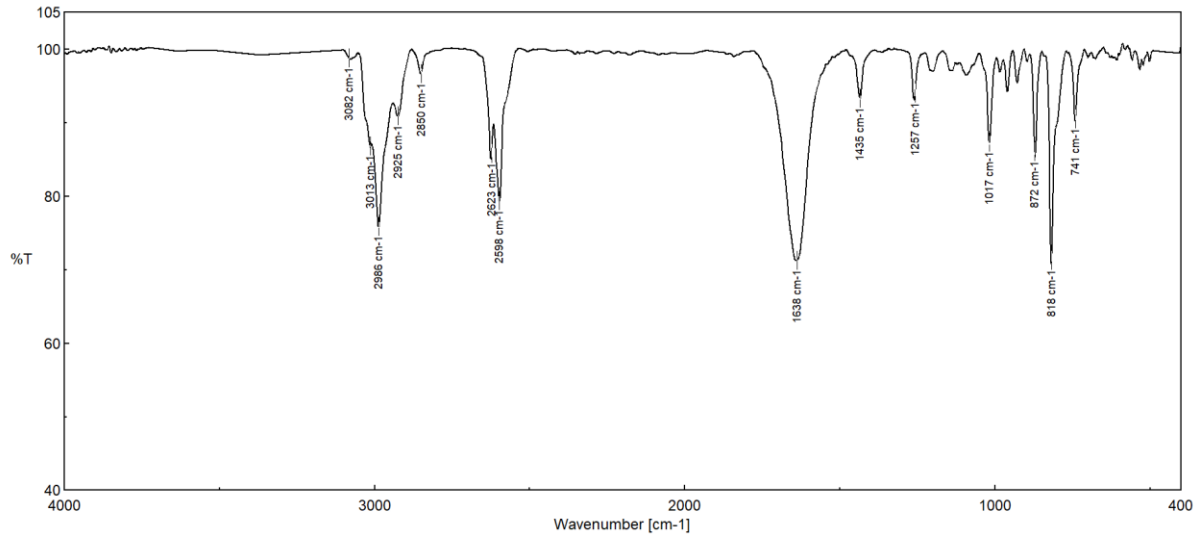

Figure S46. IR spectrum of **4b**.

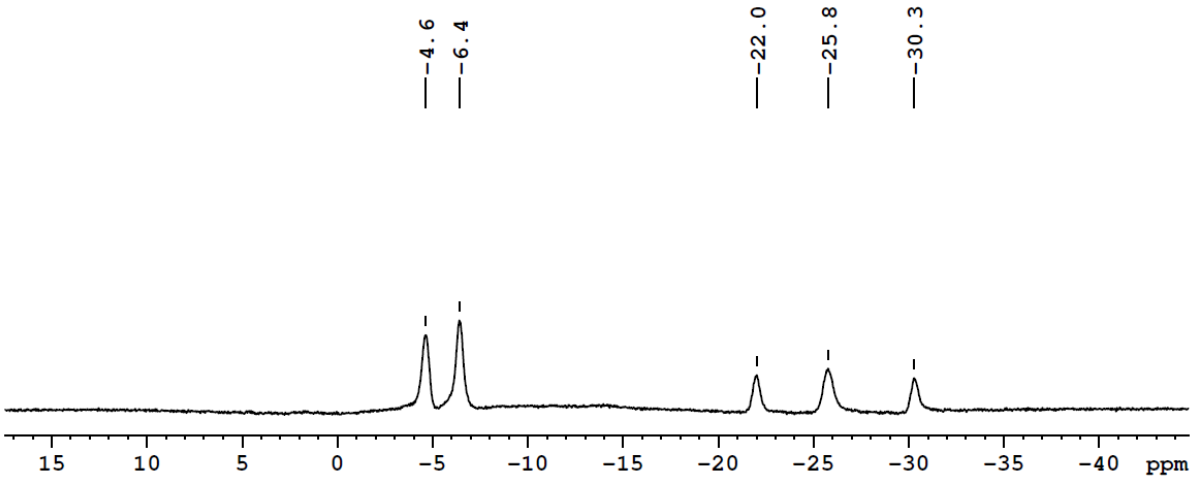

Figure S47. $^{11}B\{^{1}H\}$ NMR spectrum of **5** in $CDCl_3$.

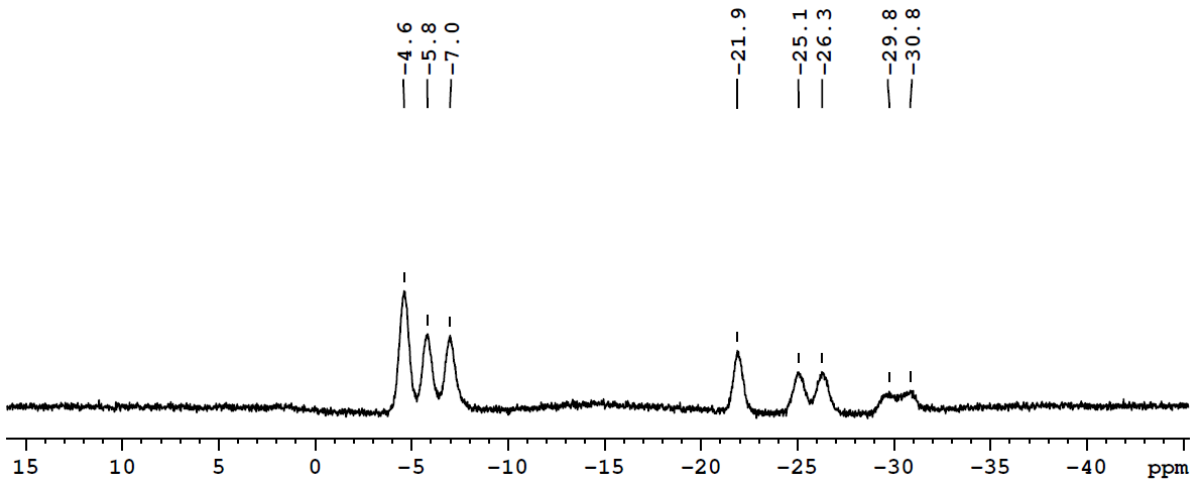

Figure S48. ^{11}B NMR spectrum of **5** in $CDCl_3$.

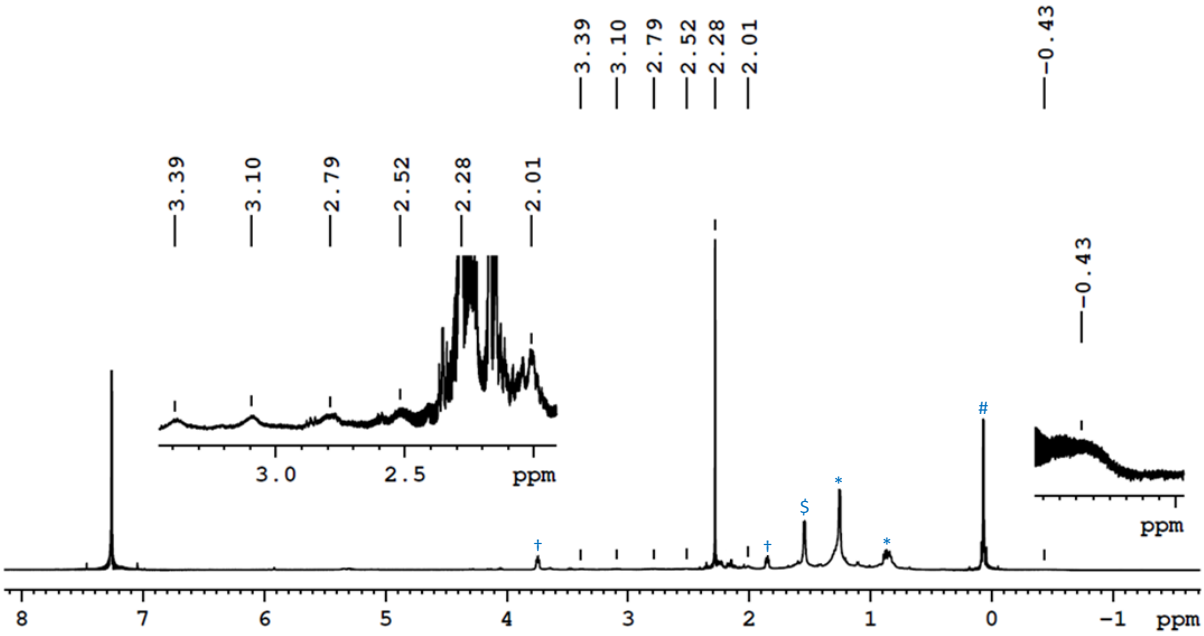

Figure S49. ^{1}H NMR spectrum of **5** in $CDCl_3$ (†Inseparable impurity, $$H_2O$, *Grease, #Silicon grease).

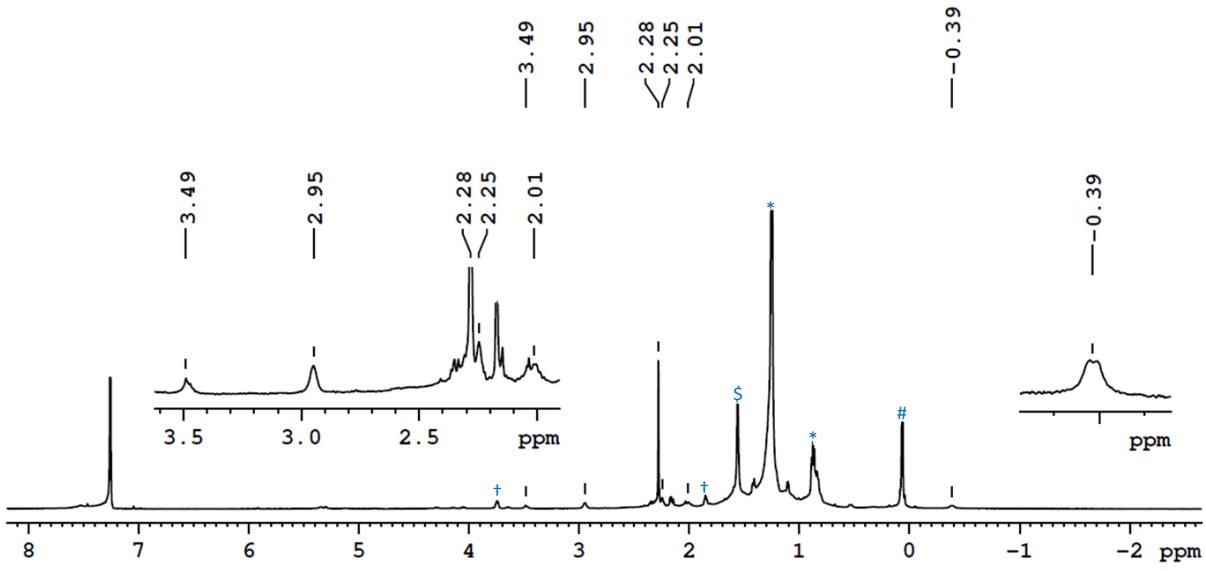

Figure S50. ^{1}H{^{11}B} NMR spectrum of **5** in $CDCl_3$ (†Inseparable impurity, $$H_2O$, *Grease, #Silicon grease).

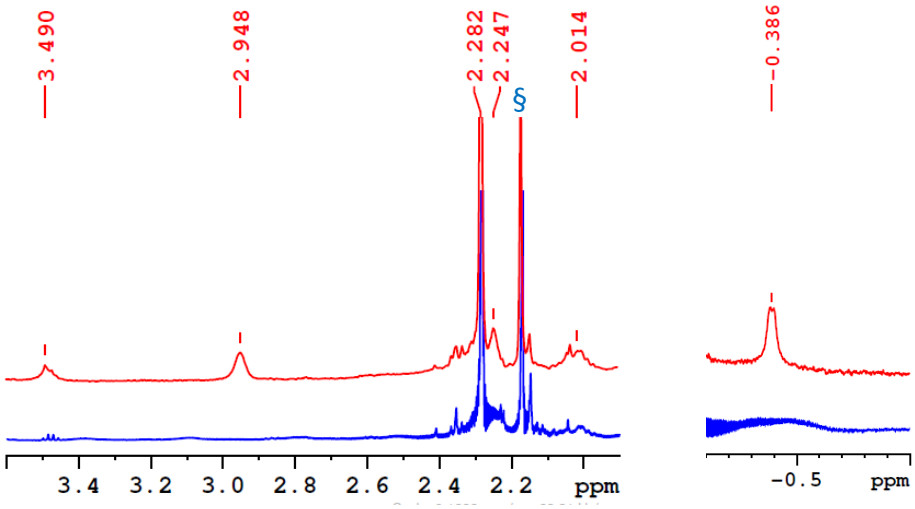

Figure S51. Stacked ^{1}H (bottom) and $^{1}H\{^{11}B\}$ NMR (top) spectra of **5** in $CDCl_3$ (§Acetone).

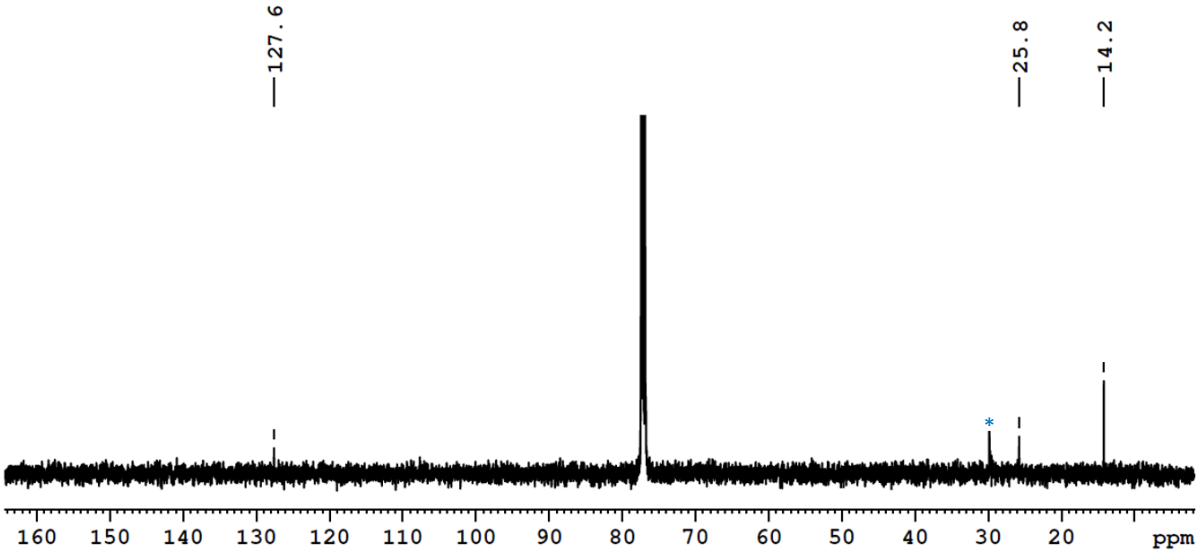

Figure S52. $^{13}C\{^{1}H\}$ NMR spectrum of **5** in $CDCl_3$ (*Grease).

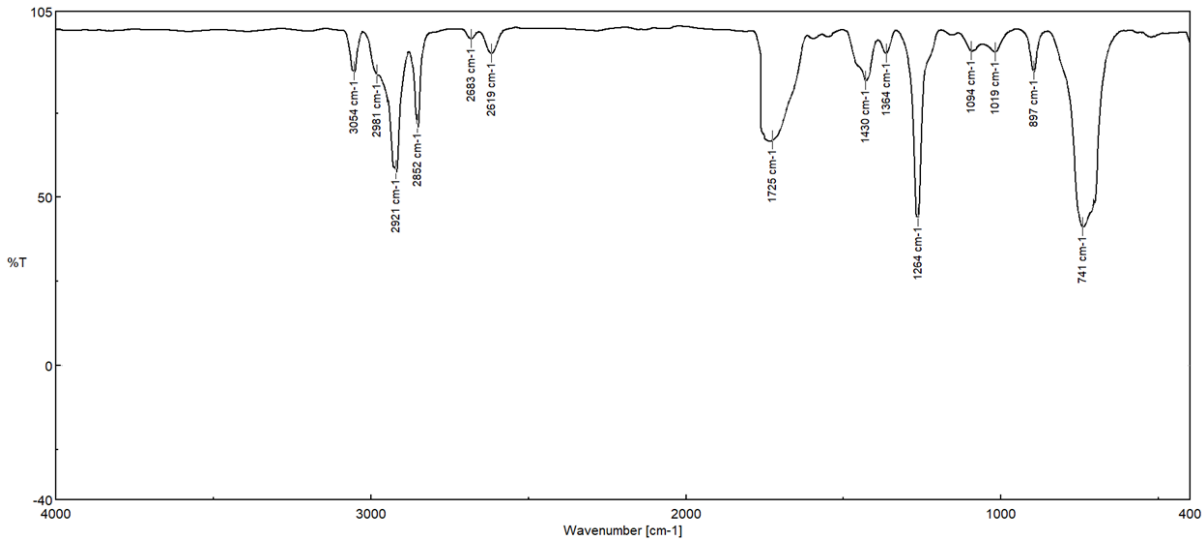

Figure S53. IR spectrum of **5**.

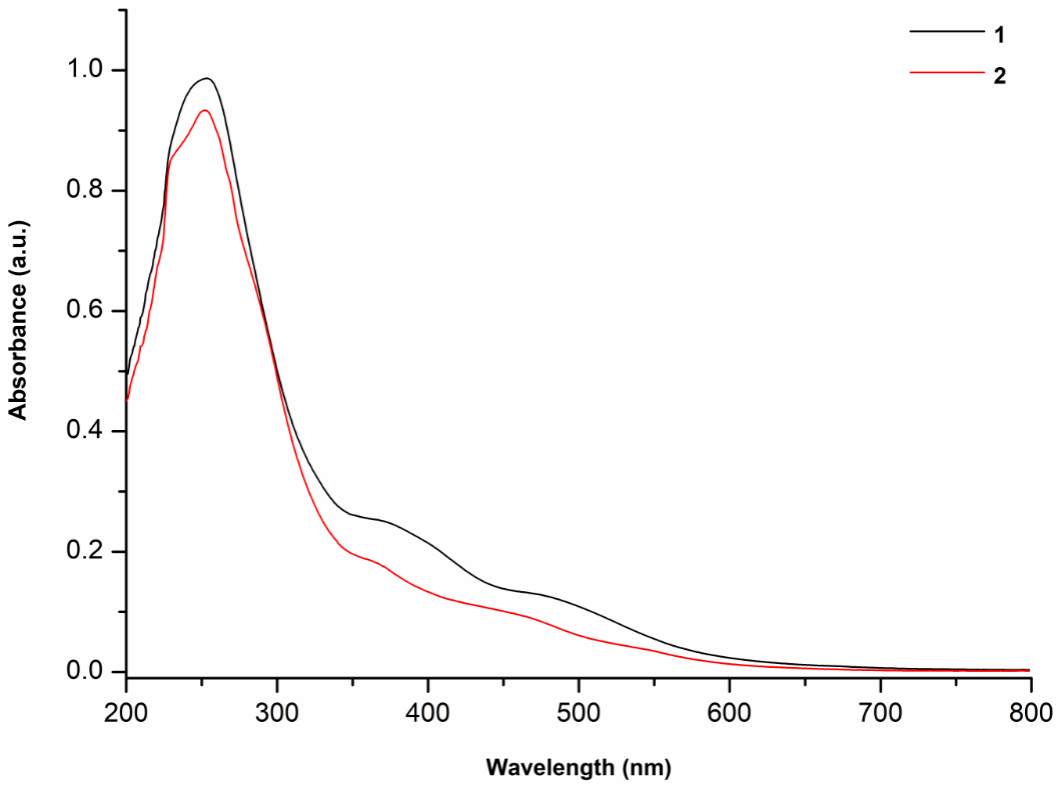

Figure S54. Combined UV-vis spectra of **1** and **2** in CH_2Cl_2.

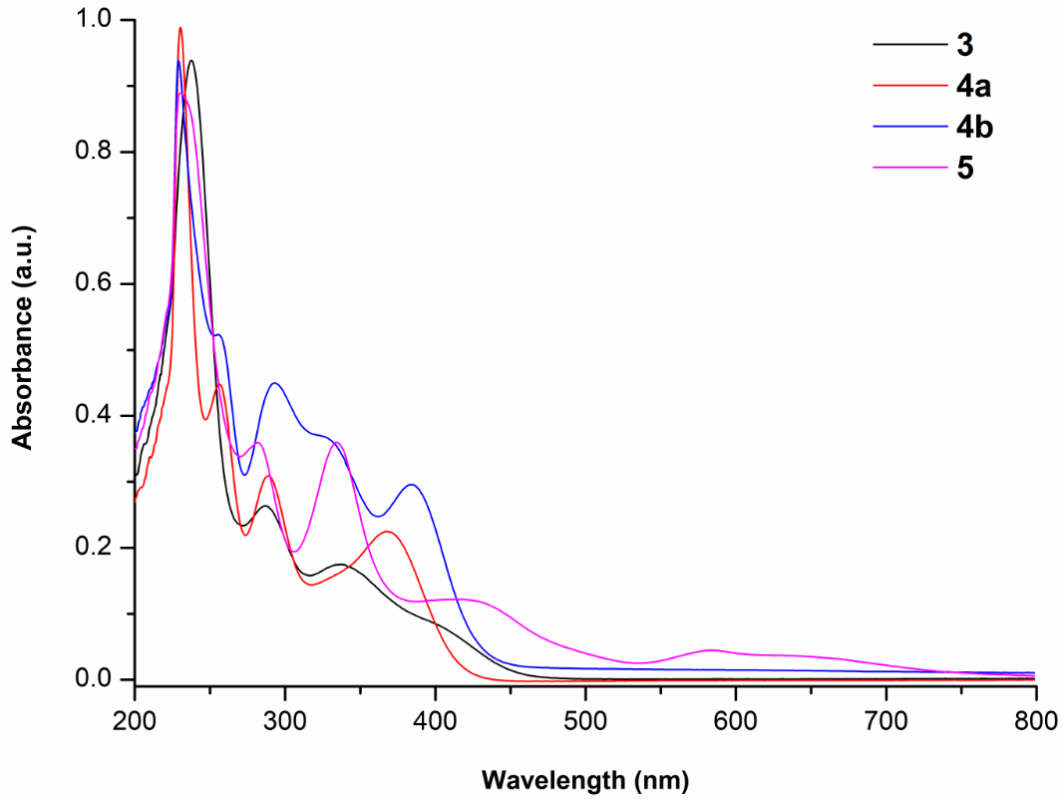

Figure S55. Combined UV-vis spectra of **3**-**5** in CH_2Cl_2.

I.4 *X-ray Analysis Details*

Suitable X-ray quality crystals of **1**-**5** were grown by slow diffusion of a hexane-dichloromethane solution at 5 ˚C. Crystal data of **1** and **2** were obtained and integrated using a Bruker V8 Venture diffractometer equipped with graphite monochromated MoKα (λ = 0.71073 Å) radiation at 300 K (for **1**) and 150 K (for **2**). Note that in **2**, all four Cp* ligands attached to the titanium centers, as well as both the C-S groups of the 1,2-dithiol-*o*-carborane ligand attached to Ti2 atom, exhibit disorder that was resolved into two positions. And crystal data of **3-5** were obtained and integrated using a Bruker APEX-II CCD diffractometer equipped with graphite monochromated MoKα (λ = 0.71073 Å) radiation at 296(2) K. The structures were solved using SIR92[11] and refined with SHELXT-2014/7, SHELXT-2018/3 and SHELXT-2019/3.[12] Using Olex2[13], the molecular structures were drawn. Crystallographic data has been deposited with the Cambridge Crystallographic Data Center as supplementary publication no CCDC - 2403346 (**1**), 2451038 (**2**), 2311787 (**3**), 2358616 (**4a**), 2311786 (**4b**), 2358617 (**5**). The data can be obtained free of charge from The Cambridge Crystallographic Data Centre via www.ccdc.cam.ac.uk/data_request/cif.

Crystal data for **1**: 2 ($C_{44}H_{80}B_{20}O_2S_{10}Ti_6$), M_r.= 2930.55, monoclinic, space group $P1_{21}/c1$, a = 13.4680(8) Å, b = 24.0416(15) Å, c = 22.5360(16) Å, α = 90°, β = 100.988(2)°, γ = 90°, V = 7163.2(8) Å^3, Z = 2, ρ_{calcd} = 0.962 g/cm^3, μ = 1.359 mm^{-1}, *F(000)* = 3008.0, R_1 = 0.0445, wR_2 = 0.1256, 14644 independent reflections [2θ ≤ 52.744°] and 759 parameters.

Crystal data for **2**: 2 ($C_{41.5}H_{65}B_5S_{7.5}Ti_5$), M_r.= 2195.86, monoclinic, space group $P1_{21}/n1$, a = 22.5923(5) Å, b = 21.4585(9) Å, c = 12.9948(10) Å, α = 90°, β = 96.7370(14)°, γ = 90°, V = 6256.3(6) Å^3, Z = 2, ρ_{calcd} = 1.166 g/cm^3, μ = 0.885 mm^{-1}, *F(000)* = 2276.0, R_1 = 0.0763, wR_2 = 0.2465, 12788 independent reflections [2θ ≤ 52.832°] and 666 parameters.

Crystal data for **3**: $C_{12}H_{27}B_{11}S_2Ti$, M_r.= 402.26, orthorhombic, space group *P*bca, a = 12.1687(9) Å, b = 12.8758(10) Å, c = 26.9268(18) Å, α = 90°, β = 90°, γ = 90°, V = 4218.9(5) Å^3, Z = 8, ρ_{calcd} = 1.267 g/cm^3, μ = 0.598 mm^{-1}, *F(000)* = 1664.0, R_1 = 0.0433, wR_2 = 0.1175 , 3705 independent reflections [2θ ≤ 49.994°] and 260 parameters.

Crystal data for **4a**: $C_{12}H_{24}B_{10}S_3Ti$, M_r.= 420.49, orthorhombic, space group *P*bca, a = 12.0927(5) Å, b = 12.8115(6) Å, c = 26.9444(9) Å, α = 90°, β = 90°, γ = 90°, V = 4174.4(3) Å^3, Z = 8, ρ_{calcd} = 1.331 g/cm^3, μ = 0.702 mm^{-1}, *F(000)* = 1712.0, R_1 = 0.0513 , wR_2 = 0.1205, 3677 independent reflections [2θ ≤ 50°] and 243 parameters.

Crystal data for **4b**: $C_7H_{14}B_{10}S_3Ti$, M_r.= 350.36, orthorhombic, space group *P*bca, a = 13.4518(6) Å, b = 12.5002(6) Å, c = 19.0272(11) Å, α = 90°, β = 90°, γ = 90°, V = 3199.4(3) Å^3, Z = 8, ρ_{calcd} = 1.455 g/cm^3, μ = 0.903 mm^{-1}, *F(000)* = 1408.0, R_1 = 0.0290, wR_2 = 0.0764, 2840 independent reflections [2θ ≤ 50.208°] and 244 parameters.

Crystal data for **5**: $C_{12}H_{24}B_9S_3V$, M_r.= 412.72, monoclinic, space group P_{21}/n, a = 10.449(2) Å, b = 14.2128(19) Å, c = 13.260(3) Å, α = 90°, β = 92.289(7)°, γ = 90°, V = 1967.6(6) Å^3, Z = 4, ρ_{calcd} = 1.393 g/cm^3, μ = 0.815 mm^{-1}, *F(000)* = 848.0, R_1 = 0.0565, wR_2 = 0.1322, 3337 independent reflections [2θ ≤ 50.078°] and 255 parameters.

II Computational Details

All molecules were fully optimized using the *Gaussian 16*[14] program employing the BP86 functional[15] in conjunction with a def2-SVP basis set from the EMSL Basis Set Exchange Library.[16] The model compounds were fully optimized in gaseous state (no solvent effect) starting from the X-ray crystallographic coordinates. Frequency calculations were performed at the same level of theory to verify the nature of the stationary states and the absence of any imaginary frequency to confirm that all structures represent minima on the potential energy hypersurface. Further, the gauge including atomic orbital (GIAO)[17-19] method was employed to compute the ^{11}B chemical shifts. The NMR chemical shifts were calculated using the hybrid Becke−Lee−Yang−Parr (B3LYP) functional[20] and the def2-SVP basis set on the BP86/def2-SVP optimized geometries. The ^{11}B NMR chemical shifts were calculated relative to B_2H_6 (B3LYP B shielding constant 84.05

ppm) and converted to the usual [$BF_3.OEt_2$] scale using the experimental δ (^{11}B) value of B_2H_6, 16.6 ppm.[21] Natural bonding analyses were performed with the natural bond orbital (NBO) partitioning scheme[22] as implemented in the Gaussian 16 suite of programs. Wiberg bond indexes (WBI)[23] were obtained from a natural bond orbital analysis. In order to understand the nature of bonding in the synthesized molecules in greater detail, the topological properties of the resultant electron density, ρ, obtained from the wave functions of all the optimized structures were analyzed with the quantum theory of atoms in molecules (QTAIM).[24] The QTAIM analysis was carried out utilizing the Multiwfn V.3.4 package[25,] whereas the wave functions were generated with Gaussian09 at the same level of theory as for geometry optimization. All the optimized structures and orbital graphics were generated using the Gaussview[26], and Chemcraft[27] visualization programs.

Table.S1. Selected geometrical parameters and Wiberg bond indices (WBI) of **1**-**5**.

1				**2**			
	Expt.	Cal.	WBI		Expt.	Cal.	WBI
Ti1···Ti2	3.250	3.308	0.077	Ti1···Ti2	3.244	3.210	0.199
Ti2···Ti3	3.110	3.162	0.064	Ti2···Ti3	3.272	3.300	0.288
Ti2-S1	2.386(9)	2.377	1.196	Ti1-S1	2.289(2)	2.297	1.101
Ti2-S2	2.407(10)	2.403	1.145	Ti2-S1	2.526(2)	2.465	0.773
Ti1-S5	2.472(6)	2.490	0.758	Ti2-S7	2.479(5)	2.399	1.137
Ti2-S5	2.396(5)	2.436	0.858	Ti2-S8	2.438(4)	2.399	1.137
Ti1-O1	1.952(12)	1.897	0.874	Ti4-S5	2.511(2)	2.515	0.710
Ti2-O1	2.044(12)	2.082	0.501	Ti5-S5	2.322(2)	2.329	1.036
C1-S1	1.798	1.800	0.962	C1-S7	1.754(16)	1.813	0.936
C2-S2	1.79(5)	1.812	0.938	C2-S8	1.906	1.813	0.936
C1-C2	1.58(6)	1.645	0.704	C1-C2	1.62(2)	1.644	0.705
C1-B1	1.72(8)	1.722	0.552	C1-B2	1.69(2)	1.723	0.552
B1-B2	1.734	1.780	0.430	B4-B8	1.810	1.794	0.526
3				**4a**			
	Expt.	Cal.	WBI		Expt.	Cal.	WBI
Ti1···B11	2.259(4)	2.240	0.591	Ti1-S1	2.3095(12)	2.326	1.192
Ti1-S1	2.3214(9)	2.341	1.194	Ti1-S2	2.3220(11)	2.327	1.192
Ti1-S2	2.3321(9)	2.341	1.192	Ti1-S3	2.3231(12)	2.332	1.667
B1-B11	1.750(5)	1.735	0.830	B1-S3	1.849(5)	1.851	1.081
B2-S1	1.851(4)	1.856	1.065	B2-S1	1.839(5)	1.855	1.073
B3-S2	1.843(4)	1.856	1.066	B3-S2	1.833(5)	1.855	1.074
B1-B2	1.811(5)	1.834	0.494	B1-B2	1.829(6)	1.853	0.474
C1-C2	1.626(6)	1.635	0.732	C1-C2	1.635(7)	1.646	0.716
C2-B10	1.720(6)	1.730	0.458	C2-B10	1.714(7)	1.721	0.466
B11-H3	0.98(4)	1.219	0.932				
B11-H2	1.03(4)	1.274	0.663				
Ti1-H2	1.93(3)	1.951	0.275				

4b				**5**			
	Expt.	Cal.	WBI		Expt.	Cal.	WBI
Ti1-S1	2.2992(7)	2.319	1.228	V1-S1	2.2194(16)	2.229	1.363
Ti1-S2	2.3182(7)	2.317	1.235	V1-S2	2.2088(18)	2.223	1.389
Ti1-S3	2.3223(7)	2.325	1.203	V1-S3	2.2099(15)	2.229	1.356
B1-S3	1.843(3)	1.851	1.080	B1-S1	1.860(6)	1.875	0.990
B2-S1	1.848(3)	1.855	1.073	B2-S2	1.860(6)	1.878	0.984
B3-S2	1.851(3)	1.856	1.070	B3-S3	1.859(6)	1.873	0.992
B1-B2	1.835(3)	1.855	0.472	B1-B2	1.837(9)	1.858	0.460
C1-C2	1.629(3)	1.646	0.716	B8-B9	1.850(11)	1.887	0.443
C2-B10	1.707(4)	1.720	0.467	B8-H1	1.15(2)	1.288	0.491
				C1-C2	1.555(8)	1.569	0.899
				C2-B5	1.695(8)	1.718	0.490

Table S2. Selected experimental and Calculated bond angles of **1**-**5**.

1			**2**		
	Expt.	Cal.		Expt.	Cal.
Ti1-Ti2-Ti3	60.57	59.96	Ti1-Ti2-Ti3	60.49	61.25
Ti2-Ti3-Ti4	93.95	93.85	Ti2-Ti3-Ti4	61.10	61.00
Ti1-S5-Ti2	83.73	84.36	Ti-S1-Ti2	84.56	84.70
Ti2-S5-Ti5	89.21	92.65	Ti2-S1-Ti3	82.00	82.24
Ti2-S1-C1	112.16	112.62	S7-Ti2-S8	81.50	84.67
C1-C2-S2	119.59	115.8	C2-S8-Ti2	114.55	111.73
Ti1-O1-Ti2	108.80	112.42	S8-C2-C1	117.20	115.94
S1-Ti2-S2	84.30	84.46	B6-C2-B9	117.90	113.67
S3-Ti2-S4	83.60	84.46			
Ti2-Ti3-S4	94.73	91.55			
3			**4a**		
	Expt.	Cal.		Expt.	Cal.
Ti1-S1-B2	81.17	80.62	Ti1-S1-B2	80.73	79.71
Ti-S2-B3	81.17	80.70	Ti1-S2-B3	80.58	79.71
S1-B2-B1	117.20	117.22	Ti1-S3-B1	80.50	79.30
B11-B1-B2	121.90	121.64	S1-B2-B1	119.10	118.83
C1-C2-B7	112.20	117.77	S3-B1-B2	119.50	120.19
			C1-C2-B7	112.0	111.75
4b			**5**		
	Expt.	Cal.		Expt.	Cal.
Ti1-S1-B2	80.89	79.44	V1-S1-B1	81.01	80.60
Ti1-S2-B3	80.48	79.45	V1-S2-B2	80.00	80.29

Ti1-S3-B1	80.33	79.02	V1-S3-B3	79.42	79.35
S1-B2-B1	118.25	118.63	S1-B1-B3	116.50	116.69
S3-B1-B2	119.54	119.96	S3-B3-B1	118.80	118.63
C1-C2-B7	111.96	111.77	C1-C2-B7	114.30	116.08

Table S3. Calculated natural charges (q) and natural valence population (Pop) of **1**-**5**.

1			**2**		
	q	Pop(val)		q	Pop(val)
Ti1	0.426	3.569	Ti1	0.159	3.840
Ti2	0.261	3.732	Ti2	-0.114	4.108
Ti3	0.261	3.732	Ti3	0.165	3.833
Ti4	0.205	3.790	Ti4	0.165	3.833
Ti5	0.205	3.790	Ti5	0.159	3.840
Ti6	0.426	3.569	S1	-0.025	6.015
S1	0.126	5.850	S2	-0.103	6.093
S2	0.074	5.903	S3	-0.003	5.991
S3	0.074	5.903	S4	-0.003	5.991
S4	0.126	5.850	S5	-0.103	6.093
S5	-0.088	6.078	S6	-0.025	6.015
S6	-0.078	6.068	S7	0.080	5.896
S7	-0.143	6.135	S8	0.080	5.896
S8	-0.078	6.068	C1	-0.580	4.555
S9	-0.088	6.078	C2	-0.580	4.555
S10	-0.143	6.134	B1	0.032	2.931
O1	-0.513	6.506	B2	0.037	2.923
O2	-0.513	6.506	B3	-0.155	3.126
C1	-0.585	4.560	B4	-0.174	3.145
C2	-0.582	4.557			
C3	-0.582	4.557			
C4	-0.585	4.560			
3			**4a**		
	q	Pop(val)		q	Pop(val)
Ti1	0.075	3.927	Ti1	0.128	3.871
S1	-0.069	6.058	S1	-0.080	6.068
S2	-0.071	6.059	S2	-0.082	6.070
C1	-0.610	4.590	S3	-0.092	6.080
C2	-0.610	4.590	C1	-0.614	4.594
B1	-0.228	3.188	C2	-0.614	4.594

B2	-0.074	3.021	B1	-0.113	3.058
B3	-0.073	3.020	B2	-0.092	3.037
B4	-0.170	3.135	B3	-0.092	3.037
B5	0.032	2.930	B4	-0.177	3.141
B6	0.033	2.928	B5	0.030	2.932
B7	0.033	2.928	B6	0.023	2.936
B8	0.032	2.931	B7	0.023	2.936
B9	0.194	2.767	B8	0.030	2.932
B10	0.228	2.730	B9	0.189	2.773
B11	-0.364	3.344	B10	0.208	2.751
4b			**5**		
	q	Pop(val)		q	Pop(val)
Ti1	0.051	3.946	V1	-0.137	5.139
S1	-0.046	6.035	S1	0.086	5.902
S2	-0.043	6.032	S2	0.083	5.903
S3	-0.057	6.046	S3	0.071	5.916
C1	-0.614	4.594	C1	-0.652	4.634
C2	-0.614	4.594	C2	-0.641	4.622
B1	-0.115	3.061	B1	-0.097	3.048
B2	-0.094	3.039	B2	-0.094	3.043
B3	-0.095	3.041	B3	-0.131	3.083
B4	-0.177	3.141	B4	-0.010	2.974
B5	0.031	2.931	B5	0.210	2.756
B6	0.023	2.936	B6	0.002	2.961
B7	0.023	2.936	B7	0.039	2.935
B8	0.031	2.931	B8	-0.303	3.274
B9	0.189	2.772	B9	0.030	2.944
B10	0.208	2.751			

Table S4. Calculated HOMO–LUMO energy gap of **1**-**5**.

	1	**2**	**3**	**4a**	**4b**	**5**
$\Delta E_{H\text{-}L}$ (eV)	1.300	0.386	2.646	2.857	2.783	1.558

Table S5. Calculated ^{11}B chemical shifts for complexes **1**-**5**.

Compounds	^{11}B NMR value (ppm)	
	Experimental	Theoretical
1[a]	-12.5 and -7.9 (vrey broad peak ranging from -11.0 to -1.0)	-17.6, -17.3, -17.1, -17.0, -15.6, -15.5, -14.0, -13.9, -10.8, -10.6
2[a]	-12.4, -9.8, -8.7, -8.4, -4.9, -3.7, -1.5, -0.8	-18.3,-17.7, -15.2, -13.7, -11.4
3	-15.8, -11.2, -10.1, -6.8, -3.1, 8.4	-25.9, -23.9, -23.8, -19.5, -18.7, -18.7, -18.4, -12.9, -10.0, 4.0, 4.3
4a	-22.3, -16.4, -12.5, -11.3, 1.3, 6.3	-31.9, -24.5, -24.3, -21.7, -19.7, -19.6, -18.6, -2.6, 2.0, 2.5
4b	-22.2, -16.6, -11.8, -10.7, 2.1, 7.1	-32.1, -24.8, -24.7, -21.5, -19.3, -19.0, -1.5, 2.6, 3.4
5	-30.3, -25.8, -22.0, -6.4, -4.6	-37.1, -35.5, -30.6, -27.0, -22.1, -17.5, -16.3, -9.6, -2.9

[a] For clusters **1** and **2**, each theoretical value corresponds to two boron atoms that are merged.

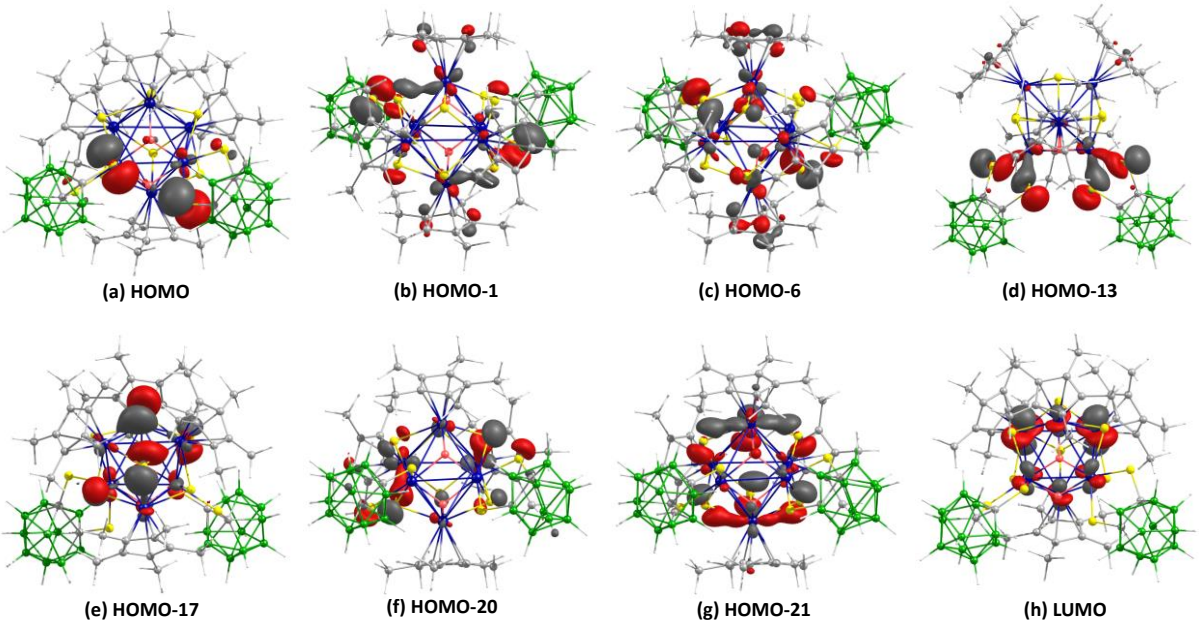

Figure S56. Selected molecular orbitals of **1** (isocontour values: ±0.045 [e.bohr^{-3}]$^{1/2}$).

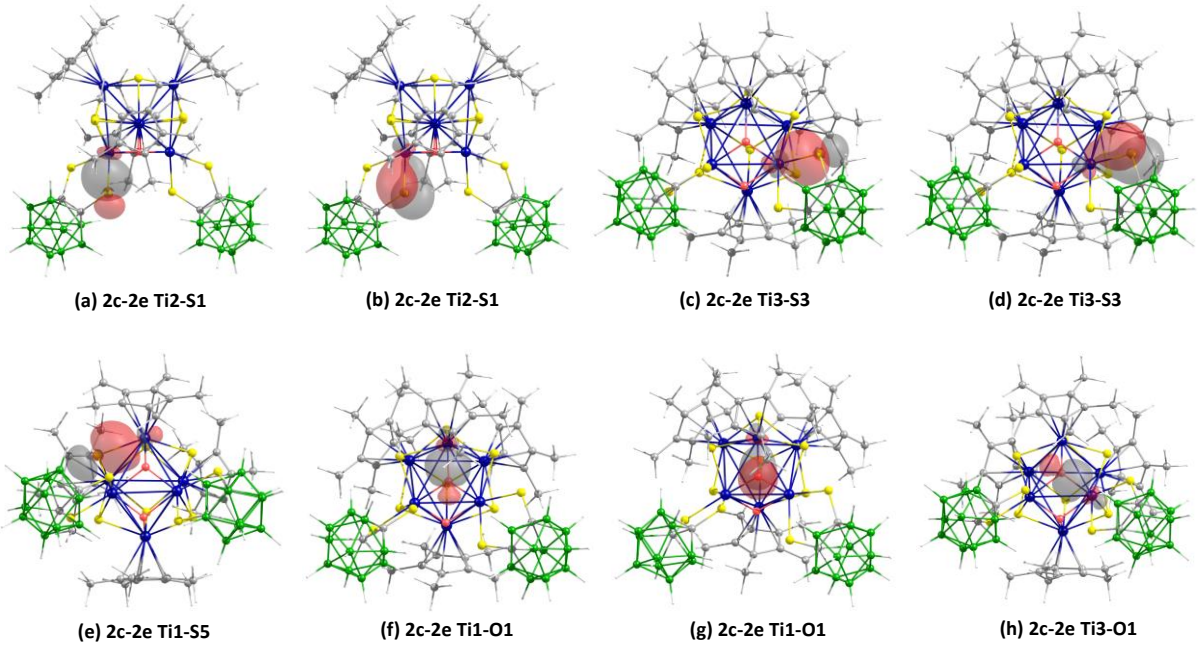

Figure S57. Selected NBO interactions of **1** (isocontour values: ±0.045 [e.bohr^{-3}]$^{1/2}$).

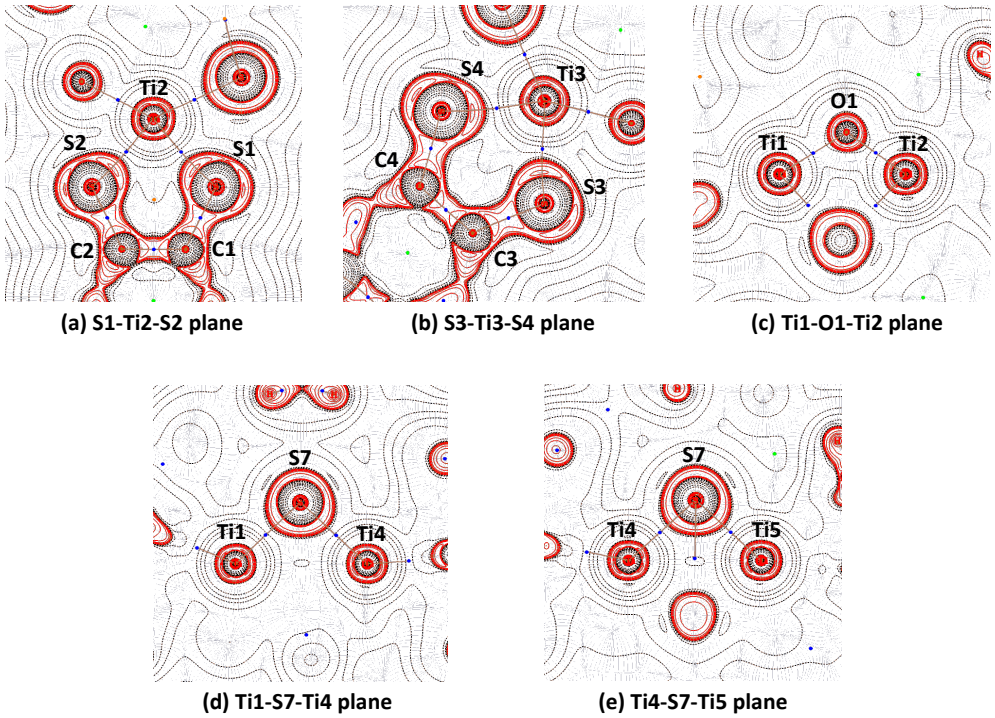

Figure S58. Contour-line diagram of the Laplacian of the electron density of **1** in selected planes. The solid brown lines are bond paths, whereas blue dots indicate the bond-critical points (BCP). Solid red lines indicate the areas of charge concentration ($\nabla^2\rho(r) < 0$), while dashed black lines show the areas of charge depletion ($\nabla^2\rho(r) > 0$).

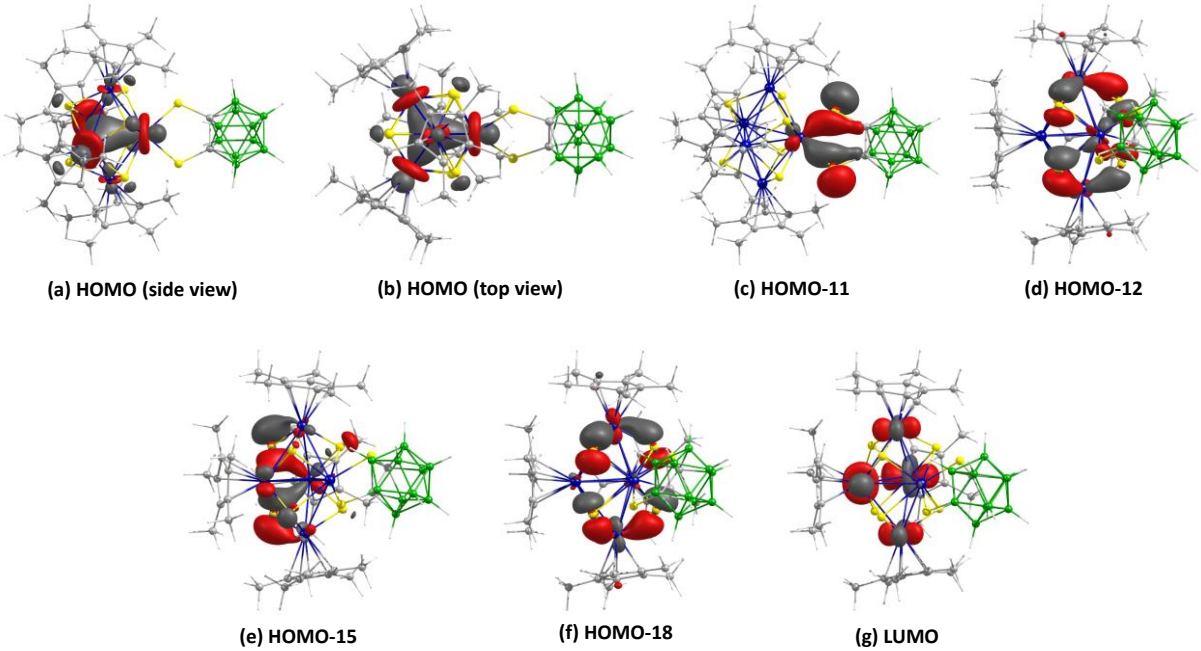

Figure S59. Selected molecular orbitals of **2** (isocontour values: ±0.045 [e.bohr^{-3}]$^{1/2}$).

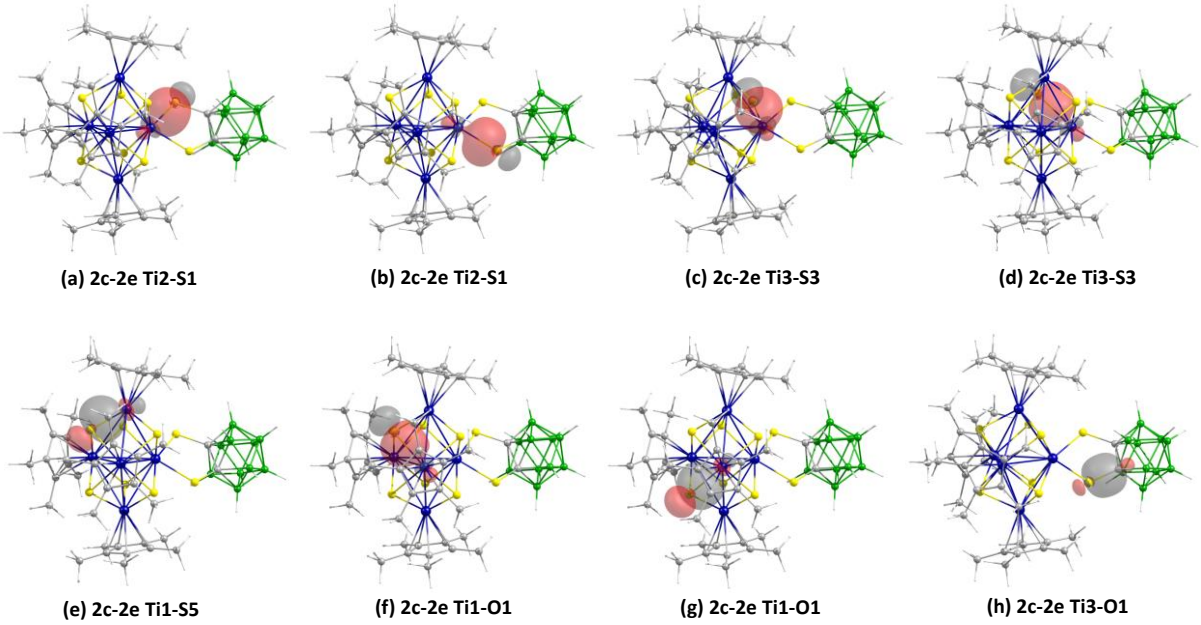

Figure S60. Selected NBO interactions of **2** (isocontour values: ±0.045 [e.bohr^{-3}]$^{1/2}$).

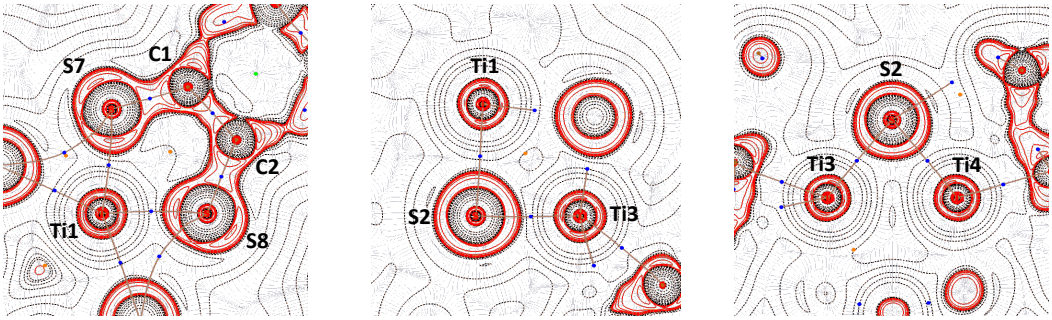

(a) S7-Ti1-S8 plane (b) Ti1-S2-Ti3 plane (c) Ti3-S2-Ti4 plane

Figure S61. Contour-line diagram of the Laplacian of the electron density of **2** in selected planes. The solid brown lines are bond paths, whereas blue dots indicate the bond-critical points (BCP). Solid red lines indicate the areas of charge concentration ($\nabla^2\rho(r) < 0$), while dashed black lines show the areas of charge depletion ($\nabla^2\rho(r) > 0$).

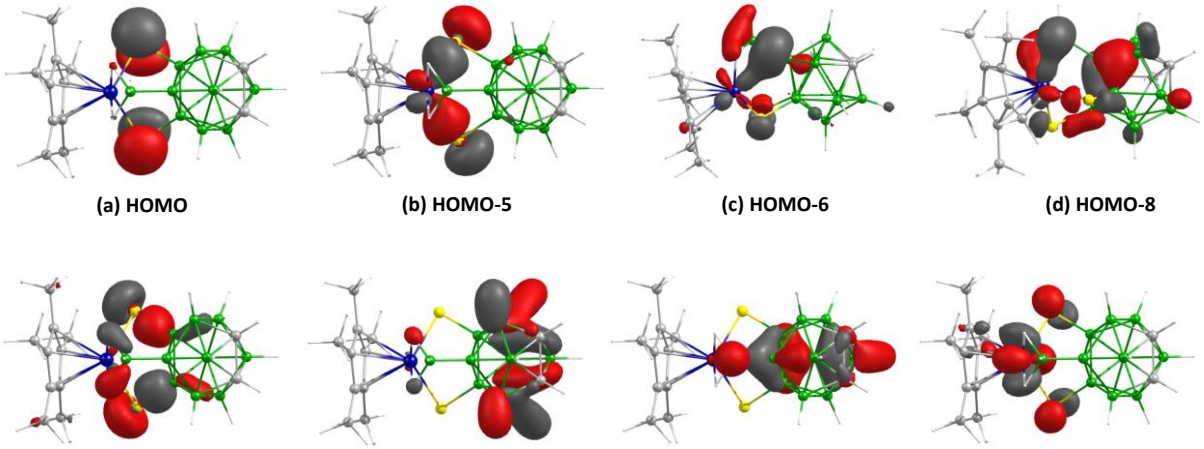

(a) HOMO (b) HOMO-5 (c) HOMO-6 (d) HOMO-8

(e) HOMO-9 (f) HOMO-12 (g) HOMO-17 (h) LUMO

Figure S62. Selected molecular orbitals of **3** (isocontour values: ±0.045 [e.bohr^{-3}]$^{1/2}$).

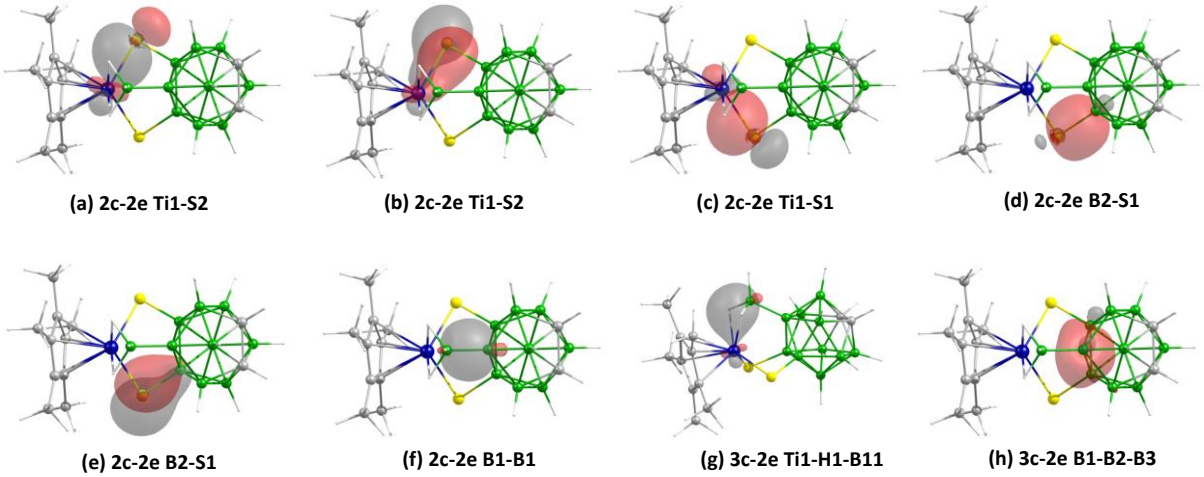

(a) 2c-2e Ti1-S2 (b) 2c-2e Ti1-S2 (c) 2c-2e Ti1-S1 (d) 2c-2e B2-S1

(e) 2c-2e B2-S1 (f) 2c-2e B1-B1 (g) 3c-2e Ti1-H1-B11 (h) 3c-2e B1-B2-B3

Figure S63. Selected NBO interactions of **3** (isocontour values: ±0.045 [e.bohr^{-3}]$^{1/2}$).

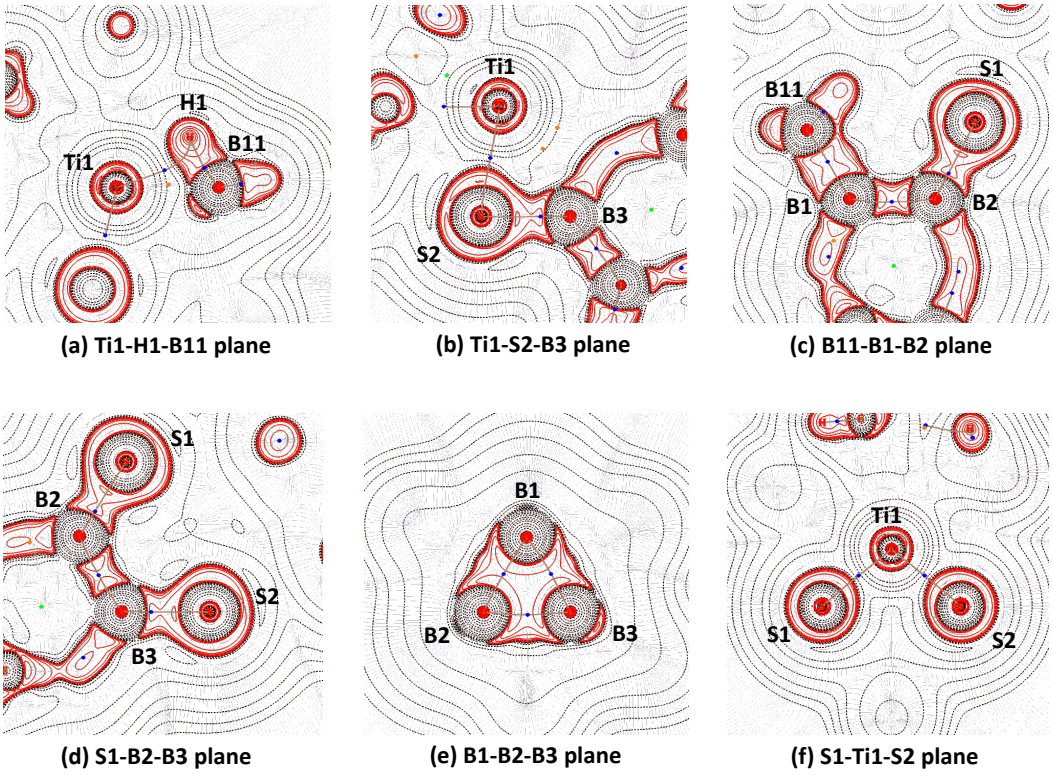

Figure S64. Contour-line diagram of the Laplacian of the electron density of **3** in selected planes. The solid brown lines are bond paths, whereas blue dots indicate the bond-critical points (BCP). Solid red lines indicate the areas of charge concentration ($\nabla^2\rho(r) < 0$), while dashed black lines show the areas of charge depletion ($\nabla^2\rho(r) > 0$).

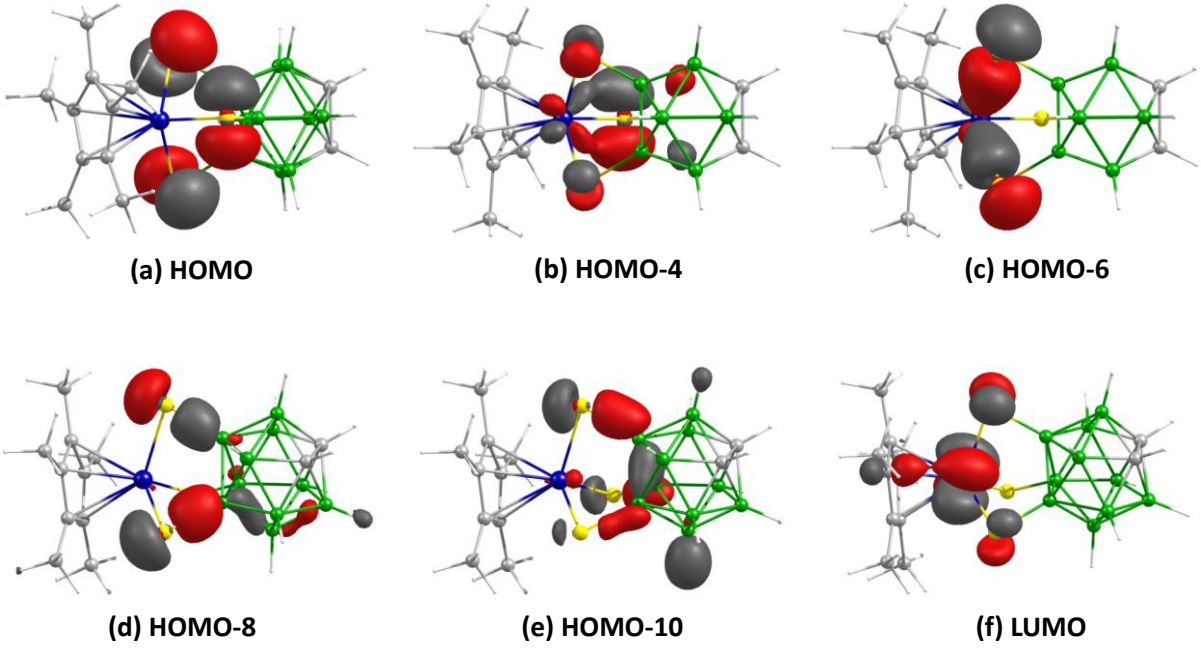

Figure S65. Selected molecular orbitals of **4a** (isocontour values: ±0.045 [e.bohr^{-3}]$^{1/2}$).

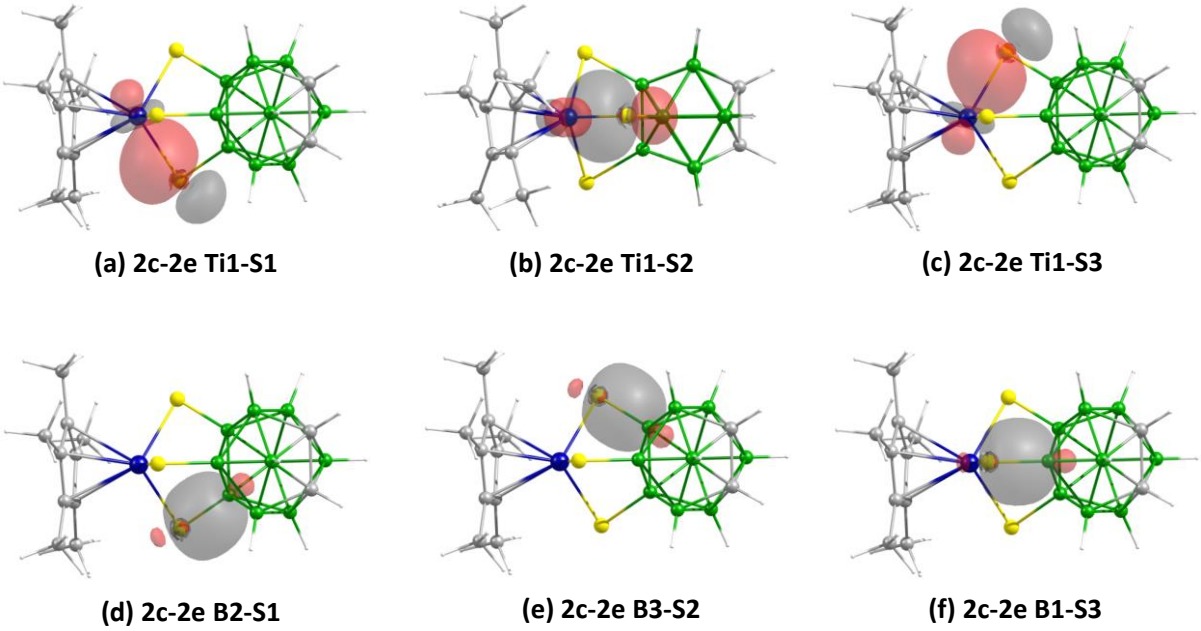

Figure S66. Selected NBO interactions of **4a** (isocontour values: ±0.045 [e.bohr^{-3}]$^{1/2}$).

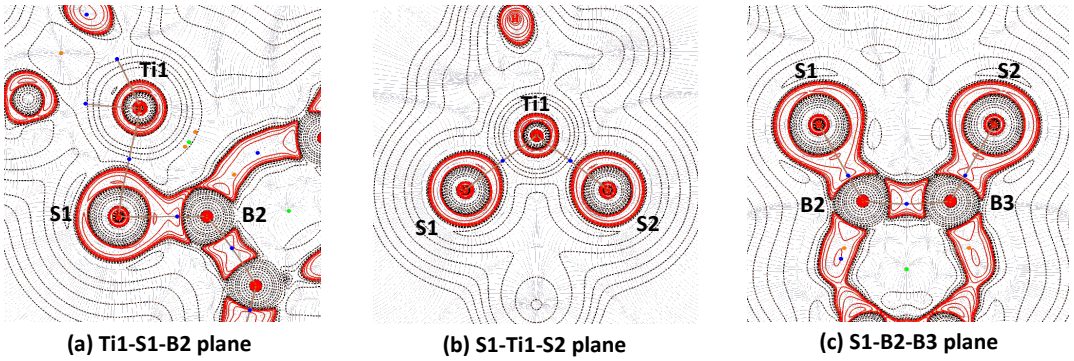

Figure S67. Contour-line diagram of the Laplacian of the electron density of **4a** in selected planes. The solid brown lines are bond paths, whereas blue dots indicate the bond-critical points (BCP). Solid red lines indicate the areas of charge concentration ($\nabla^2\rho(r) < 0$), while dashed black lines show the areas of charge depletion ($\nabla^2\rho(r) > 0$).

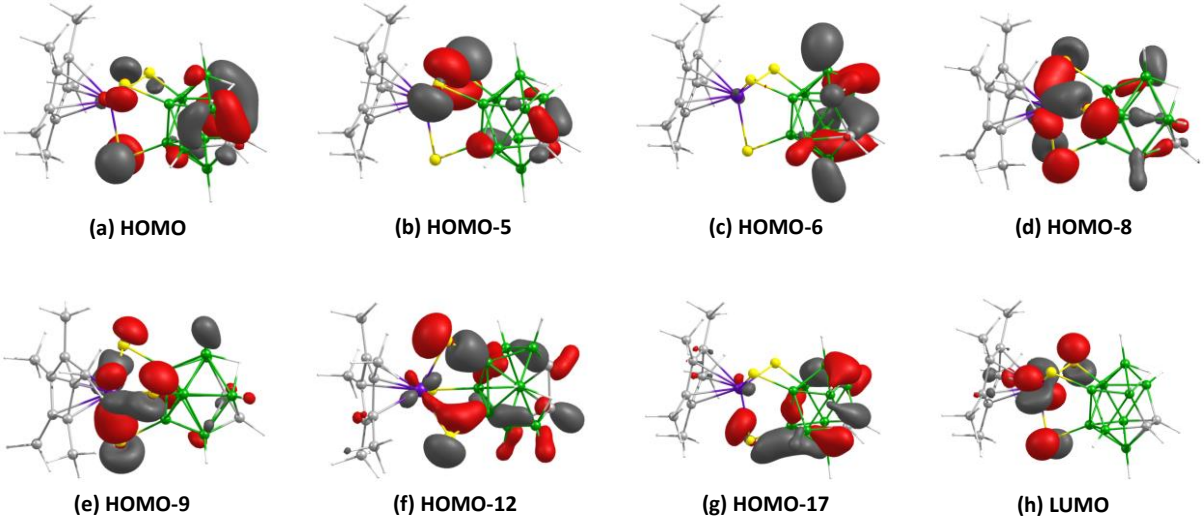

Figure S68. Selected molecular orbitals of **5** (isocontour values: ±0.045 [e.bohr^{-3}]$^{1/2}$).

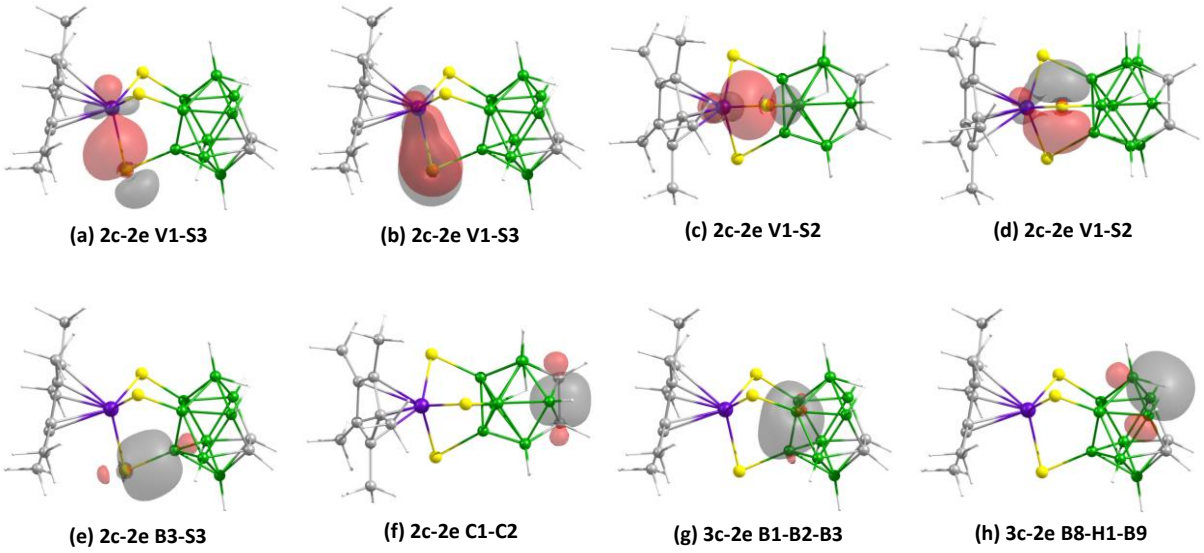

Figure S69. Selected NBO interactions of **5** (isocontour values: ±0.045 [e.bohr^{-3}]$^{1/2}$).

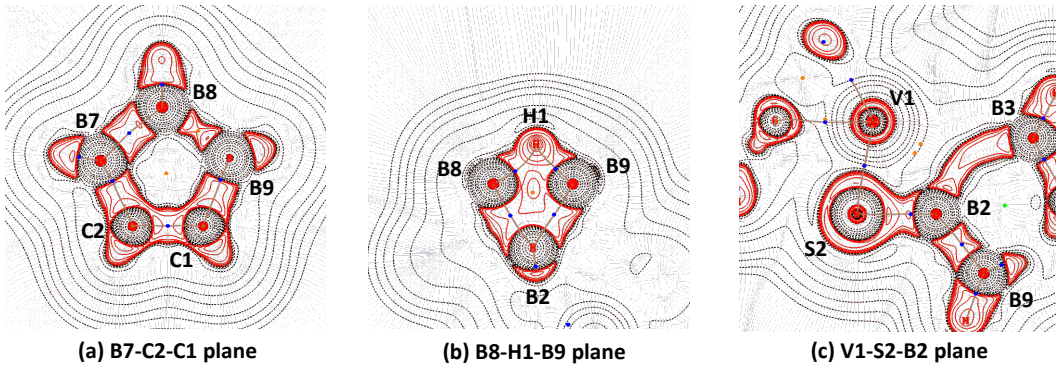

Figure S70. Contour-line diagram of the Laplacian of the electron density of **5** in selected planes. The solid brown lines are bond paths, whereas blue dots indicate the bond-critical points (BCP). Solid red lines indicate the areas of charge concentration ($\nabla^2\rho(r) < 0$), while dashed black lines show the areas of charge depletion ($\nabla^2\rho(r) > 0$).

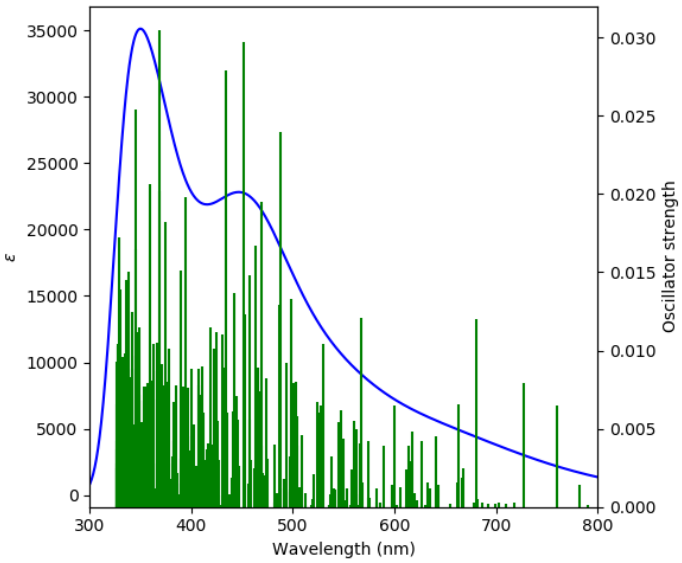

Figure S71. Absorption spectrum of **1** computed at TD-DFT- PB86/Def2-SVP level of theory (ε in $LM^{-1}cm^{-1}$).

Table S6. TD-DFT calculated energies (excitation energy (eV), λ_{calc} (nm)), oscillator strength (*f*), and main composition of the first UV−vis electronic excitations for **1**. Experimental absorption wavelengths (λ_{exp}, nm) of **1** are given for comparison.

No	Excitation Energy (eV)	Wavelength λ (nm)		Main electronic transition (% weight) [b]
		Calc. (*f*) [a]	Expt.	
1	1.822	680 (0.012)		HOMO-4→LUMO+1 (93)
2	2.184	568 (0.012)		HOMO-13→LUMO (34)
				HOMO-12→LUMO+1 (14)
				HOMO-10→LUMO+2 (28)
				HOMO→LUMO+6 (11)
3	2.487	499 (0.013)		HOMO-6→LUMO+6 (71)
4	2.544	487 (0.024)	490	HOMO-1→LUMO+8 (45)
				HOMO-8→LUMO+6 (22)
5	2.642	469 (0.020)		HOMO--18→LUMO (62)
6	2.747	451 (0.030)		HOMO-14→LUMO+5 (30)
				HOMO-4→LUMO+8 (14)
				HOMO-3→LUMO+9 (20)
7	2.853	435 (0.028)		HOMO-1→LUMO+10 (64)
8	3.359	369 (0.030)	375	HOMO-10→LUMO+11 (30)
				HOMO-5→LUMO+13 (22)
				HOMO-14→LUMO+9 (19)
9	3.448	360 (0.021)		HOMO-26→LUMO (27)
				HOMO-23→LUMO+3 (30)
				HOMO→LUMO+17 (15)
10	3.590	345 (0.025)		HOMO-14→LUMO+10 (41)
				HOMO-10→LUMO+14 (15)

[a]Oscillator strength greater than 0.010 and [b]Components with greater than 10% contribution shown.

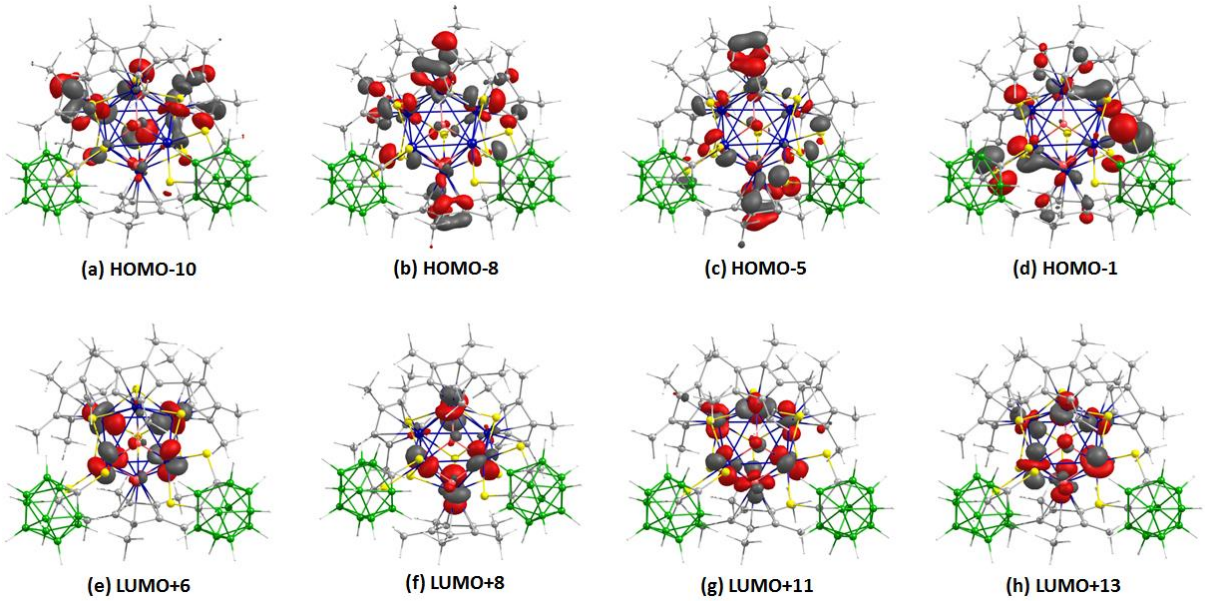

Figure S72. Selected molecular orbitals of **1** related to most intense electronic transitions [isocontour values: ±0.045 $(e/bohr^3)^{1/2}$].

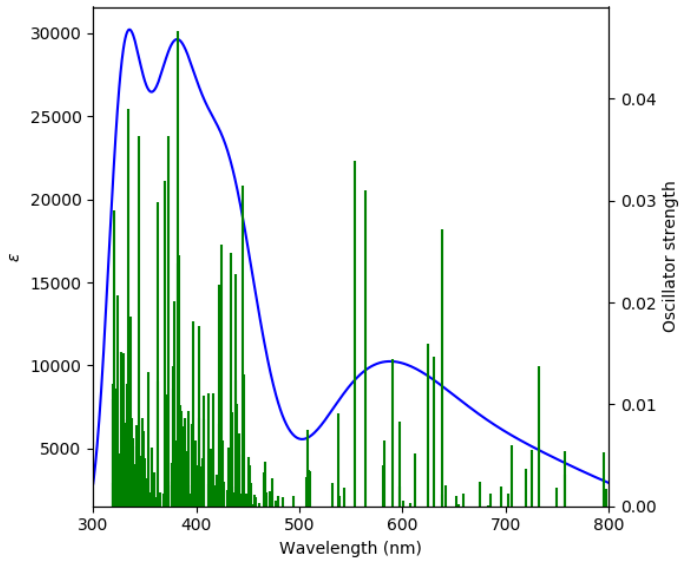

Figure S73. Absorption spectrum of **2** computed at TD-DFT-PB86/Def2-SVP level of theory (ε in $LM^{-1}cm^{-1}$).

Table S7. TD-DFT calculated energies (excitation energy (eV), λ_{calc} (nm)), oscillator strength (*f*), and main composition of the first UV−vis electronic excitations for **2**. Experimental absorption wavelengths (λ_{exp}, nm) of **2** are given for comparison.

No	Excitation Energy (eV)	Wavelength λ (nm)		Main electronic transition (% weight) [b]
		Calc. (*f*) [a]	Expt.	
1	1.693	733 (0.014)		HOMO-2→LUMO (91)
2	1.942	638 (0.027)		HOMO-6→LUMO+1(11)
				HOMO→LUMO+8 (67)
3	2.198	564 (0.031)		HOMO-9→LUMO+2 (15)
				HOMO-8→LUMO+2 (54)
4	2.240	554 (0.034)		HOMO→LUMO+10 (52)
				HOMO→LUMO+11 (16)
5	2.783	446 (0.032)	463	HOMO-5→LUMO+3 (41)
				HOMO→LUMO+18 (16)
				HOMO-1→LUMO+7 (12)
6	2.829	438 (0.023)		HOMO-7→LUMO+4 (12)
				HOMO-6→LUMO+3 (11)
				HOMO-5→LUMO+4 (22)
				HOMO-2→LUMO+7 (15)
7	2.856	434 (0.025)		HOMO-3→LUMO+6 (38)
				HOMO→LUMO+18 (12)
8	3.247	382 (0.047)		HOMO-17→LUMO+2 (10)
				HOMO-10→LUMO+6 (17)
				HOMO-1→LUMO+9 (23)
9	3.320	373 (0.036)	365	HOMO-20→LUMO+1 (77)
10	3.606	344 (0.036)		HOMO-3→LUMO+12 (64)

[a]Oscillator strength greater than 0.010 and [b]Components with greater than 10% contribution shown.

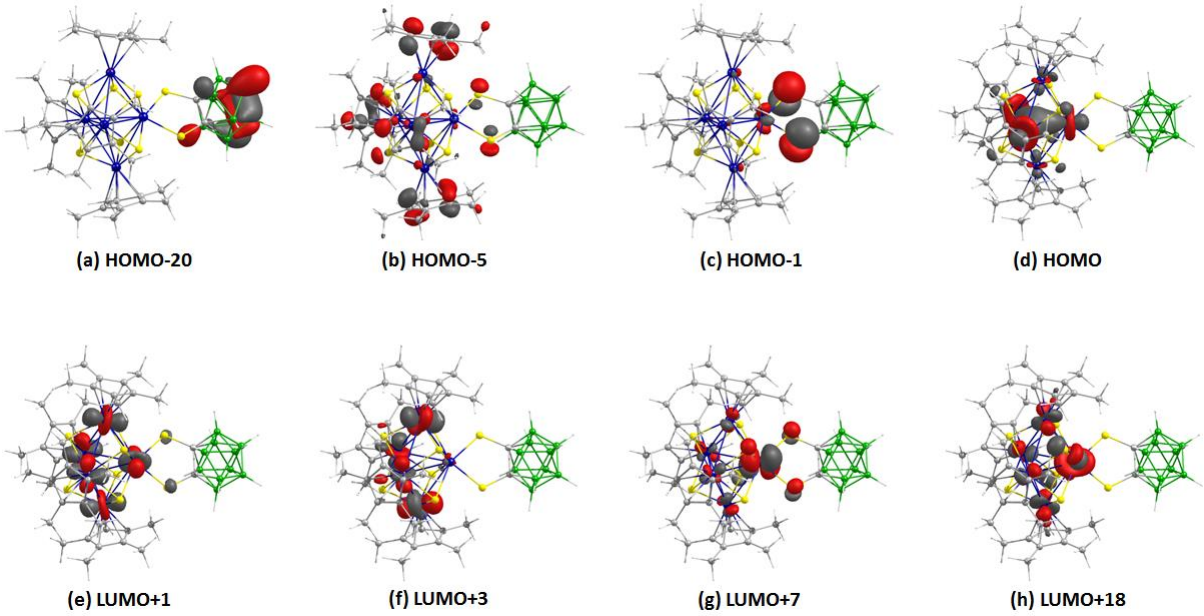

Figure S74. Selected molecular orbitals of **2** related to most intense electronic transitions [isocontour values: ±0.045 $(e/bohr^3)^{1/2}$].

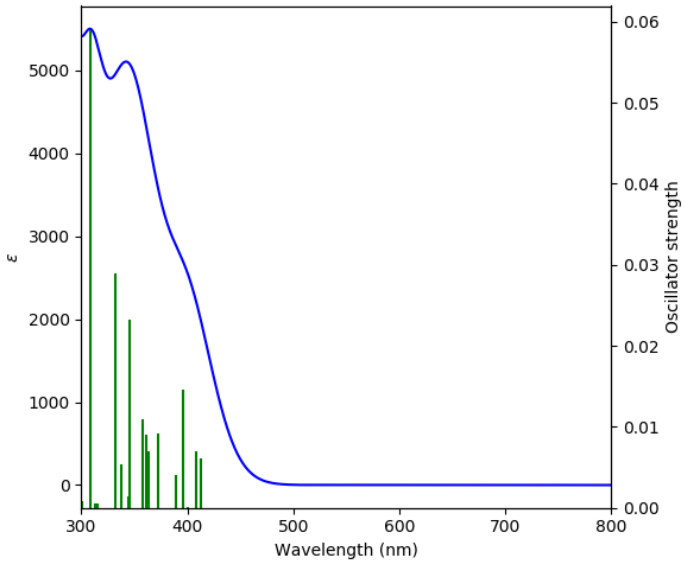

Figure S75. Absorption spectrum of **3** computed at TD-DFT-PB86/Def2-SVP level of theory (ε in $LM^{-1}cm^{-1}$).

Table S8. TD-DFT calculated energies (excitation energy (eV), λ_{calc} (nm)), oscillator strength (*f*), and main composition of the first UV−vis electronic excitations for **3**. Experimental absorption wavelengths (λ_{exp}, nm) of **3** are given for comparison.

No	Excitation Energy (eV)	Wavelength λ (nm)		Main electronic transition (% weight) [b]
		Calc. (*f*) [a]	Expt.	
1	3.131	396(0.015)		HOMO-2→LUMO (55)
				HOMO-1→LUMO+2 (11)
				HOMO→LUMO (18)
				HOMO→LUMO+1 (14)
2	3.467	358 (0.011)		HOMO-1→LUMO+2(82)
3	3.587	346 (0.023)		HOMO-2→LUMO+2 (91)
4	3.733	332 (0.029)	336	HOMO-4→LUMO (53)
				HOMO-3→LUMO (18)
10	4.011	309 (0.059)		HOMO-4→LUMO+1 (81)

[a]Oscillator strength greater than 0.010 and [b]Components with greater than 10% contribution shown.

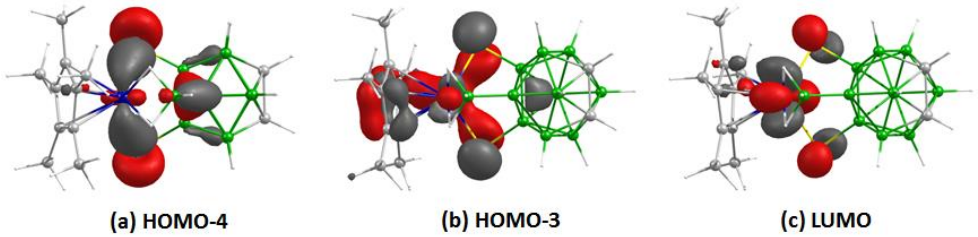

Figure S76. Selected molecular orbitals of **3** related to most intense electronic transitions [isocontour values: ±0.045 $(e/bohr^3)^{1/2}$].

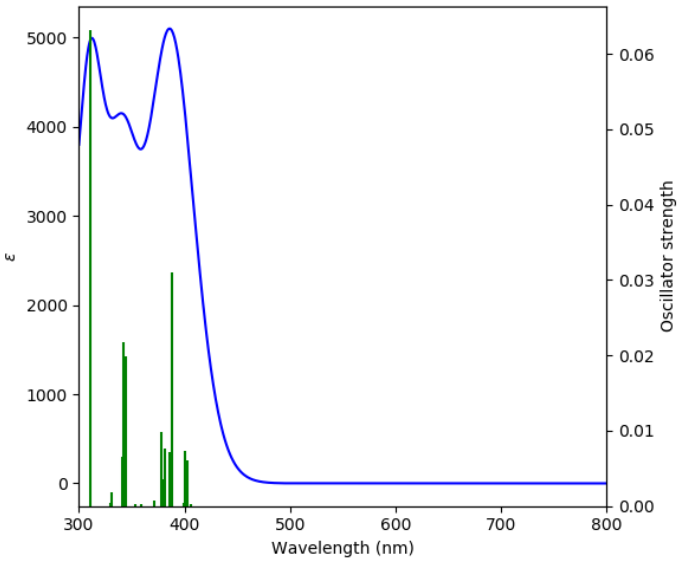

Figure S77. Absorption spectrum of **4a** computed at TD-DFT- PB86/Def2-SVP level of theory (ε in $LM^{-1}cm^{-1}$).

Table S9. TD-DFT calculated energies (excitation energy (eV), λ_{calc} (nm)), oscillator strength (*f*), and main composition of the first UV–vis electronic excitations for **4a**. Experimental absorption wavelengths (λ_{exp}, nm) of **4a** are given for comparison.

No	Excitation Energy (eV)	Wavelength λ (nm)		Main electronic transition (% weight) [b]
		Calc. (*f*) [a]	Expt.	
1	3.190	389 (0.031)	371	HOMO-1→LUMO+1 (62)
				HOMO-1→LUMO (18)
				HOMO-2→LUMO (11)
2	3.277	378 (0.010)		HOMO-2→LUMO (56)
				HOMO-2→LUMO+1 (24)
3	3.594	345 (0.020)		HOMO-4→LUMO (12)
				HOMO-3→LUMO+1 (61)
4	3.626	342 (0.022)		HOMO-4→LUMO (19)
				HOMO-4→LUMO+1 (25)
				HOMO-3→LUMO (30)
10	3.987	311 (0.063)		HOMO-5→LUMO+2 (82)

[a]Oscillator strength greater than 0.010 and [b]Components with greater than 10% contribution shown.

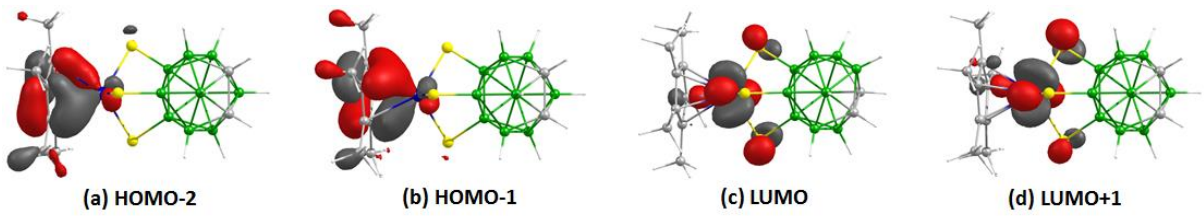

Figure S78. Selected molecular orbitals of **4a** related to most intense electronic transitions [isocontour values: ±0.045 $(e/bohr^3)^{1/2}$].

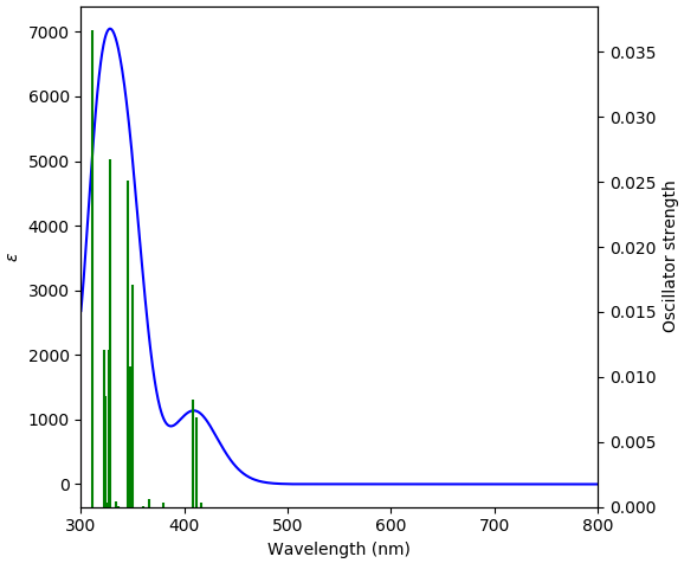

Figure S79. Absorption spectrum of **4b** computed at TD-DFT-PB86/Def2-SVP level of theory (ε in $LM^{-1}cm^{-1}$).

Table S10. TD-DFT calculated energies (excitation energy (eV), λ_{calc} (nm)), oscillator strength (*f*), and main composition of the first UV-vis electronic excitations for **4b**. Experimental absorption wavelengths (λ_{exp}, nm) of **4b** are given for comparison.

No	Excitation Energy (eV)	Wavelength λ (nm)		Main electronic transition (% weight) [b]
		Calc. (*f*) [a]	Expt.	
1	3.036	408 (0.008)	388	HOMO→LUMO+1 (76)
2	3.542	350 (0.017)		HOMO-1→LUMO (34)
				HOMO-1→LUMO+1 (37)
3	3.592	345 (0.025)		HOMO-2→LUMO+1 (37)
				HOMO-1→LUMO (21)
4	3.777	328 (0.027)	330	HOMO-5→LUMO (58)
				HOMO-4→LUMO (22)
10	3.983	311 (0.037)		HOMO-3→LUMO+2 (76)

[a]Oscillator strength greater than 0.010 and [b]Components with greater than 10% contribution shown.

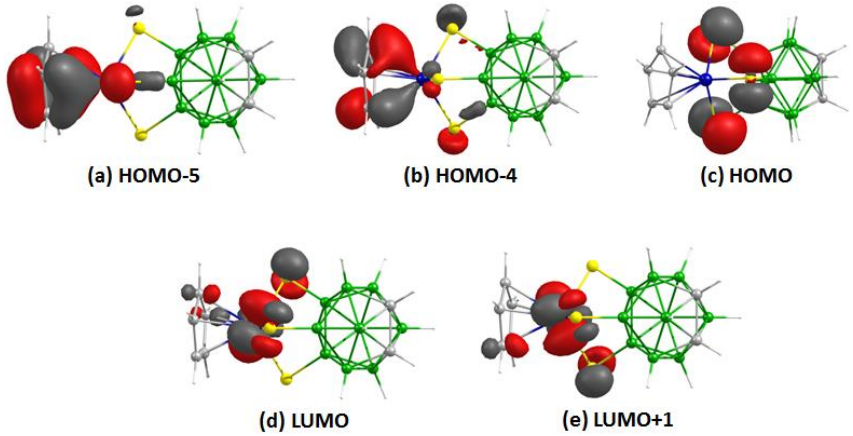

Figure S80. Selected molecular orbitals of **4b** related to most intense electronic transitions [isocontour values: ±0.045 $(e/bohr^3)^{1/2}$].

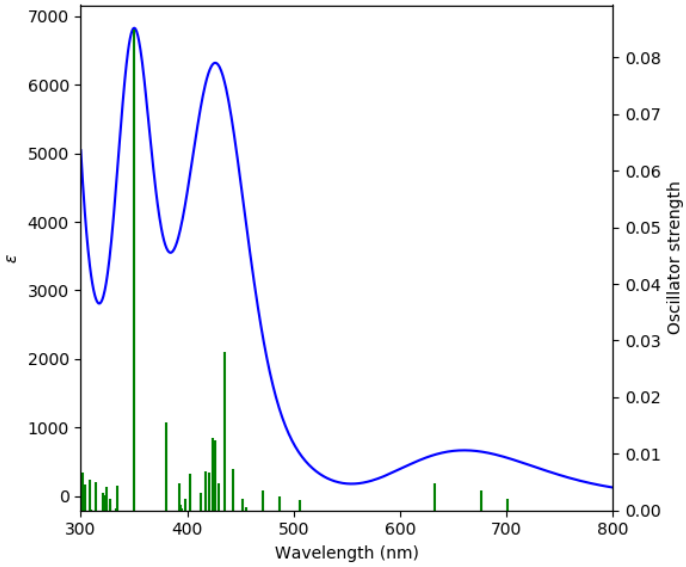

Figure S81. Absorption spectrum of **5** computed at TD-DFT-PB86/Def2-SVP level of theory (ε in $LM^{-1}cm^{-1}$).

Table S11. TD-DFT calculated energies (excitation energy (eV), λ_{calc} (nm)), oscillator strength (*f*), and main composition of the first UV−vis electronic excitations for **5**. Experimental absorption wavelengths (λ_{exp}, nm) of **5** are given for comparison.

No	Excitation Energy (eV)	Wavelength λ (nm)		Main electronic transition (% weight) [b]
		Calc. (*f*) [a]	Expt.	
1	1.960	632 (0.005)	591	HOMO→LUMO+2 (98)
2	2.847	435 (0.028)	424	HOMO-3→LUMO (65)
				HOMO-2→LUMO+2 (19)
3	2.922	424 (0.013)		HOMO-5→LUMO+1 (17)
				HOMO-2→LUMO (12)
				HOMO-2→LUMO+2 (16)
				HOMO-1→LUMO+1 (11)
4	3.262	380 (0.016)		HOMO-6→LUMO (11)
				HOMO-6→LUMO+1 (17)
				HOMO-5→LUMO+1 (13)
				HOMO-5→LUMO+2 (31)
10	3.538	350 (0.085)	335	HOMO-6→LUMO+2 (71)

[a]Oscillator strength greater than 0.010 and [b]Components with greater than 10% contribution shown.

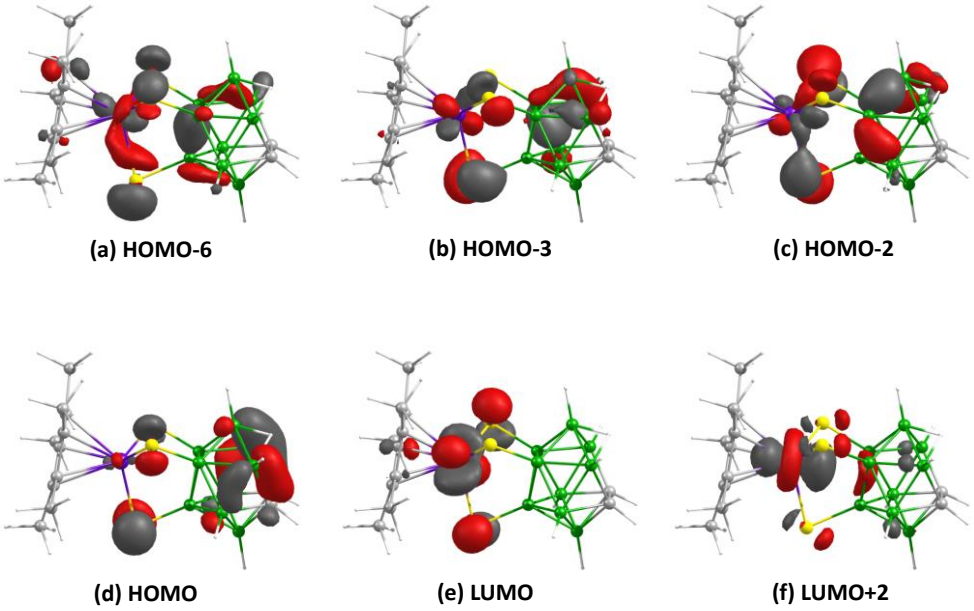

Figure S82. Selected molecular orbitals of **5** related to most intense electronic transitions [isocontour values: ±0.045 $(e/bohr^3)^{1/2}$].

III Cartesian Coordinates of all Optimized Structures

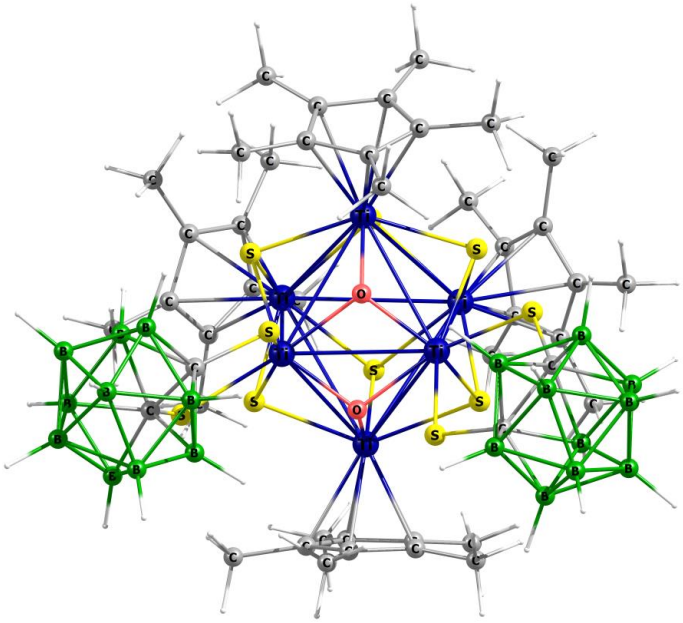

Figure S83. Optimized geometry of **1**.

Total energy = -11450.0995182 a.u.

Cartesian coordinates for the calculated structure **1** (in Å)

C	-4.154998000000	0.695467000000	-0.795999000000
C	-4.120077000000	-0.686347000000	-1.109673000000
C	-4.082435000000	-1.419629000000	0.109620000000
C	-4.107006000000	-0.480324000000	1.178105000000
C	-4.155338000000	0.821148000000	0.624317000000
C	-4.355795000000	1.797724000000	-1.776258000000
H	-3.966812000000	1.536234000000	-2.760352000000
H	-3.857089000000	2.712251000000	-1.457689000000
H	-5.425171000000	2.009436000000	-1.885314000000
C	-4.221809000000	-1.266772000000	-2.479732000000
H	-3.825751000000	-2.281645000000	-2.523542000000
H	-3.681703000000	-0.669042000000	-3.214985000000
H	-5.270461000000	-1.306585000000	-2.793258000000
C	-4.176418000000	-2.903858000000	0.241414000000
H	-5.224560000000	-3.220648000000	0.223189000000
H	-3.746290000000	-3.256343000000	1.179932000000
H	-3.668166000000	-3.421728000000	-0.573905000000
C	-4.194617000000	-0.785939000000	2.634508000000
H	-3.627998000000	-0.066586000000	3.228022000000
H	-3.821481000000	-1.782442000000	2.870178000000
H	-5.238381000000	-0.736251000000	2.964077000000
C	-4.386378000000	2.062469000000	1.414757000000
H	-5.338482000000	1.982773000000	1.950171000000
H	-4.432297000000	2.940709000000	0.774032000000
H	-3.598466000000	2.230955000000	2.151441000000
C	4.082601000000	-1.419608000000	-0.108120000000
C	4.119026000000	-0.685758000000	1.110895000000
C	4.154211000000	0.695894000000	0.796674000000
C	4.155833000000	0.821012000000	-0.623670000000
C	4.108242000000	-0.480778000000	-1.176944000000
C	4.176803000000	-2.903884000000	-0.239196000000
H	3.747922000000	-3.256748000000	-1.178147000000
H	3.667505000000	-3.421455000000	0.575660000000
H	5.224926000000	-3.220649000000	-0.219477000000
C	4.219570000000	-1.265637000000	2.481253000000
H	3.822666000000	-2.280164000000	2.525320000000
H	3.679533000000	-0.667088000000	3.215886000000
H	5.268031000000	-1.306134000000	2.795342000000
C	4.354267000000	1.798252000000	1.776946000000
H	5.423761000000	2.007531000000	1.889431000000
H	3.961335000000	1.538233000000	2.759867000000
H	3.858622000000	2.713699000000	1.456310000000
C	4.386920000000	2.062072000000	-1.414586000000
H	4.435537000000	2.940142000000	-0.773806000000
H	3.597608000000	2.231849000000	-2.149475000000
H	5.337697000000	1.981155000000	-1.952141000000
C	4.197065000000	-0.786828000000	-2.633193000000
H	3.823586000000	-1.783171000000	-2.869021000000
H	5.241172000000	-0.737810000000	-2.961791000000
H	3.631477000000	-0.067251000000	-3.227408000000
B	-0.840495000000	-1.454816000000	-1.782257000000
B	0.866019000000	-1.466005000000	-1.759395000000
B	0.009766000000	-0.158501000000	-0.960369000000
B	-0.866986000000	1.267685000000	-1.481020000000
H	-1.481276000000	1.283293000000	-2.510352000000
B	0.895944000000	1.266841000000	-1.461883000000
H	1.532432000000	1.280816000000	-2.479383000000
B	0.009411000000	2.675262000000	-0.882103000000
H	0.015908000000	3.701657000000	-1.488577000000
B	1.432248000000	2.088677000000	0.015274000000
H	2.369371000000	2.820916000000	0.025859000000
B	-0.009293000000	2.674557000000	0.882946000000

H	-0.015824000000	3.700455000000	1.490254000000
B	-1.432097000000	2.088623000000	-0.014903000000
H	-2.369258000000	2.820798000000	-0.025192000000
B	-0.895965000000	1.265612000000	1.461643000000
H	-1.532046000000	1.278885000000	2.479378000000
B	0.867103000000	1.266420000000	1.480789000000
H	1.480975000000	1.281369000000	2.510343000000
B	-0.009686000000	-0.159246000000	0.958899000000
B	-0.865967000000	-1.467517000000	1.756687000000
B	0.840578000000	-1.456298000000	1.779511000000
Ti	-2.073331000000	-0.217613000000	-0.019397000000
Ti	2.073347000000	-0.217797000000	0.017500000000
H	0.007627000000	-2.499697000000	-1.740664000000
H	1.332078000000	-1.395305000000	-2.853287000000
H	-1.276817000000	-1.377647000000	-2.887911000000
H	-1.699860000000	-1.893806000000	0.940081000000
H	1.703431000000	-1.880949000000	0.990367000000
H	1.276259000000	-1.380489000000	2.885494000000
H	-1.331476000000	-1.398084000000	2.850881000000
H	-0.007567000000	-2.501228000000	1.736391000000
H	-1.703076000000	-1.880288000000	-0.993273000000
H	1.699592000000	-1.893450000000	-0.943004000000

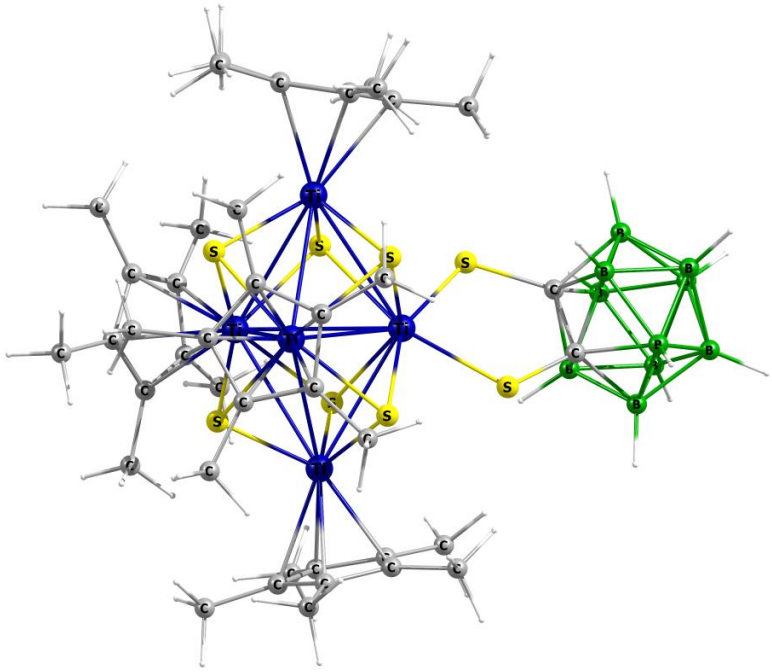

Figure S84. Optimized geometry of **2**

Total energy = -9323.13729863 a.u.

Cartesian coordinates for the calculated structure **2** (in Å)

Ti	-0.455801000	-2.673302000	-0.048789000
Ti	-0.455570000	2.673223000	0.049093000
Ti	-1.565800000	0.041743000	-1.599586000
Ti	-1.565940000	-0.041508000	1.599739000
Ti	1.320906000	-0.000009000	0.000169000
S	-2.554260000	-1.662620000	-0.037170000
S	-2.554220000	1.662927000	0.037102000
S	0.316926000	1.605048000	-1.803280000
S	0.474455000	1.482045000	1.778853000
S	0.316686000	-1.605051000	1.803472000
S	0.474574000	-1.482155000	-1.778398000
S	3.094097000	-1.183102000	1.100248000
C	4.724669000	-0.603477000	0.558874000
S	3.094088000	1.182882000	-1.100126000
B	6.058021000	-1.668267000	0.325689000
C	4.724688000	0.603247000	-0.558760000
B	5.186285000	0.989542000	1.071831000
B	6.059171000	-0.455882000	1.638961000
B	6.956305000	0.986396000	1.066950000
B	5.186265000	-0.989710000	-1.071709000
B	6.058029000	1.668031000	-0.325601000
B	6.956295000	-0.986635000	-1.066877000
B	7.506144000	-0.658788000	0.609030000
B	7.506158000	0.658551000	-0.608949000
B	6.059194000	0.455664000	-1.638885000
C	1.607142000	-4.638533000	2.021754000
C	0.666760000	-4.613479000	0.849766000
C	-0.747081000	-4.872046000	0.887018000
C	1.052718000	-4.492809000	-0.529279000
C	2.455651000	-4.327318000	-1.041366000
C	-1.236370000	-4.921050000	-0.465963000
C	-2.628796000	-5.339335000	-0.856681000
C	-0.086815000	-4.836907000	-2.839010000
C	-0.116922000	-4.699901000	-1.342131000
C	-1.535511000	-5.259452000	2.105660000
C	-3.222617000	2.607625000	3.275725000
C	-2.876787000	1.149018000	3.264731000
C	-3.708220000	0.107205000	2.730444000
C	-1.773870000	0.533042000	3.947803000
C	-0.758984000	1.222758000	4.816012000
C	-3.139984000	-1.154664000	3.111572000
C	-3.830522000	-2.478937000	2.960250000

C	-1.138257000	-1.897669000	4.636765000
C	-1.938772000	-0.894304000	3.855771000
C	-5.036184000	0.290505000	2.052086000
C	-3.830800000	2.478840000	-2.960481000
C	-3.140042000	1.154637000	-3.111554000
C	-1.938580000	0.894514000	-3.855521000
C	-3.708037000	-0.107329000	-2.730525000
C	-5.036179000	-0.291214000	-2.052683000
C	-1.773456000	-0.532784000	-3.947675000
C	-0.758313000	-1.222185000	-4.815831000
C	-3.222259000	-2.607569000	-3.275981000
C	-2.876291000	-1.148990000	-3.264683000
C	-1.138204000	1.898100000	-4.636377000
C	-2.628014000	5.339510000	0.858064000
C	-1.235918000	4.921014000	0.466427000
C	-0.747565000	4.872016000	-0.886892000
C	-0.115880000	4.699815000	1.341827000
C	-0.084853000	4.836772000	2.838685000
C	0.666312000	4.613453000	-0.850613000
C	1.605889000	4.638637000	-2.023247000
C	2.456482000	4.327390000	1.039357000
C	1.053218000	4.492789000	0.528161000
C	-1.536950000	5.259422000	-2.104901000
H	2.036081000	-5.658059000	2.146399000
H	2.449848000	-3.930638000	1.889973000
H	1.097936000	-4.370262000	2.968069000
H	2.953660000	-5.318727000	-1.132814000
H	2.475484000	-3.850017000	-2.040685000
H	3.069375000	-3.702571000	-0.362884000
H	-2.783353000	-6.420711000	-0.644914000
H	-3.407523000	-4.779182000	-0.299496000
H	-2.819777000	-5.187035000	-1.935702000
H	0.465070000	-5.758283000	-3.127931000
H	-1.102193000	-4.917692000	-3.273161000
H	0.429719000	-3.982118000	-3.322642000
H	-1.194449000	-4.726114000	3.015274000
H	-2.618730000	-5.071580000	1.978344000
H	-1.414204000	-6.347651000	2.308618000
H	-3.891522000	2.837266000	4.135707000
H	-2.322036000	3.240803000	3.379900000
H	-3.750500000	2.911721000	2.350968000
H	-1.078042000	1.182629000	5.882034000
H	0.240804000	0.749876000	4.749059000
H	-0.637246000	2.288887000	4.545854000
H	-4.711989000	-2.527263000	3.637822000
H	-4.196286000	-2.644566000	1.925805000
H	-3.164854000	-3.320353000	3.223788000
H	-1.543311000	-1.988290000	5.669898000
H	-1.170241000	-2.904684000	4.177622000
H	-0.072474000	-1.608221000	4.717593000
H	-5.857395000	0.314488000	2.803783000
H	-5.078161000	1.237709000	1.479028000
H	-5.253970000	-0.538324000	1.349760000
H	-4.713449000	2.526134000	-3.636564000
H	-3.165810000	3.320116000	-3.226179000
H	-4.194807000	2.645577000	-1.925577000
H	-5.856663000	-0.319763000	-2.805021000
H	-5.256466000	0.539585000	-1.353499000
H	-5.076544000	-1.236531000	-1.476362000
H	-1.076485000	-1.180637000	-5.882066000
H	-0.637591000	-2.288718000	-4.546819000
H	0.241756000	-0.750078000	-4.747568000
H	-3.891387000	-2.836863000	-4.135872000
H	-3.750010000	-2.911767000	-2.351171000
H	-2.321784000	-3.240850000	-3.380426000
H	-1.543941000	1.989651000	-5.669153000
H	-0.072595000	1.608277000	-4.718105000
H	-1.169394000	2.904792000	-4.176453000
H	-2.782270000	6.421070000	0.646982000
H	-3.407181000	4.779997000	0.300855000
H	-2.818572000	5.186692000	1.937085000
H	0.464783000	5.759616000	3.127256000
H	-1.100055000	4.914756000	3.273763000
H	0.434362000	3.983289000	3.321732000
H	2.034904000	5.658123000	-2.147916000
H	2.448580000	3.930575000	-1.892243000
H	1.095957000	4.370715000	-2.969267000
H	2.953939000	5.318965000	1.132011000
H	2.477063000	3.848713000	2.038015000
H	3.070261000	3.703920000	0.359764000
H	-1.416778000	6.347868000	-2.307238000
H	-1.195802000	4.726985000	-3.015006000
H	-2.619926000	5.070428000	-1.977200000
H	5.897480000	-2.836076000	0.582449000
H	8.518911000	-1.144345000	1.058003000
H	7.552035000	-1.701600000	-1.839160000
H	4.399032000	-1.602450000	-1.741410000
H	5.896922000	0.802319000	-2.782356000
H	8.518934000	1.144114000	-1.057896000
H	5.897494000	2.835843000	-0.582356000
H	7.552080000	1.701335000	1.839232000
H	4.398988000	1.602279000	1.741459000
H	5.896962000	-0.802554000	2.782436000

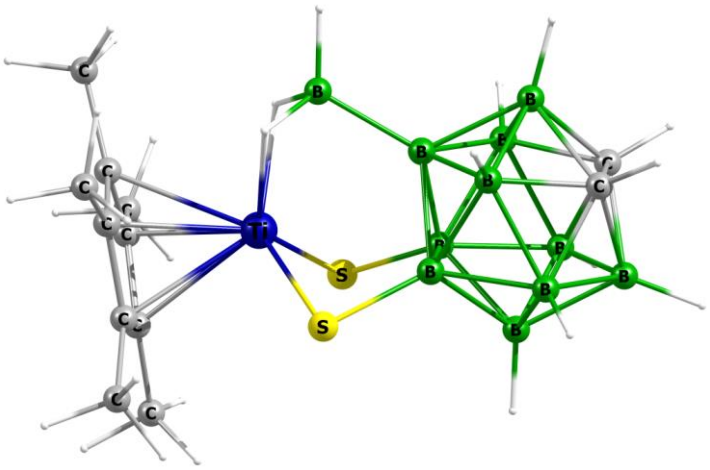

Figure S85. Optimized geometry of **3**.

Total energy = -2392.38887526 a.u.

Cartesian coordinates for the calculated structure **3** (in Å)

B	1.696365000	0.022743000	1.142592000
B	1.725486000	-0.924619000	-0.427423000
B	1.730880000	0.903474000	-0.466876000
B	2.785072000	-0.037990000	-1.599236000
H	2.608520000	-0.063061000	-2.792818000
B	3.407323000	-1.471618000	-0.714370000
H	3.779259000	-2.514869000	-1.189345000
B	2.746130000	-1.430511000	0.956749000
H	2.676656000	-2.452421000	1.592334000
B	2.754921000	1.460616000	0.895720000
H	2.691628000	2.508588000	1.488032000
B	3.416537000	1.427700000	-0.775351000
H	3.795012000	2.447684000	-1.293698000
B	4.426739000	-0.029397000	-0.948348000
H	5.502919000	-0.044099000	-1.486794000
B	3.350922000	0.031157000	1.777192000
H	3.776744000	0.053813000	2.902400000
C	-2.769945000	-0.983607000	-0.702180000
C	-2.724329000	0.383617000	-1.144334000
C	-2.810660000	1.230597000	0.017165000
C	-2.899108000	0.383711000	1.177578000
C	-2.860751000	-0.984378000	0.732661000
C	-2.879726000	-2.189332000	-1.591161000
H	-2.484521000	-3.102091000	-1.103465000
H	-2.325677000	-2.054735000	-2.540682000
H	-3.946597000	-2.379922000	-1.845575000
C	-2.700679000	0.828291000	-2.579960000
H	-2.046096000	0.179393000	-3.194974000
H	-2.327754000	1.865225000	-2.683781000
H	-3.723184000	0.789275000	-3.018254000
C	-2.918959000	2.730504000	0.016013000
H	-2.419266000	3.179269000	-0.864388000
H	-2.461986000	3.180284000	0.919605000
H	-3.987391000	3.041875000	-0.008010000
C	-3.121465000	0.840481000	2.593626000
H	-4.208168000	0.840194000	2.833782000
H	-2.745760000	1.868766000	2.760277000
H	-2.617826000	0.181051000	3.327795000
C	-3.001816000	-2.208187000	1.596889000
H	-2.727062000	-2.002863000	2.649821000
H	-2.360082000	-3.037852000	1.238810000
H	-4.053203000	-2.573198000	1.592012000
B	0.291164000	0.055667000	2.159855000
C	4.281372000	-0.814269000	0.588777000
C	4.286252000	0.820172000	0.554339000
H	5.195280000	-1.296238000	0.960143000
H	5.203145000	1.311854000	0.905262000
S	0.176372000	-1.831109000	-0.900946000
S	0.185129000	1.797596000	-0.971455000
Ti	-0.776264000	0.006924000	0.191560000
H	-0.433075000	1.041965000	1.802939000
H	0.438382000	0.096207000	3.369848000
H	-0.444938000	-0.941926000	1.863816000

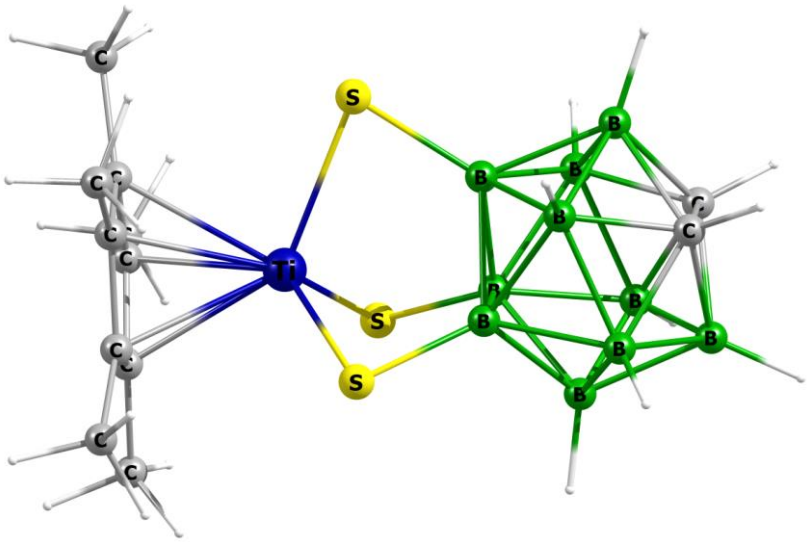

Figure S86. Optimized geometry of **4a**.

Total energy = -2763.92933711 a.u.

Cartesian coordinates for the calculated structure **4a** (in Å)

B	-0.344223000	2.566694000	1.659756000
B	-0.490019000	3.702710000	3.096798000
B	-1.684073000	2.297030000	2.913242000
B	-2.021931000	2.143685000	1.146067000
H	-2.389640000	1.145605000	0.581256000
B	-3.181268000	2.971558000	2.228351000
H	-4.327641000	2.638957000	2.375614000
B	-2.251030000	3.936303000	3.413638000
H	-2.781115000	4.212149000	4.459250000
B	-1.089971000	3.393587000	0.254030000
H	-0.836014000	3.230600000	-0.912378000
B	-0.151980000	4.354645000	1.440587000
H	0.905463000	4.857722000	1.149945000
B	-1.318619000	5.184099000	2.518741000
H	-1.227553000	6.298356000	2.967875000
B	-1.658331000	4.998113000	0.779835000
H	-1.878658000	5.914871000	0.032788000
C	2.379319000	1.171218000	5.506471000
C	2.852831000	0.569347000	4.287898000
C	2.017007000	-0.565078000	3.997650000
C	1.021308000	-0.660128000	5.033472000
C	1.240109000	0.418614000	5.959891000
C	3.053396000	2.287522000	6.254128000
H	3.556730000	2.999388000	5.570730000
H	2.336334000	2.867990000	6.867613000
H	3.826728000	1.877614000	6.941949000
C	4.060475000	1.015045000	3.510162000
H	4.152206000	2.119371000	3.494902000
H	4.992293000	0.608347000	3.963474000
H	4.021389000	0.672638000	2.458030000
C	2.210196000	-1.555564000	2.882567000
H	1.244239000	-1.944965000	2.504756000
H	2.745939000	-1.109868000	2.021848000
H	2.807881000	-2.426109000	3.235038000
C	0.025886000	-1.776578000	5.187354000
H	-0.863380000	-1.462022000	5.768304000
H	-0.333348000	-2.148766000	4.207825000
H	0.488252000	-2.635103000	5.724378000
C	0.455989000	0.688554000	7.214485000
H	-0.574062000	0.287693000	7.147252000
H	0.944728000	0.217664000	8.096831000
H	0.375022000	1.774896000	7.417655000
C	-2.840608000	4.642441000	1.993969000
C	-2.710713000	3.624942000	0.707072000
H	-3.717313000	5.303215000	2.004604000
H	-3.510643000	3.684623000	-0.042512000
S	-1.598998000	0.847000000	4.061359000
S	0.771423000	3.633456000	4.455478000
S	1.058783000	1.355620000	1.580394000
Ti	0.663601000	1.383696000	3.873280000

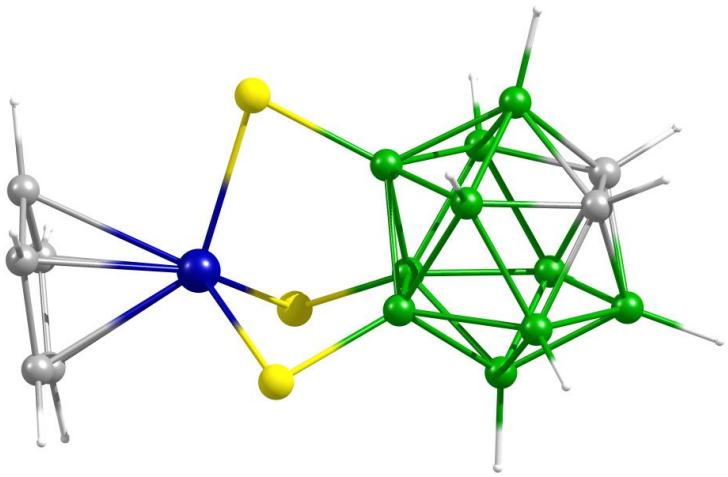

Figure S87. Optimized geometry of **4b**.

Total energy = -2567.49144199 a.u.

Cartesian coordinates for the calculated structure **4b** (in Å)

B	-1.678255000	-0.239887000	-1.037190000
B	-1.681743000	1.032449000	0.289303000
B	-1.672982000	-0.766535000	0.741238000
B	-2.717755000	-1.601678000	-0.471316000
H	-2.646266000	-2.761993000	-0.785066000
B	-3.345149000	-1.207348000	1.157903000
H	-3.767558000	-2.020631000	1.936379000
B	-2.725606000	0.406383000	1.621606000
H	-2.659866000	0.671337000	2.794350000
B	-3.362360000	-0.390829000	-1.632282000
H	-3.724360000	-0.745142000	-2.725143000
B	-2.734621000	1.224312000	-1.172559000
H	-2.541028000	2.083694000	-1.996737000
B	-3.369447000	1.614509000	0.457928000
H	-3.737258000	2.690205000	0.856043000
B	-4.381499000	0.760695000	-0.733688000
H	-5.452230000	1.154032000	-1.114831000
C	2.825256000	1.210804000	0.118518000
C	2.818381000	0.491423000	-1.114255000
C	2.819508000	-0.905091000	-0.811067000
C	2.825717000	-1.048116000	0.608923000
C	2.824262000	0.259577000	1.183798000
C	-4.250673000	0.235009000	0.911081000
C	-4.246308000	-0.904394000	-0.276466000
H	-5.170576000	0.314865000	1.505069000
H	-5.163698000	-1.497815000	-0.384478000
S	-0.155329000	-1.526647000	1.481234000
S	-0.154025000	2.036111000	0.606362000
S	-0.145392000	-0.504784000	-2.050576000
Ti	0.789383000	0.003746000	0.007279000
H	2.787193000	-1.723324000	-1.541294000
H	2.782511000	0.933148000	-2.118012000
H	2.813747000	-1.995920000	1.160785000
H	2.814099000	2.302087000	0.227460000
H	2.787129000	0.492391000	2.255748000

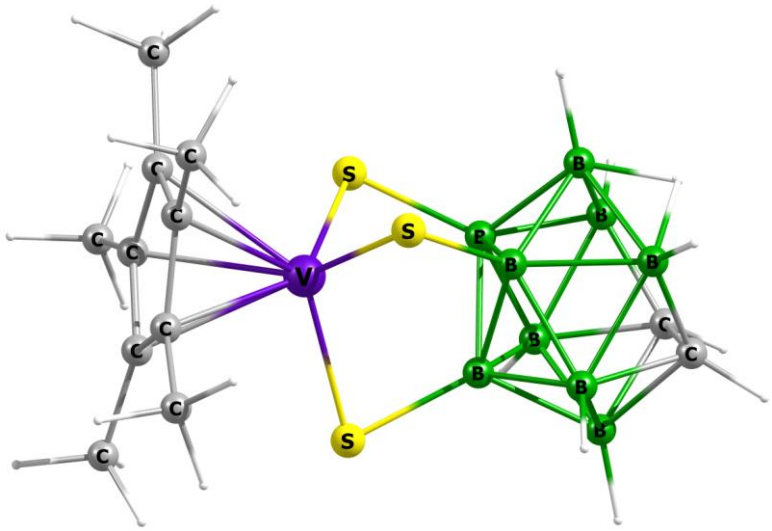

Figure S88. Optimized geometry of **5**.

Total energy = -2833.57027500 a.u.

Cartesian coordinates for the calculated structure **5** (in Å)

C	2.944491000	11.275983000	2.552201000
C	2.777411000	11.049482000	3.965247000
C	1.774457000	10.030017000	4.135852000
C	1.296686000	9.651752000	2.831474000
C	2.022073000	10.421229000	1.851514000
C	4.016793000	12.110883000	1.915498000
H	4.921635000	11.486409000	1.742968000
H	4.316805000	12.962504000	2.556610000
H	3.697572000	12.522230000	0.938542000
C	3.570396000	11.698852000	5.062345000
H	2.988453000	11.761446000	6.002008000
H	3.874319000	12.728031000	4.790025000
H	4.494422000	11.115305000	5.272437000
C	1.423511000	9.346008000	5.424437000
H	2.093262000	8.469955000	5.574224000
H	0.379135000	8.978736000	5.428314000
H	1.547482000	10.014580000	6.298414000
C	0.311356000	8.552857000	2.555504000
H	-0.167771000	8.666290000	1.564465000
H	-0.494328000	8.526070000	3.314760000
H	0.825912000	7.566193000	2.572479000
C	1.941927000	10.269330000	0.359850000
H	2.111785000	11.231932000	-0.160374000
H	0.956855000	9.883387000	0.035012000
H	2.718538000	9.553637000	0.008642000
C	-2.247574000	15.791850000	4.061346000
C	-2.565364000	15.568144000	2.540932000
B	-1.457954000	13.150904000	2.449921000
B	-0.180581000	14.336713000	3.029208000
B	-1.134883000	13.347569000	4.269163000
B	-2.792838000	13.075614000	3.633823000
B	-2.931862000	14.051152000	2.105520000
B	-1.314550000	14.746492000	1.702005000
H	-0.971988000	15.002341000	0.572273000
B	-0.944847000	15.947905000	2.970046000
H	-0.421808000	17.011419000	2.750611000
B	-0.775521000	15.077512000	4.519601000
H	-0.093478000	15.528139000	5.407979000
B	-2.431354000	14.415682000	4.912411000
S	-0.839792000	11.564067000	1.663873000
S	1.624610000	13.917159000	2.754003000
S	-0.193083000	11.979131000	5.146663000
V	0.786769000	11.889998000	3.153501000
H	-3.291631000	11.999130000	3.880875000
H	-3.665696000	13.797547000	1.175782000
H	-2.729811000	14.377685000	6.084553000
H	-2.513094000	16.765417000	4.498581000
H	-3.052754000	16.408973000	2.024494000
H	-3.524495000	14.000259000	4.154490000

References

1 G. H. Llinás, M. Mena, F. Palacios, P. Royo and R. Serrano, *J. Organomet. Chem.*, 1988, **340**, 37.

2 C. D. Abernethy, F. Bottomley and A. Decken, *Organometallics*, 1997, **16**, 1865.

3 A. R. Popescu, A. D. Musteti , A. Ferrer-Ugalde, C. Vinas , R. Nunez and F. Teixidor, *Chem.-Eur. J.*, 2012, **18**, 3174.

4 J. Plešek, Z. Janousek and S. Hermanek, *Collect. Czech. Chem. Commun.*, 1980, **45**, 1775.

5 X. Zhang, X. Tang, J. Yang, Y. Li, H. Yan and V. I. Bregadze, *Organometallics*, 2013, **32**, 2014.

6 *(a*) J. J. Led and H. Gesmar, *Chem. Rev.*, 1991, **91**, 1413; (*b*) L. Yang, R. Simionescu, A. Lough and H. Yan, *Dyes Pigm.* 2011, **91**, 264; (*c*) R. Weiss and R. N. Grimes, *J. Am. Chem. Soc.*, 1978, **100**, 1401.

7 P. Govindaswamy, Y. A. Mozharivskyj and M. R. Kollipara, *Polyhedron*, 2005, **24**, 1710.

8 *a*) C. E. Rao, S. K. Barik, K. Yuvaraj, K. Bakthavachalam, T. Roisnel, V. Dorcet, J.-F. Halet and S. Ghosh, *Eur. J. Inorg. Chem.*, 2016, 4913; *b*) A. Haridas, S. Kar, B. Raghavendra, T. Roisnel, V. Dorcet and S. Ghosh, *Organometallics*, 2020, **39**, 58.

9 S. Bairagi, S. Giri, G. Joshi, E. D. Jemmis and S. Ghosh, *Angew. Chem. Int. Ed.*, 2025, **64**, e202417170

10 S. Bairagi, A. N. Pradhan, M. Cordier, T. Roisnel and S. Ghosh, *Eur. J. Inorg. Chem.*, 2023, **26**, e202300060.

11 A. Altomare, G. Cascarano, C. Giacovazzo, A. Guagliardi, M. C. Burla, G. Polidori and M. Camalli, *J. Appl. Crystallogr*., 1994, **27**, 435.

12 *a*) G. M. Sheldrick, *Acta Cryst.*, 2015, **C71**, 3; *b*) L. J. Bourhis, O. V. Dolomanov, R. J. Gildea, J. A. K. Howard, H. Puschmann*, Acta Cryst.*, 2015, **A71**, 59.

13 O. V. Dolomanov, L. J. Bourhis, R. J. Gildea, J. A. K. Howard and H. Puschmann, *J. Appl. Cryst*., 2009, **42**, 339.

14 M. J. Frisch, G. W. Trucks, H. B. Schlegel, G. E. Scuseria, M. A. Robb, J. R. Cheeseman, G. Scalmani, V. Barone, B. Mennucci, G. A. Petersson, H. Nakatsuji, M. Caricato, X. Li, H. P. Hratchian, A. F. Izmaylov, J. Bloino, G. Zheng, J. L. Sonnenberg, M. Hada, M. Ehara, K. Toyota, R. Fukuda, J. Hasegawa, M. Ishida, T. Nakajima, Y. Honda, O. Kitao, H. Nakai, T. Vreven, J. A. Montgomery Jr., J. E. Peralta, F. Ogliaro, M. Bearpark, J. J. Heyd, E. Brothers, K. N. Kudin, V. N. Staroverov, R. Kobayashi, J. Normand, K. Raghavachari, A. Rendell, J. C. Burant, S. S. Iyengar, J. Tomasi, M. Cossi, N. Rega, J. M. Millam, M. Klene, J. E. Knox, J. B. Cross, V. Bakken, C. Adamo, J. Jaramillo, R. Gomperts, R. E. Stratmann, O. Yazyev, A. J. Austin, R. Cammi, C. Pomelli, J. W. Ochterski, R. L. Martin, K. Morokuma, V. G. Zakrzewski, G. A. Voth, P. Salvador, J. J. Dannenberg, S. Dapprich, A. D. Daniels, Ö. Farkas, J. B. Foresman, J. V. Ortiz, J. Cioslowski and D. J. Fox, *Gaussian 09, Revision C.01*, Gaussian, Inc., Wallingford, CT, 2010.

15 *a*) H. L. Schmider and A. D. Becke, *J. Chem. Phys.*, 1998, **108**, 9624; *b*) J. P. Perdew, *Phys. Rev. B: Condens. Matter Mater. Phys.*, 1986, **33**, 8822.

16 EMSL Basis Set Exchange Library. https://bse.pnl.gov/bse/portal

17 F. London, *J. Phys. Radium*., 1937, **8**, 397.

18 R. Ditchfield, *Mol. Phys.*, 1974, *27*, 789.

19 K. Wolinski, J. F. Hinton and P. Pulay, *J. Am. Chem. Soc.*, 1990, **112**, 8251.

20 *a*) A. D. Becke, *Phys. Rev. A.*, 1988, **38**, 3098; *b*) C. Lee, W. Yang and R. G. Parr, *Phys. Rev. B.*, 1988, **37**, 785; *c*) A. D. Becke, *J. Chem. Phys.*, 1993, **98**, 5648.

21 T. P. Onak, H. L. Landesman, R. E. Williams and I. Shapiro, *J. Phys.Chem.*, 1959, **63**, 1533.

22 *a*) E. D. Glendening, A. E. Reed, J. E. Carpenter and F. Weinhold, *NBO Program 3.1*, W. T. Madison, 1988; *b*) A. E. Reed, F. Weinhold and L. A. Curtiss, *Chem. Rev.*, 1988, **88**, 899; *c*) F. Weinhold and R. Landis, *Valency and bonding: A natural bond orbital donor-acceptor perspective;* Cambridge University Press: Cambridge, U.K, 2005.

23 K. Wiberg, *Tetrahedron*, 1968, **24**, 1083.

24 *a*) R. F. W. Bader, *Atoms in Molecules: A Quantum Theory*; Oxford University Press: Oxford, U. K., 1990; *b*) R. F. W. Bader, *J. Phys. Chem. A.*, 1998, **102**, 7314; *c*) R. F. W. Bader, *Chem. Rev.*, 1991, **91**, 893.

25 T. Lu, F. Chen, *J. Comput. Chem.*, 2012, **33**, 580.

26 I. I. Dennington, R. T. Keith, J. Millam, K. Eppinnett, W. L. Hovell and R. Gilliland, *GaussView, Version 3.09*; Semichem Inc.: Shawnee Mission, KS, 2003.

27 G. A. Zhurko, http://www.chemcraftprog.com.